AFRL-IF-RS-TR-2005-310
Final Technical Report
August 2005

ULTRA-PRECISE CLOCK SYNCHRONIZATION VIA DISTANT ENTANGLEMENT

Massachusetts Institute of Technology

APPROVED FOR PUBLIC RELEASE; DISTRIBUTION UNLIMITED.

AIR FORCE RESEARCH LABORATORY
INFORMATION DIRECTORATE
ROME RESEARCH SITE
ROME, NEW YORK

STINFO FINAL REPORT

This report has been reviewed by the Air Force Research Laboratory, Information Directorate, Public Affairs Office (IFOIPA) and is releasable to the National Technical Information Service (NTIS). At NTIS it will be releasable to the general public, including foreign nations.

AFRL-IF-RS-TR-2005-310 has been reviewed and is approved for publication

APPROVED: /s/

DONALD J. NICHOLSON
Project Engineer

FOR THE DIRECTOR: /s/

WARREN H. DEBANY, JR., Technical Advisor
Information Grid Division
Information Directorate

REPORT DOCUMENTATION PAGE

Form Approved
OMB No. 074-0188

1. AGENCY USE ONLY (Leave blank)

2. REPORT DATE
AUGUST 2005

3. REPORT TYPE AND DATES COVERED
Final Aug 01 – Aug 04

4. TITLE AND SUBTITLE
ULTRA-PRECISE CLOCK SYNCHRONIZATION VIA DISTANT ENTANGLEMENT

5. FUNDING NUMBERS
C - F30602-01-2-0546
PE - 62712E
PR - M253
TA - QU
WU - AN

6. AUTHOR(S)
Selim Shahriar,
Franco Wong and
Ulvi Yurtsever

7. PERFORMING ORGANIZATION NAME(S) AND ADDRESS(ES)
Massachusetts Institute of Technology
Research Laboratory of Electronic
77 Massachusetts Avenue
Cambridge Massachusetts 02139

8. PERFORMING ORGANIZATION REPORT NUMBER
N/A

9. SPONSORING / MONITORING AGENCY NAME(S) AND ADDRESS(ES)
Air Force Research Laboratory/IFGC
525 Brooks Road
Rome New York 13441-4505

10. SPONSORING / MONITORING AGENCY REPORT NUMBER
AFRL-IF-RS-TR-2005-310

11. SUPPLEMENTARY NOTES

AFRL Project Engineer: Donald J. Nicholson/IFGC/(315) 330-7437/ Donald.Nicholson@rl.af.mil

12a. DISTRIBUTION / AVAILABILITY STATEMENT
APPROVED FOR PUBLIC RELEASE; DISTRIBUTION UNLIMITED.

12b. DISTRIBUTION CODE

13. ABSTRACT *(Maximum 200 Words)*
We have demonstrated a spectrally bright source of entangled photon pairs that are necessary for transferring entanglement from photons to a pair of atoms at significant distance. We have shown how a measurement of the degree of entanglement may be used to deduce the relative speed between two frames, without direct measurement of velocities.

14. SUBJECT TERMS
Clock Synchronization, Entangled Sources, Satellite

15. NUMBER OF PAGES
73

16. PRICE CODE

17. SECURITY CLASSIFICATION OF REPORT	18. SECURITY CLASSIFICATION OF THIS PAGE	19. SECURITY CLASSIFICATION OF ABSTRACT	20. LIMITATION OF ABSTRACT
UNCLASSIFIED	UNCLASSIFIED	UNCLASSIFIED	UL

Table of Contents

1. OBJECTIVE:

The objective of the experimental part of this project was to investigate the use of distant entanglement between atoms for synchronizing clocks, even in the presence of random fluctuations of the intervening path-length. The objective of the theoretical part of this project was to study the role of special and general relativity as well as decoherence in this process.

2. APPROACH:

A key step in our approach was to establish a degenerate entanglement between two distant atoms, in a manner that is independent of the distance between the atoms, and no timing information is transmitted. Each atom would then be excited by its local atomic clock, thus producing a non-degenerate entanglement. Next, an interference between the co- and counter-rotating terms in the Hamiltonian, followed by a measurement induced collapse of the entanglement, would be used to teleport the wavelength of one clock to the other location, thereby realizing frequency locking. Given an initial synchronization, frequency locking is of primary importance in keeping the clocks synchronized.

In order to realize this protocol, it would necessary first to create two building blocks: a trapped atom quantum memory, and an ultra-bright source of entangled photon pairs. Each bit of the quantum memory would be realized by trapping a single atom in a dipole force field, co-located at the center of a high-finesse super-cavity. This would be achieved by catching a group of atoms first in a magneto-optic trap, followed by a vertical launch as an atomic fountain, and capture of a single atom in a far-off-resonant trap (FORT). The entangled photon pairs would be realized by using optical parametric amplifiers (OPAs).

In addition to the frequency locking, it would be useful to have a protocol for transmitting absolute timing signals, which can be achieved --- with an accuracy beyond the classical limit of shot-noise --- by using a frequency-entangled source of laser pulses. The noise-reduction factor is $\sqrt{N}$, where N is the number of frequencies entangled. Non-linear processes involving frequency down-conversions would be used to produce a source of this nature.

For the theoretical tasks, a relativistic formulation of quantum entanglement would be applied to the specific protocol for clock synchronization. Effects of both special and general relativity would be considered Furthermore, the issue of how various sources of decoherence may affect the fidelity of entanglement generation and thereby the accuracy of the clock synchronization would be studied, first in the non-relativistic context, and then including relativity.

3. SUMMARY OF ACCOMPLISHMENTS:

The work performed by the people suppported under this project has resulted in thirty eight journal publications, and many conference presentations. Some of the most important journal publications are included as attachments, and **the content of these attached papers represent the primary body of this report**. In what follows, we present a summary of the key accomplishments under this project. Details of these results can be found in the attached papers.

3.1. Most Significant Theoretical Accomplishments

1. A basic Lorentz invariant model for distant entanglement was constructed
2. A concrete scheme was established for measuring the absolute phase of a field in real time using a thermal atomic beam, via making use of a novel photon-echo type process that eliminates the dephasing from the velocity spread.
3. A protocol was developed for remote frequency locking via wave-length teleportation using the Bloch-Siegert Oscillation based phase mapping.
4. A protocol was developed for transmitting absolute timing signals, which can be achieved --- with an accuracy beyond the classical limit of shot-noise --- by using a frequency-entangled source of laser pulses. The noise-reduction factor is $\sqrt{N}$, where N is the number of frequencies entangled. Non-linear processes involving frequency down-conversions could be used to produce a source of this nature.
5. An explicit scheme was developed for generating the so-called Difference Beam (DB), for achieving the sub-shot-noise accuracy in transmitting timing signal using the protocol of item 4 above.
6. The fundamental constraints on any protocol for clock synchronization using distant entanglement was established using a general framework
7. A proof was developed, via a Lorentz-invariant analysis, that it is not possible to purify the so-called Preskill phase asynchronously.
8. It was proven that the BSO is negligible if a two level system is excited by an off-resonant Raman transition, and prominent BSO requires the use of direct RF excitation.
9. A detailed theoretical mdoel was developed to show how the degree of entanglement between a pair of particles --- either massive or massless --- located in one reference frame and observed from another reference frame, depends on the relative boost between the frames.
10. The model of item 9 was used to show how a measurement of the degree of entanglement may be used to deduce the relative speed between two frames, without direct measurement of velocities. Such a deduction can be used to enhance the accuracy of clock synchronization as well

3.2. Most Significant Experimental Accomplishments

11. We have demonstrated a down-converter with a KTP crystal in a cavity, achieving a fidelity of about 68%.
12. We have demonstrated a single-pass, broadband PPKTP crystal based down-converter with a coincidence count of up to 50,000 per second, and a fidelity of more than 97%.
13. We have realized a novel dual-pumped downconversion source that yields the highest flux of polarization-entangled photon pairs. We have detected a 795-nm pair flux of 11000/s/mW of pump power at a 90% visibility level in quantum interference

measurements. This is the brightest (by at least an order of magnitude) source of entangled photon pairs to date, and is ideally suited for the clock synchronization protocol based on the Bloch-Siegert effect.

14. We have demonstrated an extended phase-matched second-harmonic generation in PPKTP with an observed fundamental bandwidth of ~100 nm, centered at 1585 nm. This represents an important step toward realizing the coincident-frequency entangled state for use in the frequency-entanglement clock synchronization protocol.
15. We have demonstrated a FORT that catches atoms at the top of an atomic fountain launched from a MOT. We have also demonstrated coupling between two cavities and an upside down atomic beam traveling through the cavities.
16. We have observed the Bloch-Siegert Oscillation (BSO) using an atomic beam, as a spectral signature at twice the frequency of the one used to drive a Zeeman transition. In addition, we have demonstrated directly that the BSO is phaselocked with the driving frequency.
17. We have demonstrated an ultrabright source of polarization-entangled photons. The total output flux is entangled without spectral, spatial, or temporal filtering. The novel configuration uses bi-directional pumping and collinear propagation. The 795-nm center wavelength is ideal for coupling to trapped Rb atoms.
18. We have demonstrated extended phase matching in PPKTP with a 100 nm phase-matching bandwidth for second harmonic generation. This is to be used for demonstrating coincident-frequency entanglement.
19. We have demonstrated that by applying a DC field parallel to the oscillating field, it is possible to observe a BSO that is at the same frequency as the driving phase, and phase locked, without the 180 degree ambiguity that occurs for the BSO at twice the frequency. Furthermore, we have shown that BSO may be readily observed in an atomic ensemble, even without any optical pumping for state preparation. This is a critical results that paves the way for using dipole-blockaded clusters of rubidium atoms in Rydberg states for the clock synchronization protocol.
20. We have demonstrated that by monitoring the transition rate, and the first and second harmonics attributable to the BSO, it is possible to realize an ultra-precise vector magentometer.
21. We have demonstrated launching (from a MOT) and catching (using a FORT) of a small number of rubidium atoms using two separate chambers, as required for the clock synchronization protocol. In one of these chambers, a magnetic guide was used to keep the launched atoms collimated until they reach the FORT. In the other chamber, the FORT was brought physically closer to the MOT.
22. We have demonstrated generation of paired photons at the Stokes and Anti-Stokes Frequencies simultaneously, using a Raman transition in a rubidium vapor cell. This serves as an indirect evidence of the vapor cell acting as a quantum memory. The next step would be to use a pair of vapor cells to demonstrate generation of entanglement between distant atomic clusters. If atoms in Rydberg states are used, under conditions of dipole blockade, this process may be used to realize the clock synchronization protocol without having to use the high Q cavities.

3.3 Overview of Project Achievement and Future Directions

As discussed above, the primary objective of this project was to investigate the use of distant entanglement between atoms for synchronizing clocks, even in the presence of random fluctuations of the intervening path-length. The protocol to be employed for this task makes use of the so-called Bloch-Siegert Oscillation. In order to achieve this goal, it was necessary to demonstrate first two new processes: (a) encoding of the absolute phase of a microwave oscillator on to a set of two-level atoms, and (b) establishment of distant, degenerate entanglement between a pair of trapped, single atoms in an asynchronus manner. During the period of this project, we have accomplished the first goal completely. The second goal is very challenging, and represents a holy grail in the field of distributed quantum information processing and quantum communication. We have made steady progress in this regard, and the work is continuing beyond the end of this project, given that such a source of distant entanglement is necessary for another project currently underway. Specifically, we have demonstrated a spectrally bright source of entangled photon pairs that are necessary for transferring entanglement from photons to a pair of atoms located at significant distance. Furthermore, we have built the pair of single-atom-in-a-cavity trap systems that are necessary for demonstrating the clock synchronization protocol. Additional time and effort is necessary to finalize the demonstraion of the synchronization protocol.

In parallel to these experimental developments, we carried out theoretical investigations in support of this project. For example, we have investigated the feasibility of a novel method of atom-interferomteric nanolithography that could be employed for creating the arrays of trapped atoms pairs for demonstrating the synchronization protocol in a practical system. Furthermore, we have established the relativistic validity of our protocol, and developed the framework for Lorentz invariance for entanglement. In particular, we have shown how a measurement of the degree of entanglement may be used to deduce the relative speed between two frames, without direct measurement of velocities. Such a deduction can be used to enhance the accuracy of clock synchronization as well. We have also established the fundamental constraints in quantum clock synchronization, and have estabslished several new protocols that can work in conjuction with our primary protocol to enhance the accuracy of clock synchronization. The most significant one of these new protocols is the one that shows that transmitting absolute timing signals can be achieved --- with an accuracy beyond the classical limit of shot-noise --- by using a frequency-entangled source of laser pulses. The noise-reduction factor for this protocol is $\sqrt{N}$, where N is the number of frequencies entangled. An explicit scheme was developed for generating the so-called Difference Beam (DB), for achieving this sub-shot-noise accuracy in transmitting timing signal.

The work performed by the people suppported under this project has resulted in thirty eight journal publications, and many conference presentations. Some of the most important journal publications are included as attachments, and the content of these attached papers represent the primary body of this report. This project has established the feasibility of quantum-effects induced enhancement in clock synchronization, and has paved the way for future efforts to realize a functional system of practical usage.

4. TECHNOLOGY TRANSITION

None

5. LIST OF JOURNAL PUBLICATIONS

The project has resulted in the publication of thirty eight journal papers, as well as a large number of conference papers. The journal papers only are listed below. Some of the co-authors in each of these papers was supported by this project for doing the work. It should be noted that not enough care was taken in making sure that this project is explicitly acknowledged as a source of support for each of these papers.

1. “Long Distance, Unconditional Teleportation of Atomic States Via Complete Bell State Measurements,” S. Lloyd, M.S. Shahriar, J.H. Shapiro and P.R. Hemmer, *Phys. Rev. Letts.87, 167903 (2001)*

2. “Frequency Stabilization of an Extended Cavity Semiconductor Laser for Chirped Cooling,” J.A. Morzinsky, P.S. Bhatia, and M.S. Shahriar, Review of Scientific Instruments, **73**, 10, pp. 3449-3453 (2002)

3. “Two-Dimensional Atomic Interferometry for Creation of Nanostructures,”Y. Tan, J. Morzinski, A.V. Turukhin, P.S. Bhatia, and M.S. Shahriar, *Opt. Commun.*, **206**,1, pp. 141-147 (2002).

4. "Limits to clock synchronization induced by completely dephasing communication channels," V. Giovannetti, S. Lloyd, L. Maccone, and M.S. Shahriar, Phys. Rev. A 65, 062319 (2002).

5. "Driver Phase Correlated Fluctuations in the Rotation of a Strongly Driven Quantum Bit," M. S. Shahriar, P. Pradhan, and J. Morzinski, Phys. Rev. A **69**, 032308 (2004)

6. "Super Efficient Absorption Filter for Quantum Memory using Atomic Ensembles in a Vapor," A. Heifetz, A. Agarwal, G. Cardoso, V. Gopal, P. Kumar, and M.S. Shahriar, *Opt. Commun.* 232 (2004) 289–293

7. “Infrastructure for the Quantum Internet,” S. Lloyd, J.H. Shapiro, N.C. Wong, P. Kumar, M.S. Shahriar, and H. Yuen, in ACM SIGCOMM Computer Communication Review (Oct. 2004)

8. "Continuously Guided Atomic Interferometry Using a Single-Zone Optical Excitation: Theoretical Analysis," M.S. Shahriar, M. Jheeta, Y. Tan, P. Pradhan, and A. Gangat, Optics Communications, Volume **243**, Issue 1-6, p. 183-201, 21 (December 2004)

9. "Demonstration Of A Continuously Guided Atomic Interferometer Using A Single-Zone Optical Excitation," M.S. Shahriar, Y. Tan, M. Jheeta, J. Morzinksy, P.R. Hemmer and P. Pradhan, *J. Opt. Soc. Am. B.,* Vol. **22**, No. 7 (July 2005).

10. "Two-dimensional Arbitrary Pattern Nanolithography Using Atom Interferometry," A. Gangat, P. Pradhan, G. Pati, and M.S. Shahriar, Physical Review A **71**, 043606 (2005).

11. “In-Situ Detection of The Temporal and Initial Phase of The Second Harmonic of a Microwave Field via Incoherent Fluorescence,” G. Cardoso, P. Pradhan, J. Morzinski, and M.S. Shahriar, *Phys. Rev. A.* **71**, 063408 (2005).

12. "Wavelength Teleportation via Distant Quantum Entanglement Using the Bloch-Siegert Oscillation," M.S. Shahriar, P. Pradhan, V. Gopal, J. Morzinski, G. Cardoso, and G.S. Pati, to appear in *Optics Communications*

13. "Suppression of the Bloch-Siegert Oscillation Induced Error in Qubit Rotations via the Use of Off-Resonance Raman Excitation," P. Pradhan, G. Cardoso, J. Morzinski, and M.S. Shahriar , submitted to *Optics Communications.*

14. "Multi-Spectral Characteristics of Raman Scattering under Gain Condition for Collective Excitation in Rubidium Atomic Vapor," G.S. Pati, J. Vornehm, V. Gopal, G. Cardoso, P. Kumar, and M.S. Shahriar, submitted to *Physical Review A*.

15 "A Vecor Magneto-meter Using the First and Second Harmonic Bloch-Siegert Oscillator," M.S. Shahriar, P. Pradhan, G. Cardoso, K. Salit, and M. Messal, to be submitted to Phys. Rev. Letts.

16. "Quantum Communication and Computing With Atomic Ensembles Using Light-Shift Imbalance Induced Blockade of Collective Excitations Beyond the Lowest Order**,"** M.S. Shahriar, P. Pradhan, G.S. Pati, K. Salit and J.H. Shapiro, submitted to *Phys. Rev. Letts*.

17. "Quantum Atomic Clock Synchronization Based on Shared Prior Entanglement," Richard Jozsa, Daniel S. Abrams, Jonathan P. Dowling, Colin P. Williams, *Physical Review Letters* 85, (28 August 2000) 2010-2013

18. "Reply to 'Comment on "Quantum Clock Synchronization Based on Shared Prior Entanglement'," Richard Jozsa, Daniel S. Abrams, Jonathan P. Dowling, and Colin P. Williams, *Physical Review Letters* 87 (29 August 2001) 129802 (1)

19. "A Lorentz-Invariant Look at Quantum Clock Synchronization Protocols Based on Distributed Entanglement," Ulvi Yurtsever & Jonathan P. Dowling, Physical Review A 65 (01 May 2002) 052317 (1-6)

20. "Quantum Entanglement of Moving Bodies," Robert M. Gingrich and Christoph Adami, Physical Review Letters, 89, 270402 (2002)

21. Attila J. Bergou, Robert M. Gingrich, and Christoph Adami "Entangled Light in Moving Frames," Phys Rev. A. 68, 042102 (2003)

22. "The Holographic Entropy Bound and Local Quantum Field Theory", Ulvi Yurtsever, Phys. Rev. Letts., 91, 041302 (2003).

23. "Single Photons on Demand from 3D Photonic Band-Gap Structures," Marian Florescu, Stefan Scheel, Hartmut Häffner, Hwang Lee, Dmitry V. Strekalov, Peter L. Knight, and Jonathan P. Dowling, Europhysics Letters 69 (01 March 2005) 945-951.

24. "Distributed Entanglement as a Probe for the Quantum Structure of Spacetime," Pieter Kok, Ulvi Yurtsever, Samuel L. Braunstein, Jonathan P. Dowling, quant-ph/0206082.

25. "Interferometry with Entangled Atoms," Ulvi Yurtsever, Dmitry V. Strekalov, and Jonathan P. Dowling, *European Physical Journal D* 22 (01 March 2003) 365-371.

26. "Clock Synchronization with Dispersion Cancellation," V. Giovannetti, S. Lloyd, L. Maccone, and F.N.C. Wong,*Phys. Rev. Letts.* 87, 117902 (2001)

27. "Quantum-enhanced positioning and clock synchronization," V. Giovannetti, S. Lloyd, and L. Maccone, Nature 412, 417-419 (2001).

28. "Positioning and clock synchronization through entanglement," V. Giovannetti, S. Lloyd, and L. Maccone, Phys. Rev. A, 65, 022309 (2001).

29. "Generating entangled two-photon states with coincident frequencies," V. Giovannetti, L. Maccone, J. H. Shapiro, and F. N. C. Wong, Phys. Rev. Lett. 88, 183602 (2002).

30. "A high-flux entanglement source based on a doubly-resonant optical parametric amplifier," C. E. Kuklewicz, E. Keskiner, F. N. C. Wong, and J. H. Shapiro, J. Opt. B: Quantum and Semiclass. Opt. 4, S162-S168 (2002).

31. "Efficient generation of tunable photon pairs at 0.8 and 1.6 μm," E. J. Mason, M. A. Albota, F. König, and F. N. C. Wong, Opt. Lett. 27 , 2115 (2002).

32. "Clock synchronization and dispersion", V. Giovannetti, S. Lloyd, L. Maccone, and F. N. C. Wong, J. Opt. B: Quantum Semiclass. Opt. 4, S415, (2002).

33. "Extended phase-matching conditions for improved entanglement generation", V. Giovannetti, L. Maccone, J. Shapiro, and F.N.C. Wong, Phys. Rev. A 66, 043813 (2002).

34. "Generation of ultrabright tunable polarization entanglement without spatial, spectral, or temporal constraints," M. Fiorentino, G. Messin, C.E. Kuklewicz, F.N.C. Wong, and J.H. Shapiro, Phys. Rev. A, 69, 041801(R), 2004.

35. "Efficient single-photon counting at 1.55 μm by means of frequency upconversion," M.A. Albota and F.N.C. Wong,Opt. Lett. 29, 1449-1451 (2004).

36. "Conveyor-belt clock synchronization," V. Giovannetti, S. Lloyd, L. Maccone, J.H. Shapiro, and F.N.C. Wong, Phys. Rev. A 70, 043808 (2004).

37. "Source of polarization entanglement in a single periodically poled KTiOPO4 crystal with overlapping emission cones," M. Fiorentino, C.E. Kuklewicz, and F.N.C. Wong,Opt. Express 13, 127-135 (2005).

38. "Efficient and spectrally bright source of polarization-entangled photons," F. König, E.J. Mason, F.N.C. Wong, and M.A. Albota, Phys. Rev. A 71, 033805 (2005).

6. ATTACHMENTS

The papers attached below show the details of the most important parts of the theoretical and experimental accomplishments summarized above. **These papers constitute the primary body of this report.** As mentioned above, some of the co-authors in each of these papers was supported by this project for doing the work. It should be noted that not enough care was taken in making sure that this project is explicitly acknowledged as a source of support for each of these papers.

The following papers are attached in sequence:

1. “In-Situ Detection of The Temporal and Initial Phase of The Second Harmonic of a Microwave Field via Incoherent Fluorescence,” G. Cardoso, P. Pradhan, J. Morzinski, and M.S. Shahriar, *Phys. Rev. A.* **71**, 063408 (2005).

2. “Wavelength Teleportation via Distant Quantum Entanglement Using the Bloch-Siegert Oscillation,” M.S. Shahriar, P. Pradhan, V. Gopal, J. Morzinski, G. Cardoso, and G.S. Pati, to appear in *Optics Communications*

3. "Driver Phase Correlated Fluctuations in the Rotation of a Strongly Driven Quantum Bit," M. S. Shahriar, P. Pradhan, and J. Morzinski, Phys. Rev. A **69**, 032308 (2004)

4. "Limits to clock synchronization induced by completely dephasing communication channels," V. Giovannetti, S. Lloyd, L. Maccone, and M.S. Shahriar, Phys. Rev. A 65, 062319 (2002).

5. "Super Efficient Absorption Filter for Quantum Memory using Atomic Ensembles in a Vapor," A. Heifetz, A. Agarwal, G. Cardoso, V. Gopal, P. Kumar, and M.S. Shahriar, *Opt. Commun.* 232 (2004) 289–293

6. "A Lorentz-Invariant Look at Quantum Clock Synchronization Protocols Based on Distributed Entanglement," Ulvi Yurtsever & Jonathan P. Dowling, Physical Review A 65 (01 May 2002) 052317 (1-6)

7. "Quantum Entanglement of Moving Bodies," Robert M. Gingrich and Christoph Adami, Physical Review Letters, 89, 270402 (2002)

8. Attila J. Bergou, Robert M. Gingrich, and Christoph Adami "Entangled Light in Moving Frames," Phys Rev. A. 68, 042102 (2003)

9. “Quantum-enhanced positioning and clock synchronization,” V. Giovannetti, S. Lloyd, and L. Maccone, Nature 412, 417-419 (2001).

10. “Efficient generation of tunable photon pairs at 0.8 and 1.6 μm,” E. J. Mason, M. A. Albota, F. König, and F. N. C. Wong, Opt. Lett. 27 , 2115 (2002).

11. "Generation of ultrabright tunable polarization entanglement without spatial, spectral, or temporal constraints," M. Fiorentino, G. Messin, C.E. Kuklewicz, F.N.C. Wong, and J.H. Shapiro, Phys. Rev. A, 69, 041801(R), 2004.

12. “Efficient and spectrally bright source of polarization-entangled photons,“ F. König, E.J. Mason, F.N.C. Wong, and M.A. Albota, Phys. Rev. A 71, 033805 (2005).

Appendix A:

In-Situ detection of the temporal and initial phase of the second harmonic of a microwave field via incoherent fluorescence

George C. Cardoso,[1] Prabhakar Pradhan,[1] Jacob Morzinski,[2] and M. S. Shahriar[1,2]
[1] *Department of Electrical and Computer Engineering, Northwestern University, Evanston, Illinois 60208, USA*
[2] *Research Laboratory of Electronics, Massachusetts Institute of Technology, Cambridge, Massachusetts 02139, USA*
(Received 26 October 2004; published 23 June 2005)

Measuring the amplitude and absolute (i.e., temporal and initial) phase of a monochromatic microwave field at a specific point of space and time has many potential applications, including precise qubit rotations and wavelength quantum teleportation. Here we show how such a measurement can indeed be made using resonant atomic probes via detection of incoherent fluorescence induced by a laser beam. This measurement is possible due to self-interference effects between the positive- and negative-frequency components of the field. In effect, the small cluster of atoms here act as a highly localized pickup coil, and the fluorescence channel acts as a transmission line.

DOI: 10.1103/PhysRevA.71.063408 PACS number(s): 32.80.Qk, 03.67.Hk, 03.67.Lx

Measurement of the amplitude and the absolute (i.e., temporal and initial) phase of a monochromatic wave is challenging because in the most general condition the spatial distribution of the field around a point is arbitrary. Therefore, one must know the impedance of the system between the point of interest and the detector, and ensure that there is no interference with the ambient field. It is recently shown in the literature that the absolute phase measurement can be used for accurate qubit rotations [1–3] and quantum wavelength teleportation [4–6].

Before we describe the physics behind this process, it is instructive to define precisely what we mean by the term "absolute phase." Consider, for example, a microwave field such that the magnetic field at a position $\boldsymbol{R}$ is given by $\boldsymbol{B}(t)=B_0\cos(\omega t+\phi)\hat{x}$, where ω is the frequency of the field and ϕ is determined simply by our choice of the origin of time. The absolute phase is the sum of the temporal and initial phases—i.e., $\omega t+\phi$. In order to illustrate how this phase can be observed directly, consider a situation where a cluster of noninteracting atoms is at rest at the same location. For simplicity, we assume each atom to be an ideal two-level system where a ground state $|0\rangle$ is coupled to an excited state $|1\rangle$ by this field $\mathbf{B}(t)$, with the atom initially in state $|0\rangle$. The Hamiltonian for this interaction is

$$\hat{H}=\varepsilon(\sigma_0-\sigma_z)/2+g(t)\sigma_x, \tag{1}$$

where $g(t)=-g_0\cos(\omega t+\phi)$, g_0 is the Rabi frequency, σ_i are the Pauli matrices, and the driving frequency $\omega=\varepsilon$ corresponds to resonant excitation. We consider g_0 to be of the form $g_0(t)=g_{0M}[1-\exp(-t/\tau_{sw})]$ with a switching time τ_{sw} relatively slow compared to other time scales in the system—i.e., $\tau_{sw}\gg\omega^{-1}$ and g_{0M}^{-1}.

As we have shown before [2,3], without the rotating-wave approximation (RWA) and to the lowest order in $\eta\equiv(g_0/4\omega)$, the amplitudes of $|0\rangle$ and $|1\rangle$ at any time t are as follows:

$$C_0(t)=\cos[g_0'(t)t/2]-2\eta\Sigma\sin[g_0'(t)t/2], \tag{2}$$

$$C_1(t)=ie^{-i(\omega t+\phi)}\{\sin[g_0'(t)t/2]+2\eta B\Sigma^*\cos[g_0'(t)t/2]\}, \tag{3}$$

where $\Sigma\equiv(i/2)\exp[-i(2\omega t+2\phi)]$ and $g_0'(t)\equiv(1/t)\int_0^t g_0(t')dt'=g_0\{1-(t/\tau_{sw})^{-1}[1-\exp(-t/\tau_{sw})]\}$. If we produce this excitation using a $\pi/2$ pulse [i.e., $g_0'(\tau)\tau=\pi/2$] and measure the population of state $|1\rangle$ after the excitation terminates (at $t=\tau$), we get a signal

$$|C_1(g_0'(\tau),\phi)|^2=1/2+\eta\sin[2(\omega\tau+\phi)]. \tag{4}$$

This signal contains information of both the amplitude and phase of the field $\boldsymbol{B}(t)$. The second term of Eq. (3) is related to the Bloch-Siegert shift [7,8], and we have called it the Bloch-Siegert oscillation (BSO) [2,3]. It is attributable to an interference between the so-called corotating and counterrotating parts of the oscillating field, with the atom acting as the nonlinear mixer. For $\eta=0$, we have the conventional Rabi flopping that is obtained with the RWA. For a stronger coupling field, where the RWA is not valid, the second term of Eq. (3) becomes important [2,3], and the population will depend now both on the Rabi frequency and the phase of the driving field. In recent years, this effect has also been observed indirectly using ultrashort optical pulses [9–11] under the name of carrier-wave Rabi flopping. However, to the best of our knowledge, the experiment we report here represents the first direct, real-time observation of this effect.

From the oscillation observed, one can infer the value of $2(\omega t+\phi)$, which represents the absolute phase of the second harmonic. This is equivalent to determine the absolute phase of the fundamental field, $(\omega t+\phi)$, modulo π. In principle, a simple modification of the experiment can be used to eliminate the modulus π uncertainty. Specifically, if one applies a dc magnetic field parallel to the rf field, it leads to a new oscillation (in the population of either level) at the fundamental frequency, with exactly the same phase as that of the driving field. In the experiment described here, we have restricted ourselves to the case of determining the absolute phase of the second harmonic only.

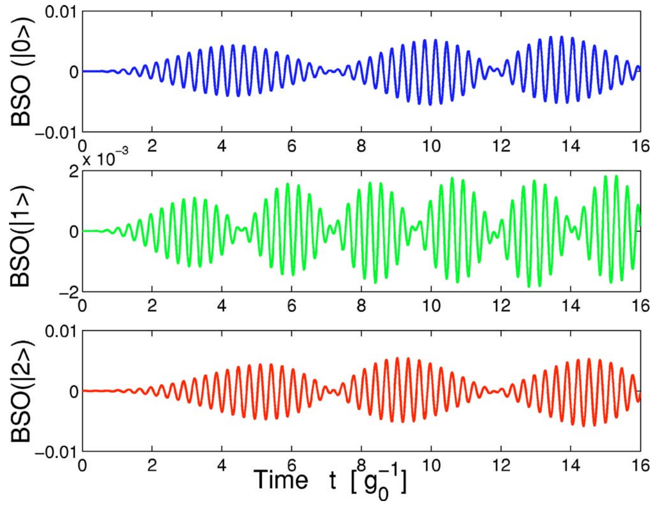

FIG. 1. BSO amplitude versus time t (in units of g_0^{-1}) plots for all the levels of a three-level system. The initial densities of the levels are $\rho_{00}(t=0)=0.5$, $\rho_{11}(t=0)=0.3$, and $\rho_{22}(t=0)=0.2$, the Rabi frequency $g_0=1$, and the resonant frequencies $\omega_{02}=\omega_{21}=10$.

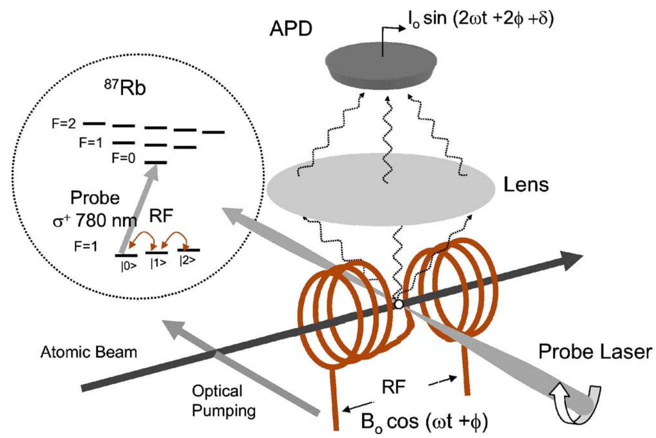

FIG. 2. Experimental setup. The 1-mm cross section rubidium atomic beam passes through the symmetry axis of the rf coil whose magnetic field is along the beam. The rf field of frequency ω is fed by a power amplifier connected to the resonant coil. A circularly polarized probe laser beam is focused down to 30 μm in diameter through a gap in the middle of the rf coil and perpendicularly to the atomic beam. The atomic fluorescence is collected by the lens and detected by an avalanche photodiode (APD). The phase signature appears in the fluorescence signal encoded in an oscillation at a frequency 2ω due to the Bloch-Siegert oscillations. In the picture, δ is an additional phase delay due to the APD circuits and cabling. Inset: Diagram of the relevant sublevels of the D_2 line of ^{87}Rb. The numbers on the left represent the total angular momentum of the respective levels. The strong driving rf field couples to the ground-state Zeeman sublevels. The probe beam must be resonant with an appropriate optical transition for the observation of the phase-locked signal, as discussed in the main text.

While the above analytical model presented here is based on a two level system, practical examples of which are presented in Ref. [2], the effect is more generic, and is present even in three-level or multilevel systems. In particular, we employed a three-level system to observe this effect, due primarily to practical considerations. The specific system used consists of three equally spaced Zeeman sublevels of ^{87}Rb ($5\,^2S_{1/2}$: $F=1$: $m_F=-1$, 0, and 1, denoted as states $|0\rangle$, $|1\rangle$, and $|2\rangle$, respectively), where the degeneracy can be lifted by applying an external bias field. We have performed numerical simulations to confirm the presence of the BSO signature in the population dynamics of such a system as described below.

Consider an equally spaced, ladder-type three-level system ($|0\rangle$, $|1\rangle$, and $|2\rangle$). The transition frequencies for $|0\rangle$-$|1\rangle$ and $|1\rangle$-$|2\rangle$ are of the same magnitude ε. We also consider that a direct transition between $|0\rangle$ and $|2\rangle$ is not allowed. Now, let the system be pumped by the same field at a frequency ω. Consider also that the Rabi frequency for the $|0\rangle$-$|1\rangle$ transition is g_0 and that for $|1\rangle$-$|2\rangle$ is also g_0. Then, the Hamiltonian of the three-level system in a rotating frame can be written as

$$\hat{\tilde{H}}' = - g_0[1 + \exp(- i2\omega t - i2\phi)](|0\rangle\langle 1| + |1\rangle\langle 2|) + \text{c.c.}, \tag{5}$$

where $\omega=\varepsilon$. The amplitudes of the three levels are calculated numerically by solving the Schrödinger equation for the above Hamiltonian. The BSO amplitudes are then calculated by subtracting the population amplitude of each level *with* the RWA from the population amplitude *without* the RWA. The BSO oscillations for all the levels of such a system are shown in Fig. 1.

The experimental configuration, illustrated schematically in Fig. 2, uses a thermal, effusive atomic beam. The rf field is applied to the atoms by a coil, and the interaction time τ is set by the time of flight of the individual atoms in the rf field before they are probed by a strongly focused and circularly polarized laser beam. The rf field couples the sublevels with $|\Delta m|=1$, as detailed in the inset of Fig. 2. Optical pumping is employed to reduce the populations of states $|1\rangle$ and $|2\rangle$ compared to that of state $|0\rangle$ prior to the interaction with the microwave field.

A given atom interacts with the rf field for a duration τ prior to excitation by the probe beam that couples state $|0\rangle$ to an excited sublevel in $5\,^2P_{3/2}$. The rf field was tuned to 0.5 MHz, with a power of about 10 W, corresponding to a Rabi frequency of about 4 MHz for the $|0\rangle \rightarrow |1\rangle$ as well as the $|1\rangle \rightarrow |2\rangle$ transition. The probe power was 0.5 mW focused to a spot of about 30 μm diameter, giving a Rabi frequency of about 60 Γ, where Γ(6.06 MHz) is the lifetime of the optical transition. The average atomic speed is 500 m/s, so that the effective pulse width of the probe, τ_{LP}, is about 60 ns, which satisfies the constraint that $\tau_{LP} \leqslant 1/\omega$. Note that the resolution of the phase measurement is essentially given by the ratio of $\min[\tau_{LP}, \Gamma^{-1}]$ and $1/\omega$, and can be increased further by making the probe zone shorter. The fluorescence observed under this condition is essentially proportional to the population of level $|0\rangle$, integrated over a duration of τ_{LP}, which corresponds to less than 0.3 Rabi period of the rf driving field [for $g_{0M}/(2\pi)=4$ MHz]. Within a Rabi oscillation cycle, the BSO signal is maximum for $g_0(\tau)\tau/2 =(2n+1)\pi/2$, where $n=0,1,2,\ldots$, so that there is at least one maximum of the BSO signal within the region of the probe.

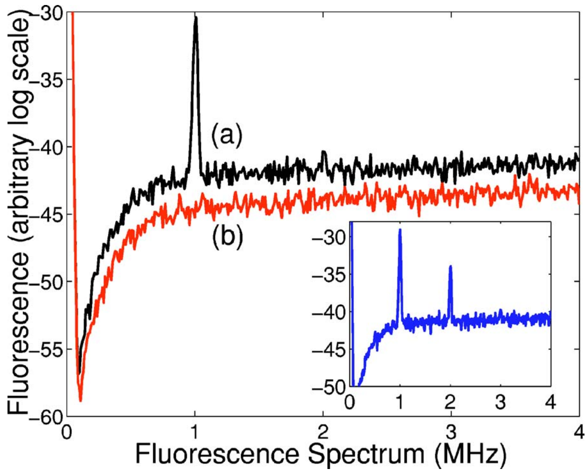

FIG. 3. Bloch-Siegert oscillation spectra. rf at 0.5 MHz and Rabi frequency around 4 MHz. (a) Probe beam resonant with the $5S_{1/2}$, $F=1 \leftrightarrow 5S_{3/2}$, $F'=0$ transition. The signal appears at 1 MHz with a linewidth less than 1 kHz (resolution limited by the spectrum analyzer). (b) Probe beam blocked. The dip structure around 100 kHz is an artifact due to the amplifier gain curve. Inset: Spectrum for same configuration and rf Rabi frequency around 10 MHz. Notice the 2-MHz harmonic which corresponds to the higher-order BSO at 4ω.

Note that atoms with different velocities have different interaction times with the rf field and produce a spread in the BSO signal amplitude within the probe region. However, *the phase of the BSO signal is the same for all the atoms*, since it corresponds to the value of $(\omega\tau+\phi)$ at the time and location of interaction. Thus, there is no washout of the BSO signal due to the velocity distribution in the atomic beam.

Figure 3 shows the spectrum of the observed BSO signal. In Fig. 3(a), we show that the BSO stays mainly at 2ω. When the probe beam is blocked, there is no signal [Fig. 3(b)]. When the rf intensity is increased a component of the BSO at 4ω begins to develop, as predicted. For the data in Fig. 4, the second harmonic of the driving field is used to trigger a 100-MHz digital oscilloscope and the fluorescence signal is averaged 256 times. When the probe beam is tuned to the $F=1 \leftrightarrow F'=0$ transition, the population at $m=-1$ state is probed. When the probe is tuned to $F=1 \leftrightarrow F'=1$, the combined populations of $m=-1$ and $m=0$ states are probed. That results in an effective detection of the complement of the population of $m=1$. On the other hand, when the probe beam is locked to the $F=1 \leftrightarrow F'=2$ transition, all three Zeeman sublevels of $F=1$ are simultaneously probed and the phase information is not clearly present, since the total population of level $F=1$ is a constant. The observed residual phase information is a result of different coupling efficiencies for each of the three ground Zeeman sublevels. We observed that the BSO signal amplitude varies as a function of an external magnetic field applied in the $\hat{z}$ direction, with a peak corresponding to a Zeeman splitting matching the applied frequency of 0.5 MHz.

In Fig. 5, we show that the fluorescence signal is phase locked to the second harmonic of the driving field. First, we placed a delay line of 0.4 μs on the cable of the reference field used to trigger the oscilloscope and recorded the fluorescence [Fig. 5(a)]. Then, we put the 0.4-μs delay line on the BSO signal cable and recorded the fluorescence [Fig. 5(b)]. The phase difference between the signals recorded in Figs. 5(a) and 5(b) is approximately 0.8 μs, as expected for a phase locked fluorescence signal. The data presented were for the probe resonant with the transition $F=1 \leftrightarrow F'=1$, but the same results were observed for $F=1 \leftrightarrow F'=0$.

To summarize, we report the first direct observation of the absolute phase of the second harmonic of an oscillating elec-

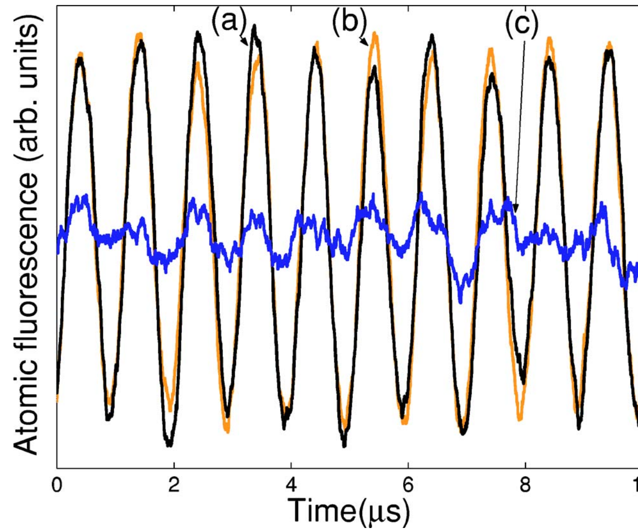

FIG. 4. Time dependence of the fluorescence signal at 2ω when the probe beam is resonant to different excited states. The lines (a), (b), and the noisy line (c) correspond to the probe locked to the transitions $F=1 \rightarrow F'=0$, $F=1 \rightarrow F'=1$, and $F=1 \rightarrow F'=2$, respectively, of the $5S_{1/2} \rightarrow 5P_{3/2}$ transition in ^{87}Rb.

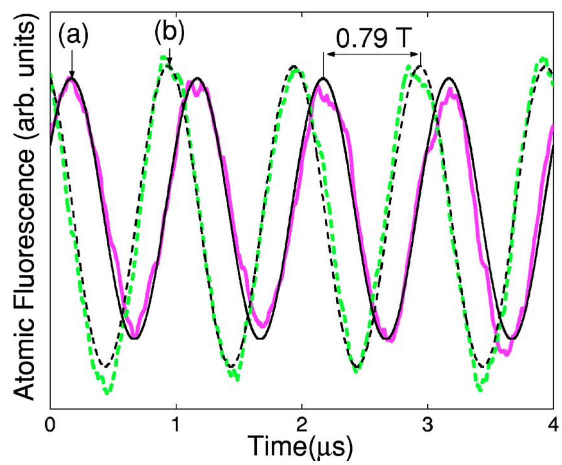

FIG. 5. Demonstration of phase-locked fluorescence. T is the period of the Bloch-Siegert oscillation. (a) Population vs time when a $0.4T$ delay line was inserted in the reference field cable. (b) Population vs time when the same $0.4T$ delay line was placed in the fluorescence signal cable. The figure shows that signal (b) is about $0.8T$ ahead of signal (a), confirming that the atomic fluorescence carries phase information which is locked to the absolute rf field phase. The solid and dashed sinusoidal smooth curves are fittings to the experimental data and were used for period and delay determination.

tromagnetic field using self-interference in an atomic resonance. This process is important in the precision of quantum bit rotations at a high speed. The knowledge of the absolute phase of a rf field at a particular point of space may also be useful for single-atom quantum optics experiments. For example, an extension of this concept may possibly be used to teleport the wavelength of an oscillator, given the presence of degenerate distant entanglement, even in the presence of unknown fluctuations in the intervening medium [4–6,12]. Finally, this localized absolute phase detector may prove useful in mapping of radio-frequency fields in microcircuits. Although a particular alkali-metal atom was used in the present experiment, the mechanism is robust and could be observed in virtually any atomic or molecular species.

This work was supported by DARPA Grant No. F30602–01–2–0546 under the QUIST program, ARO Grant No. DAAD19–001–0177 under the MURI program, NRO Grant No. NRO-000–00–C-0158, and AFOSR Grants: No. F49620–02–1-0400 and No. FA9550–04–1–0189.

[1] D. Jonathan, M. B. Plenio, and P. L. Knight, Phys. Rev. A **62**, 042307 (2000).
[2] M. S. Shahriar, P. Pradhan, and J. Morzinski, Phys. Rev. A **69**, 032308 (2004).
[3] P. Pradhan, G. C. Cardoso, and M. S. Shahriar, e-print quant-ph/0402112.
[4] R. Jozsa, D. S. Abrams, J. P. Dowling, and C. P. Williams, Phys. Rev. Lett. **85**, 2010 (2000).
[5] M. S. Shahriar, P. Pradhan, G. C. Cardoso, V. Gopal, and G. Pati, e-print quant-ph/0309085.
[6] E. Burt, C. Ekstrom, and T. Swanson, e-print quant-ph/0007030.
[7] L. Allen and J. Eberly, *Optical Resonance and Two-Level Atoms* (Wiley, New York, 1975).
[8] F. Bloch and A. J. F. Siegert, Phys. Rev. **57**, 522 (1940).
[9] G. G. Paulus *et al.*, Nature (London) **414**, 182 (2001).
[10] O. D. Mücke, T. Tritschler, M. Wegener, U. Morgner, and F. X. Kärtner, Phys. Rev. Lett. **87**, 057401 (2001).
[11] O. D. Mücke, T. Tritschler, M. Wegener, U. Morgner, and F. X. Kärtner, Phys. Rev. Lett. **89**, 127401 (2002).
[12] S. Lloyd, M. S. Shahriar, J. H. Shapiro, and P. R. Hemmer, Phys. Rev. Lett. **87**, 167903 (2001).

Appendix B:

Wavelength Teleportation via Distant Quantum Entanglement Using the Bloch-Siegert Oscillation

M.S. Shahriar[1,2], P. Pradhan[1], V. Gopal[1], J. Morzinski[2], G. Cardoso[1], and G.S. Pati[1]

[1]*Dept. of Electrical and Computer Engineering, Northwestern University*
Evanston, IL 60208
[2]*Research Laboratory of Electronics, Massachusetts Institute of Technology*
Cambridge, MA 02139

Abstract

Recently, we have shown theoretically [1] as well as experimentally [2] how the phase of an electromagnetic field can be determined by measuring the population of either of the two states of a two-level atomic system excited by this field, via the so-called Bloch-Siegert oscillation resulting from the interference between the co- and counter-rotating excitations. Here, we show how a degenerate entanglement, created without transmitting any timing signal, can be used to teleport this phase information. This phase-teleportation process may be applied to achieve wavelength teleportation, which in turn may be used for frequency-locking of remote oscillators.

PACS Number(s): 03.67.-a, 03.67.Hk, 03.67.Lx, 32.80.Qk

The task of synchronizing a pair of oscillators that are separated in space is important for many practical applications, such as the global positioning system (GPS) [3] and the very large base interferometry (VLBI) [4]. Conventionally, this is performed by transmitting timing signals between the oscillators. Consider first the *ideal* situation where the intervening medium is stable and fully characterized. The accuracy of the synchronization process is then limited by the uncertainty in the timing signal. The best result achievable is limited by the signal to noise ratio (SNR). It is generally possible in most cases to eliminate sources of systematic noises, so that the fundamental constraint is the shot noise limit (SNL). In principle, specially prepared quantum states can reduce the effective noise below the SNL. However, since the level of signal in this case is typically much weaker, the actual SNR achievable this way is far below what can be achieved using classical states. Most of the recent proposals [5-9] for achieving improved oscillator synchronization (OS) using quantum processes suffer from the same constraint, so that in practice they are inferior to classical approaches. Thus, given the current state of technology, quantum mechanical effects is not likely to help in the process of OS under the *ideal* situation.

In a real-life application such as in the field of GPS, the density of the intervening medium fluctuates randomly, leading to a corresponding fluctuation in the time needed for a signal to travel between the oscillators. Under this condition, it is *fundamentally* impossible to synchronize the oscillators to an accuracy higher than the corresponding fluctuation in the travel time . This follows from the principle of special relativity, which is built on the axiom that there exists a maximum speed --- namely, the speed of light in vacuum --- at which information can propagate. As such, the notion of oscillator synchrony is *defined* with respect to the time it takes for light to traverse the distance between the oscillators. It then follows that if this travel time itself is fluctuating, then the oscillator synchrony is undefined, and cannot be achieved on the timescale of the fluctuation. One can define and establish only an *average* synchrony, valid only for timescales longer than that of the fluctuation. In all situations of practical interest, OS always implies the achievement of this *average synchrony*. This conclusion also holds for the clever technique demonstrated by Ma *et al.* [10].

An alternative way to improve the average synchrony is through frequency locking. Specifically, consider a typical application where each oscillator is locked to a metastable atomic transition. Most of the recent proposals about oscillator synchronization, including the Jozsa protocol [9], make the assumption that each oscillator continues to operate at some ideal transition frequency. In practice, however, this is not the case. The frequency of each oscillator undergoes shifts and drifts due to a host of reasons. These fluctuations lie at the heart of oscillator asynchrony. As such, minimizing the relative drifts in the frequencies is perhaps the most effective way to minimize the error in OS. This approach opens up new possibilities for exploring whether quantum mechanical effects may outperform classical approaches. In this paper, we propose a new technique for locking the frequencies of two distant oscillators, via the process of *wavelength teleportation*.

The process underlying this technique is the so-called Bloch-Siegert Oscillation (BSO), which results from an interference between the co- and counter-rotating parts of a two-level excitation. Recently, we have analyzed the basic features of the BSO theoretically [1], in the context of how it may affect the accuracy of the rotation of a quantum bit. We have also observed the key feature of the BSO using an atomic beam [2], showing specifically that the excited state population of a two-level system driven by a strong microwave field reveals an oscillation that is in phase with the second harmonic of the driving field. In applying the BSO to the task of frequency locking, the phase variation of an oscillator is first mapped by Alice (keeper of the first oscillator) to the wave-functions of an array of atoms, by making use of the fact that the amplitude of the excited state (as well as that of the ground state) depends explicitly on the phase of the driving field. The maximum number of atoms needed to encode the phase variation can be very small, and is given by the Nyquist sampling criterion. Distant entanglement, produced using an asynchronous technique [11], is used to teleport the quantum state of each of these atoms to a matching atom with Bob (keeper of the second oscillator). Bob can thus recreate the exact phase variation of Alice's oscillator locally, and compare with the same for his oscillator. We discuss the potential constraints and advantages of this approach after presenting the scheme in detail.

Consider first a situation where Alice and Bob each has an atom that has two degenerate ground states (|1> and |2>), each of which is coupled to a higher energy state (|3>), as shown in Fig. 1. We assume the 1-3 and 2-3 transitions are magnetic dipolar, and orthogonal to each other, with a transition frequency ω. For example, in the case of ^{87}Rb, |1> and |2> correspond to $5^2P_{1/2}$:|F=1,m_F=-1> and $5^2P_{1/2}$:|F=1,m_F=1> magnetic sublevels, respectively, and |3> corresponds to $5^2P_{1/2}$:|F=2,m_F=0> magnetic sublevel [2]. Left and right circularly polarized magnetic fields, perpendicular to the quantization axis, are used to excite the 1-3 and 2-3 transitions, respectively. We take ω to be the same as the oscillator frequency ω_c.

We assume that Alice and Bob's fields at ω have the form $B_A=B_{A0}Cos(\omega t+\phi)$ and $B_B=B_{B0}Cos(\omega t+\chi)$, respectively. The origin of the time variable, t, is therefore arbitrary, and does not affect the phase difference, $\Omega\equiv(\phi-\chi)$. The oscillators are assumed to be in phase if $\Omega=0$, so that if Bob determines that at some instant his magnetic field is maximum and positive in some direction $\boldsymbol{r}_B$, then Alice will also find her magnetic field to be maximum and positive in some direction $\boldsymbol{r}_A$ at the same instant. As long as Alice and Bob agree on this definition of phase-locking, and use the same definitions all the time, then $\boldsymbol{r}_B$ and $\boldsymbol{r}_A$ do not have to be the same. During the magnetic resonance excitations, the value of any dc magnetic field will be assumed to be vanishing. Symmetry then dictates that any physical observable will be independent of the choice of the quantization axis, as long as it is perpendicular to $\boldsymbol{r}_A$ for Alice, and perpendicular to $\boldsymbol{r}_B$ for Bob. In order to describe our protocol, we now summarize briefly the theory behind the Bloch-Siegert oscillation that occurs when a two-level interaction is considered without the rotating wave approximation (RWA) [12-16], and is presented in greater detail in ref. [1]. We also describe the condition for the time reversal of an arbitrary evolution under this condition, another necessary element of our protocol.

We consider an ideal two-level system where a ground state |1> is coupled to a higher energy state |3>. We assume that the 1-3 transition is magnetic dipolar, with a transition frequency ω, and the magnetic field is of the form $B=B_0 Cos(\omega t+\phi)$. In the dipole approximation, the Hamiltonian can be written as:

$$\hat{H} = \varepsilon(\sigma_0 - \sigma_z)/2 + g(t)\sigma_x \tag{1}$$

where $g(t) = -g_o\,[\exp(i\omega t+i\phi) + c.c.]/2$, σ_i are the Pauli matrices, and $\varepsilon=\omega$ corresponding to resonant excitation. The state vector is written as:

$$\left|\xi(t)\right\rangle = \begin{bmatrix} C_1(t) \\ C_3(t) \end{bmatrix}. \tag{2}$$

We perform a rotating wave transformation by operating on $|\xi(t)>$ with the unitary operator $\hat{Q} = (\sigma_0 + \sigma_z)/2 + \exp(+i\omega t + i\phi)(\sigma_0 - \sigma_z)/2$. The Schroedinger equation then takes the form (setting $\hbar$=1): $\dfrac{\partial\,|\,\tilde{\xi}(t)>}{\partial t} = -i\tilde{H}(t)\,|\,\tilde{\xi}(t)>$, where the effective Hamiltonian is given by:

$$\tilde{H} = \alpha(t)\sigma_+ + \alpha^*(t)\sigma_-, \tag{3}$$

with $\alpha(t) = -g_0[\exp(-i2\omega t-i2\phi)+1]/2$, and the rotating frame state vector is:

$$|\,\tilde{\xi}(t)> \equiv \hat{Q}\,|\,\xi(t)> = \begin{bmatrix} \tilde{C}_1(t) \\ \tilde{C}_3(t) \end{bmatrix}. \tag{4}$$

The general solution, without RWA, to Eq.4 can be written in the form:

$$|\,\tilde{\xi}(t)> = \sum_{n=-\infty}^{\infty} \begin{pmatrix} a_n \\ b_n \end{pmatrix} \exp(n(-i2\omega t - i2\phi)), \tag{5}$$

with the couplings described by

$$\dot{a}_n = i2n\omega a_n + ig_o(b_n + b_{n-1})/2\,, \tag{6a}$$

$$\dot{b}_n = i2n\omega b_n + ig_o(a_n + a_{n+1})/2\,. \tag{6b}$$

We consider $g_0 \equiv g_0(t) = g_{0M}(1-e^{-t/\tau_{sw}})$ to have a slower time-dependence compared to other characteristic timescales such as 1/ω and 1/g_{0M}, where g_{0M} is the peak value of g_0 and τ_{sw} is the switching time. Under this condition, one can solve these equations by employing the method of adiabatic elimination, which is valid to first order in $\eta \equiv (g_0/4\omega)$. As derived in refs. [1] and [2], the solutions are:

$$C_1(t) = Cos(g_0^{'}(t)t/2) - 2\eta\Sigma \cdot Sin(g_0^{'}(t)t/2)\ , \tag{7a}$$

$$C_3(t) = ie^{-i(\omega t+\phi)}[Sin(g_0^{'}(t)t/2) + 2\eta\Sigma^* \cdot Cos(g_0^{'}(t)t/2)]\ , \tag{7b}$$

where $\Sigma \equiv (i/2)\exp[-i(2\omega t + 2\phi)]$ and $g_0^{'}(t) = 1/t\int_0^t g_0(t^{'})dt^{'} = g_0[1-(t/\tau_{sw})^{-1}\exp(-t/\tau_{sw})]$.

To lowest order in η this solution is normalized at all times. Note that if Alice were to carry this excitation on an ensemble of atoms through for a π/2 pulse, and measure the population of the state $|3>_A$ immediately (at t=τ, the moment when the π/2 excitation ends), the result would be a signal given by [1+2ηSin(2ωτ+2ϕ)]/2, which contains information related to the amplitude and phase of her field.

Next, we consider the issue of exact time reversal of such an excitation. The Schroedinger eqn. (4) has the formal solution:

$$|\tilde{\xi}(t_2)> = \exp[-i\int_{t_1}^{t_2}\tilde{H}(t')dt']\,|\tilde{\xi}(t_1)>\ . \tag{8}$$

If the RWA is made, then $\tilde{H}$ is time independent. In that case, if one starts an evolution at t_1, proceed for *any* duration T, then reverses the sign of $\tilde{H}$ by shifting the phase of the magnetic field by π, and continues with the evolution for another duration T, then the system returns back to the starting state. Here, however, RWA is not made, so that $\tilde{H}$ depends on time. Therefore, the exact reversal can be achieved in this manner only if T=mπ/ω for any integer value of m. [9,1,2]

Returning to the task at hand, our protocol starts by using a scheme, developed earlier by us [11] to produce a degenerate entanglement of the form $|\psi>=(|1>_A|2>_B - |2>_A|1>_B)/\sqrt{2}$. Recalling briefly, in this technique, a pair of entangled photons, produced by a parametric down converter, for example, are transmitted to Alice and Bob, each receiving one of the photons. The capturing process is checked indirectly, using a quantum non-demolition measurement. If the verification process confirms the capture of the photons, then the quantum states of the atoms remain undisturbed. Otherwise, the process is re-initialized (placing each atm in state |1>) and repeated until it succeeds. An optically off-resonant Raman transition (with one leg corresponding to a pump frequency, and the other corresponding to one of the entangled photons) coupling |1> to |2> is used by Alice as well as Bob to capture the photons, resulting in the entangled state shown above. Next, Alice attenuates her field so that the counter-rotating term in the Hamiltonian can be ignored (this assumption is not essential for our conclusion, but merely simplifies the algebra somewhat), and excites a π-pulse coupling $|2\rangle_A$ to $|3\rangle_A$, and then stops the excitation. The degree of attenuation is such that the Rabi frequency is much less than the transition freuency, so that the RWA is valid. Similarly, Bob uses a field, attenuated as above, to excite a π-pulse coupling $|2\rangle_B$ to $|3\rangle_B$, and then stops the excitation. Using digital communications over a classical channel, Alice and Bob wait until they both know that these excitations have been completed. The resulting state is then given by :

$$|\psi(t)\rangle=[|1\rangle_A|3\rangle_B\exp(-i\omega t-i\chi) - |3\rangle_A|1\rangle_B\exp(-i\omega t-i\phi)]/\sqrt{2}. \tag{9}$$

The next step is for Alice to make a measurement along the $|1\rangle_A\leftrightarrow|3\rangle_A$ transition. For this process, she chooses a much larger value of g_o, so that the RWA can not be made. The state she wants to measure is the one that would result if one were to start from state $|1\rangle_A$, and evolve the system for a $\pi/2$ pulse using this stronger g_{oM}:

$$|+\rangle_A \equiv \frac{1}{\sqrt{2}}\left[\{1-2\eta\Sigma\}|1\rangle_A + ie^{-i(\omega t+\phi)}\{1+2\eta\Sigma^*\}|3\rangle_A\right] \tag{10}$$

where we have made use of Eq. (9). The state orthogonal to $|+\rangle_A$ results from a $3\pi/2$ pulse:

$$|-\rangle_A \equiv \frac{1}{\sqrt{2}}\left[\{1+2\eta\Sigma\}|1\rangle_A - ie^{-i(\omega t+\phi)}\{1-2\eta\Sigma^*\}|3\rangle_A\right] \tag{11}$$

To first order in η, these two states are each normalized, and orthogonal to each other. As such, one can re-express the state of the two atoms in Eq. (9) as:

$$|\psi(t)\rangle = \frac{1}{\sqrt{2}}\left[|+\rangle_A|-\rangle_B - |-\rangle_A|+\rangle_B\right] \tag{12}$$

here we have defined:

$$|+\rangle_B \equiv \frac{1}{\sqrt{2}}\left[\{1-2\eta\Sigma\}|1\rangle_B + ie^{-i(\omega t+\chi)}\{1+2\eta\Sigma^*\}|3\rangle_B\right], \tag{13a}$$

$$|-\rangle_B \equiv \frac{1}{\sqrt{2}}\left[\{1+2\eta\Sigma\}|1\rangle_B - ie^{-i(\omega t+\chi)}\{1-2\eta\Sigma^*\}|3\rangle_B\right]. \tag{13b}$$

She can measure the state $|+\rangle_A$ by taking the following steps: (i) Shift the phase of the B-field by π, (ii) Fine tune the value of g_o so that $g_0'(t)=\omega/2m$, for an integer value of m, (iii) apply the field for a duration of $T=\pi/2\,g_0'(T)$, and (iv) detect state $|1\rangle_A$. Note that the constraint on g_o ensures that $T=m\pi/\omega$, which is necessary for time reversal to work in the absence of the RWA. Once Alice performs this measurement, the state for Bob collapses to $|-\rangle_B$, given in eqn. (14). Note that if η is neglected, then the measurement produces a $|-\rangle_B$ that contains no information about the phase of Alice's oscillator, which is analogous to the Jozsa protocol [9].

In the present case, $|-\rangle_B$ does contain information about the amplitude and the phase of Alice's oscillator signal. In order to decipher this, Bob measures his state $|1\rangle_B$. The probability of success is:

$$p_\phi \equiv \left|{}_B\langle 1|-\rangle_B\right|^2 = \frac{1}{2}\left[1+2\eta\sin(2\phi)\right]. \tag{14}$$

where we have kept terms only to the lowest order in η. Of course, the value of ϕ (mod 2π), the phase difference, can not be determined from knowing *Sin*(2ϕ) alone. However, this whole process can be repeated after, for example, Alice shifts the phase of her B-field by π/2, so that Bob can determine the value of Cos(2ϕ). It is then possible to determine the value of ϕ (mod 2π) unambiguously.

The overall process can be carried out in one of two ways. First, consider the situation where Alice and Bob starts with X pairs of atoms, and entangle each pair in the form of equation (13). Then, over a digital communication channel, Alice sends Bob a list of the M atoms she found in state $|1\rangle_A$ after performing her measurement process described above. Bob performs his measurement only on this subset of atoms. Suppose he finds L number of atoms in state $|1\rangle_B$. Then:

$$\zeta \equiv \left(\frac{L}{M}-\frac{1}{2}\right) \rightarrow \eta Sin(2\phi) \qquad , \qquad \textit{for large M} \tag{15}$$

Thus, the value of η determined asymptotically for a large number of entangled pairs will reveal the value of Sin(2ϕ). Alternatively, if only a single pair of atoms is available, then the same result can be obtained by repeating the whole process X times, assuming that ϕ remains unchanged during the time needed for the process.

Note that what is determined by Bob is ϕ, not Ω. Thus, it is not possible to measure the absolute phase difference in this manner. However, one could use this approach of phase teleportation in order to achieve frequency locking of two remote oscillators. This is illustrated in figure 2. Briefly, assume that Bob has an array of N atoms. Assume further that Alice also has an identical array of atoms. For our protocol, the physical separations between the neighboring atoms do not have to match. In principle, one can create such an identical pair of arrays by embedding N rows of atoms (or quantum dots) in a substrate patterned lithographically, with two atoms in each row, and then splitting it in two halves. To start with, the corresponding atoms in each array are entangled with each other using the asynchronous approach of Ref. 11. Here, we assume that the two oscillators may differ in frequency. The frequency-locking algorithm then proceeds as follows. Alice and Bob both apply their fields parallel to their arrays of atoms, so that the phase variation is 2π over their respective wavelengths. After Alice makes her measurements of the state $|+\rangle_A$, using the same set of steps as described above, she informs Bob, over a classical communication channel, the indices of her atoms that were found in this state. Bob now measures the state $|-\rangle_B$ for this subgroup of atoms only, using an analogous set of time-reversed excitation steps which ends in observing his atom in state $|3\rangle_B$. For a given atom in this subgroup, the phase of his field at that location at the time Bob starts the measurement affects the probability of success in finding the atom in state $|3\rangle_B$ at the end of the measurement process. This phase is varied as Bob repeats the measurement for different measurement-starting-times (modulo $2\pi/\omega_B$, where ω_B is the frequency of Bob's oscillator). It is easy to show that there exists a choice of this phase for which the probability of success is 100%. However, the success probability for atoms (in the post-selection subgroup) would vary with location if the frequencies of Bob's and Alice's oscillators are not the same. This effect can be used by Bob to adjust his oscillator frequency, thereby achieving frequency locking. The Nyquist sampling criterion dictates that the number of atoms in this subgroup can be as low as only two, so that N can be quite small, thus making this protocol potentially practicable.

The optimal SNR that may be achievable in the protocol outlined here will be determined fundamentally by the SNL. For a measurement interval of τ, the SNR in this case would be $\eta\sqrt{(M\tau/\tau_o)}$, where τ_o ($<<\tau$) is the time needed to carry out a single sequence in the protocol. The values of all these parameters (η, M and τ_o) would depend on the actual technology to be employed in realizing the protocol. As a concrete example, let us assume a value of η to be 0.025, corresponding to a case where $(g_0/\omega)=0.1$. The values of M and τ_o are not independent of each other; the bigger the M, the bigger the amount of time that would be necessary to carry out a single sequence of the protocol. Note that τ_o determines the speed with which one wants to update the frequencies of the oscillator (i.e., the inverse of the bandwidth of the frequency locking servo). Let us assume a servo bandwidth of 1 kHz, corresponding to a value of τ_o=(1 msec/2π). For a lithographically patterned substrate, it is easy to envision a value of M as large as 10^4. For an averaging time of 1 second, the SNR is then close to 200. Given that, to the best of our knowledge, this is the only technique for performing frequency locking in a manner that is independent of the fluctuations in the intervening optical path length, it is not possible to compare this value to any other technique directly.

To summarize, previously we have shown how the phase of an electromagnetic field can be determined by measuring the population of either of the two states of a two-level atomic system excited by this field, via the so-called Bloch-Siegert oscillation. Here, we show how a degenerate entanglement, created without transmitting any timing signal, can be used to teleport this phase information. This in turn makes it possible to achieve wavelength teleportation, one possible application of which is frequency-locking of remote oscillators.

This work was supported by DARPA grant No. F30602-01-2-0546 under the QUIST program, ARO grant No. DAAD19-001-0177 under the MURI program, and NRO grant No. NRO-000-00-C-0158.

References:

[1] M. S. Shahriar, P. Pradhan, and J. Morzinski, Phys. Rev. A **69**, 032308 (2004).

[2] G. Cardoso, P. Pradhan, J. Morzinski, and M.S. Shahriar, "In-Situ Absolute Phase Detection of a Microwave Field via Incoherent Fluorescence," to appear in *Phys. Rev. A*.

[3] P. Misra and P. Enge, *Global Positioning System: Signals, Measurements, and Performance* (Ganga-Jamuna Press, 2001); National Research Council Staff, *The Global Positioning System: A Shared National Asset* (National Academy Press, Washington, D.C., 1995).
[4] G. S. Levy *et al.*, Acta Astonaut. **15**, 481 (1987).
[5] I. L. Chuang, Phys. Rev. Lett. **85**, 2006 (2000).
[6] V. Giovannetti, S. Lloyd, L. Maccone, Nature **412**, 2001.
[7] V. Giovannetti, S. Lloyd, L. Maccone, and F.N.C. Wong, Phys. Rev. Lett. **87**, 117902 (2001).
[8] V. Giovannetti, S. Lloyd, L. Maccone, and M. S. Shahriar, Phys. Rev. A **65**, 062319 (2002).
[9] R. Jozsa, D.S. Abrams, J.P. Dowling, and C.P. Williams, Phys. Rev. Lett. **85**, 2010 (2000).
[10] L-S. Ma, P. Jungner, J. Ye, and J. L. Hall, Optics. Lett. **19**, 1777 (1994).
[11] S.Lloyd, M.S. Shahriar, J.H. Shapiro, and P.R. Hemmer, Phys. Rev. Lett. **87**, 167903 (2001).
[12] A. Corney, *Atomic and Laser Spectroscopy* (Oxford University Press, 1977).
[13] L. Allen and J. Eberly, *Optical Resonance and Two Level Atoms* (Wiley, 1975).
[14] F. Bloch and A.J.F. Siegert, Phys. Rev. **57**, 522 (1940) .
[15] J. H. Shirley, Phys. Rev. **138**, 8979 (1965).
[16] S. Stenholm, J. Phys. B **6**, 1650 (1973).

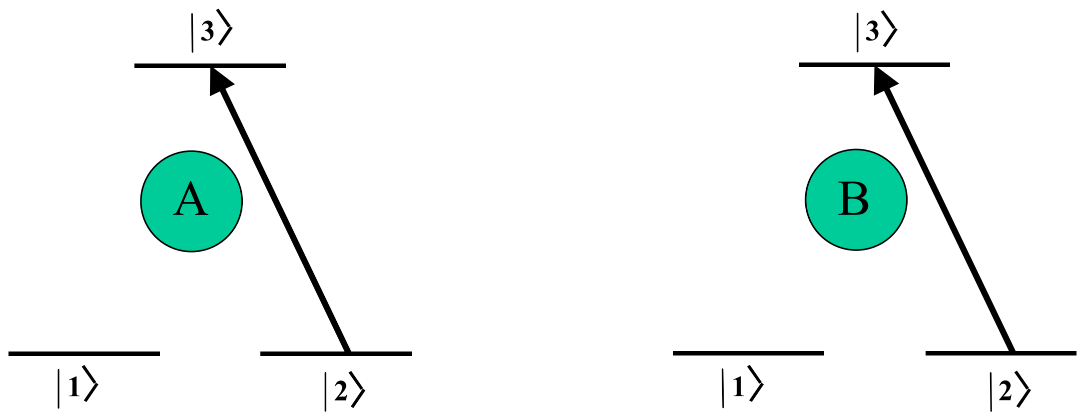

Fig. 1. Schematic illustration of the basic protocol for phase locking two remote oscillators, one with Alice (A), and the other with Bob (B), without transmitting a oscillator signal directly. The model energy levels can be realized, for example, using the metastable hyperfine Zeeman sublevels of ^{87}Rb atoms, as detailed in the text.

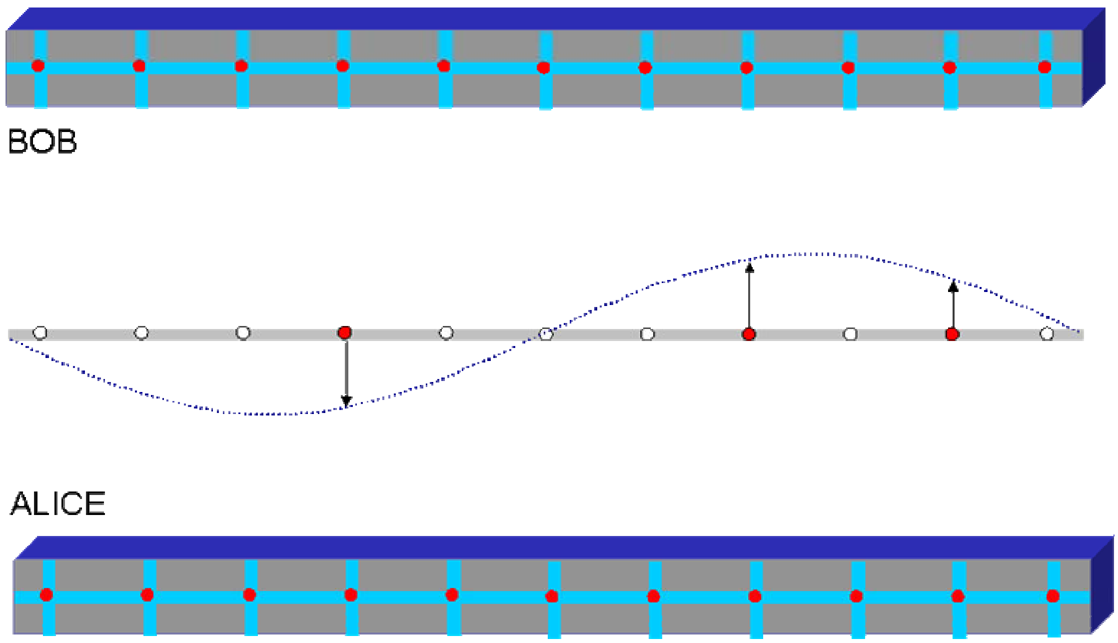

Fig. 2. Schematic illustration of the process to be employed for remote frequency locking. The top (bottom) array shows the atoms co-located with and excited by Bob (Alice). The degree of correlation observed after executing the frequency-locking protocol displays a spatial variation only if the frequencies of Bob's and Alice's oscillators are different, as shown in the middle. Elimination of such a variation leads to frequency locking.

Appendix C:

Driver-phase-correlated uctuations in the rotation of a strongly driven quantum bit

M. S. Shahriar,[1,2] Prabhakar Pradhan,[1,2] and Jacob Morzinski[2]

[1]*Department of Electrical and Computer Engineering, Northwestern University, Evanston, Illinois 60208, USA*

[2]*Research Laboratory of Electronics, Massachusetts Institute of Technology, Cambridge, Massachusetts 02139, USA*

(Received 20 July 2002; published 16 March 2004)

The need to maximize the number of operations of a quantum bit within its decoherence time may require the ratio of Rabi frequency to transition frequency to be large enough to invalidate the rotating-wave approximation. The state of the quantum bit under any initial condition then depends explicitly on the phase of the driving eld, resulting in driver-phase-correlated uctuations and a violation of the rule that the degree of excitation depends only on the pulse area. This is due to the interference of the excitations caused by the corotating and counterrotating elds, and is a signi cant source of error, correctable only by controlling the driver phase. We present a scheme for observing this effect under currently realizable parameters.

DOI: 10.1103/PhysRevA.69.032308 PACS number(s): 03.67.Hk, 03.67.Lx, 32.80.Qk

In order to minimize the decoherence rate of a two-state quantum bit (qubit) embodied in a massive particle, one often chooses to use low-energy transitions. In general, one is interested in performing these transitions as fast as possible [1–5] which demands a strong Rabi frequency. The ratio of Rabi frequency to qubit transition frequency is therefore not necessarily very small, thus invalidating the so-called rotating-wave approximation (RWA). A key effect due to violation of the RWA (VRWA) is the so-called Bloch-Siegert shift [6–9] which is negligible in optical transitions, but is manifested in nuclear magnetic resonance [10]. Here, we show that VRWA leads to another important effect, which can lead to controllable errors that are signi cant on the scale of precisions envisioned for a functioning quantum computer [11]. Speci cally , we show that under VRWA the population difference between the two levels of the quantum bit, with any initial condition, depends explicitly on the phase of the driving eld at the onset of an excitation pulse, which is a violation of the rule [6] that for a two-level system starting in the ground state, the population difference is a function of the integral of the eld amplitude over the pulse duration and does not depend on the phase of the eld. We provide a physical interpretation of this effect in terms of an interference of the excitations caused by the corotating and counterrotating elds, and present a scheme for observing this effect under currently realizable parameters.

To see the implication of this result, consider a scenario where one has a qubit, initialized to the ground state, and would like to prepare it to be in an equal superposition of the ground and excited states. To this end, one would apply a resonant pulse with an area of $\pi/2$ starting at a time $t=t_0$. Under the RWA, one does not have to know what the absolute phase of the eld, ϕ_P, is at t_0, and the population difference for the qubit would be zero. Under VRWA, however, the desired excitation would only occur if $\phi_P=0$. Otherwise, the population difference would have a component varying as $\eta \sin(2\phi_P)$, where η is a parameter that is proportional to the ratio of Rabi frequency to transition frequency. Suppose one has to apply this pulse to many such qubits, with a potentially different ϕ_P for each (e.g., because the pulses are applied at different times or the qubits are spatially separated), but with identical pulse areas. The population difference for the qubits will then exhibit a uctuation, correlated to their respective values of ϕ_P. For a quantum computer, this variation would represent a source of error. For some experiments (e.g., Ref. [5]), the value of η is already close to 0.01, so that the magnitude of this error is much larger than the ultimate accuracy ($10^{\;6}$) desirable for a large-scale quantum computer [11] and must be controlled.

To illustrate this effect, we consider an ideal two-level system where a ground state $|0\rangle$ is coupled to a higher-energy state $|1\rangle$. We also assume that the $0 \leftrightarrow 1$ transition is magnetic dipolar, with a transition frequency ω, and the magnetic eld is of the form $B=B_0\cos(\omega t+\phi)$. We now summarize brie y the two-level dynamics without the RWA. In the dipole approximation, the Hamiltonian can be written as

$$\hat{H} = \epsilon(\sigma_0 \quad \sigma_z)/2 + g(t)\sigma_x, \tag{1}$$

where $g(t)= \;\; g_0[\exp(i\omega t+i\phi)+\text{c.c.}]/2$, σ_i are the Pauli matrices, and $\epsilon=\omega$ corresponds to resonant excitation. The state vector is written as

$$|\xi(t)\rangle = \begin{bmatrix} C_0(t) \\ C_1(t) \end{bmatrix}. \tag{2}$$

We perform a rotating-wave transformation by operating on $|\xi(t)\rangle$ with the unitary operator $\hat{Q}$, where

$$\hat{Q} = (\sigma_0 + \sigma_z)/2 + \exp(i\omega t + i\phi)(\sigma_0 \quad \sigma_z)/2. \tag{3}$$

The Schrödinger equation then takes the form (setting $\hbar=1$) $|\dot{\tilde{\xi}}\rangle = \;\; i\tilde{H}(t)|\tilde{\xi}(t)\rangle$ where the effective Hamiltonian is given by

$$\tilde{H} = \alpha(t)\sigma_+ + \alpha^*(t)\sigma \;\;, \tag{4}$$

with $\alpha(t)= \;\; (g_0/2)[\exp(\;\; i2\omega t \;\; i2\phi)+1]$, and in the rotating frame the state vector is

$$|\widetilde{\xi}(t)\rangle \equiv \hat{Q}|\xi(t)\rangle = \begin{bmatrix} \widetilde{C}_0(t) \\ \widetilde{C}_1(t) \end{bmatrix}. \qquad (5)$$

Now, one may choose to make the RWA, corresponding to dropping the fast-oscillating term in $\alpha(t)$. This corresponds to ignoring effects (such as the Bloch-Siegert shift) of the order of (g_0/ω), which can easily be observable in an experiment if g_0 is large [6–10]. On the other hand, by choosing g_0 to be small enough, one can make the RWA for any value of ω. We explore both regimes in this paper. As such, we find the general results without the RWA.

From Eqs. (4) and (5), one gets two coupled differential equations

$$\widetilde{C}_0(t) = \quad (g_0/2)[1+\exp(\quad i2\omega t \quad i2\phi)]\widetilde{C}_1(t), \qquad (6a)$$

$$\widetilde{C}_1(t) = \quad (g_0/2)[1+\exp(+i2\omega t+i2\phi)]\widetilde{C}_0(t). \qquad (6b)$$

We assume $|C_0(t)|^2=1$ to be the initial condition and proceed further to nd an approximate analytical solution of Eq. (6). Given the periodic nature of the effective Hamiltonian, the general solution to Eq. (6) can be written in the form

$$|\widetilde{\xi}(t)\rangle = \sum_{n=\ \infty}^{\infty} \begin{bmatrix} a_n \\ b_n \end{bmatrix} \exp[n(\quad i2\omega t \quad i2\phi)]. \qquad (7)$$

Inserting Eq. (7) into Eq. (6) and equating coefficients with same the frequencies, one gets for all n,

$$a_n = i2n\omega a_n + ig_0(b_n + b_{n\ 1})/2, \qquad (8a)$$

$$b_n = i2n\omega b_n + ig_0(a_n + a_{n+1})/2. \qquad (8b)$$

Here, the coupling between a_0 and b_0 is the conventional one present when the RWA is made. The couplings to the nearest neighbors, $a_{\pm 1}$ and $b_{\pm 1}$, are detuned by an amount 2ω and so on. To the lowest order in (g_0/ω), we can ignore terms with $|n|>1$, thus yielding a truncated set of six equations

$$a_0 = ig_0(b_0 + b_{\ 1})/2, \qquad (9a)$$

$$b_0 = ig_0(a_0 + a_1)/2, \qquad (9b)$$

$$a_1 = i2\omega a_1 + ig_0(b_1 + b_0)/2, \qquad (9c)$$

$$b_1 = i2\omega b_1 + ig_0 a_1/2, \qquad (9d)$$

$$a_{\ 1} = \quad i2\omega a_{\ 1} + ig_0 b_{\ 1}/2, \qquad (9e)$$

$$b_{\ 1} = \quad i2\omega b_{\ 1} + ig_0(a_{\ 1} + a_0)/2. \qquad (9f)$$

We consider g_0 to have a time dependence of the form $g_0(t)=g_{0M}[1 \quad \exp(\quad t/\tau_{sw})]$, where the switching time constant $\tau_{sw} \gg \omega^{\ 1}, g_{0M}^{\ 1}$. We can solve these equations by employing the method of adiabatic elimination, which is valid to rst order in $\eta \equiv (g_0/4\omega)$. Note that η is also a function of time and can be expressed as $\eta(t)=\eta_0[1 \quad \exp(\quad t/\tau_{sw})]$, where $\eta_0 \equiv (g_{0M}/4\omega)$. We consider rst Eqs. (9e) and (9f). In order to simplify these two equations further, one needs to diagonalize the interaction between $a_{\ 1}$ and $b_{\ 1}$. De ne $\mu \equiv (a_{\ 1} \quad b_{\ 1})$ and $\mu_+ \equiv (a_{\ 1} + b_{\ 1})$, which now can be used to reexpress these two equations in a symmetric form as

$$\mu \ = \quad i(2\omega + g_0/2)\mu \quad ig_0 a_0/2, \qquad (10a)$$

$$\mu_+ = \quad i(2\omega \quad g_0/2)\mu_+ + ig_0 a_0/2. \qquad (10b)$$

Adiabatic following then yields (again, to lowest order in η) $\mu \approx \quad \eta a_0$ and $\mu_+ \approx \eta a_0$, which in turn yields $a_{\ 1} \approx 0$ and $b_{\ 1} \approx \eta a_0$. In the same manner, we can solve Eqs. (9c) and (9d), yielding $a_1 \approx \quad \eta b_0$ and $b_1 \approx 0$.

Note that the amplitudes of $a_{\ 1}$ and b_1 are vanishing (each proportional to η^2) to lowest order in η and thereby justifying our truncation of the in nite set of relations in Eq. (9). It is easy to show now

$$a_0 = ig_0 b_0/2 + i\Delta(t)a_0/2, \qquad (11a)$$

$$b_0 = ig_0 a_0/2 \quad i\Delta(t)b_0/2, \qquad (11b)$$

where $\Delta(t)=g_0^2(t)/4\omega$ is essentially the Bloch-Siegert shift. Equation (11) can be thought of as a two-level system excited by a eld detuned by Δ. For simplicity, we assume that this detuning is dynamically compensated for by adjusting the driving frequency ω. This assumption does not affect the essence of the results to follow, since the resulting correction to η is negligible. With the initial condition of all the population in $|0\rangle$ at $t=0$, the only nonvanishing (to lowest order in η) terms in the solution of Eq. (9) are

$$a_0(t) \approx \cos[g_0'(t)t/2], \quad b_0(t) \approx i \sin[g_0'(t)t/2],$$

$$a_1(t) \approx \quad i\eta \sin[g_0'(t)t/2], \quad b_{\ 1}(t) \approx \eta \cos[g_0'(t)t/2],$$

where

$$g_0'(t) = 1/t\int_0^t g_0(t')dt' = g_0[1 \quad (t/\tau_{sw})^{\ 1} \exp(\quad t/\tau_{sw})].$$

We have veri ed this solution via numerical integration of Eq. (6) as shown later. Inserting this solution into Eq. (6) and reversing the rotating-wave transformation, we get the following expressions for the components of Eq. (2):

$$C_0(t) = \cos[g_0'(t)t/2] \quad 2\ \eta\Sigma \sin[g_0'(t)t/2], \qquad (12a)$$

$$C_1(t) = ie^{\ i(\omega t+\phi)}\{\sin[g_0'(t)t/2] + 2\eta\Sigma^* \cos[g_0'(t)t/2]\}, \qquad (12b)$$

where we have de ned $\Sigma \equiv (i/2)\exp[\quad i(2\omega t+2\phi)]$. To lowest order in η, this solution is normalized at all times. Note that if one wants to carry this excitation on an ensemble of atoms using a $\pi/2$ pulse and measure the population of the state $|1\rangle$ after the excitation terminates [at $t=\tau$ when $g'(\tau)\tau/2=\pi/2$], the result would be an output signal given by

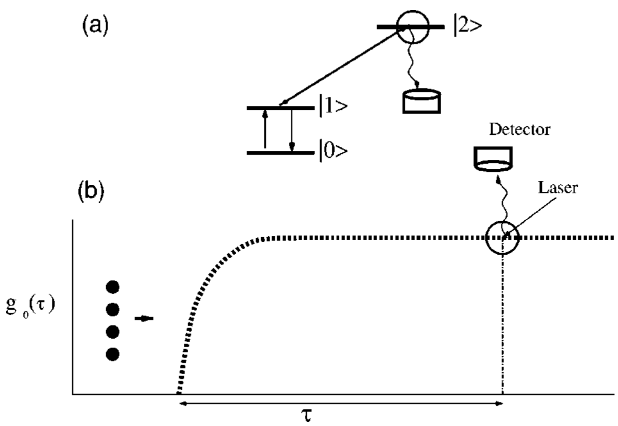

FIG. 1. Schematic illustration of an experimental arrangement for measuring the phase dependence of the population of the excited state $|1\rangle$: (a) The microwave eld couples the ground state ($|0\rangle$) to the excited state ($|1\rangle$). A third level, $|2\rangle$, which can be coupled to $|1\rangle$ optically, is used to measure the population of $|1\rangle$ via uorescence detection. (b) The microwave eld is turned on adiabatically with a switching time constant τ_{sw}, and the uorescence is monitored after a total interaction time of τ.

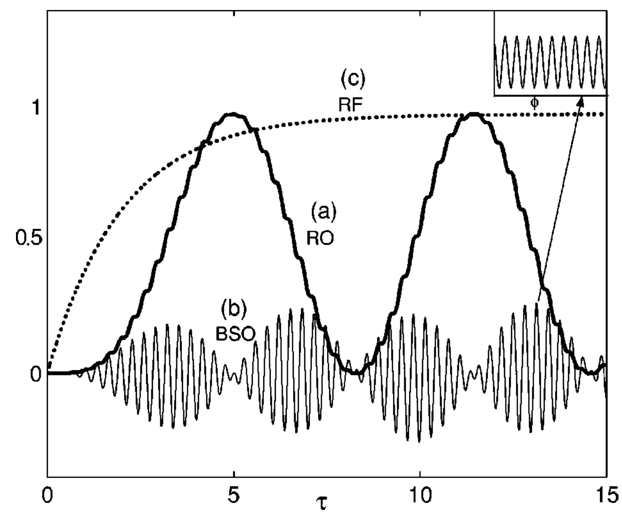

FIG. 2. Illustration of the Bloch-Siegert oscillation (BSO): (a) the population of state $|1\rangle$, as a function of the interaction time τ, showing the BSO superimposed on the conventional Rabi oscillation; (b) the BSO oscillation (ampli ed scale) by itself, produced by subtracting the Rabi oscillation from the plot in (a); and (c) the time dependence of the Rabi frequency. Inset: BSO as a function of the absolute phase of the eld.

$$|C_1(g_0'(\tau),\phi)|^2 = \frac{1}{2}[1 + 2\eta \sin(2\phi_\tau)], \qquad (13)$$

where we have defined the phase of the field at $t=\tau$ to be $\phi_\tau \equiv \omega\tau + \phi$. This signal contains information of both the amplitude and phase of the driving field.

This result can be appreciated best by considering an experimental arrangement of the type illustrated in Fig. 1. Consider, for example, a collection of ^{87}Rb atoms, caught in a dipole force trap, where the states $|0\rangle \equiv 5^2S_{1/2}:|F=1, m=1\rangle$ and $|1\rangle \equiv 5^2S_{1/2}:|F=2, m=2\rangle$ form the two-level system. These states differ in frequencies by 6.683 47 GHz. When illuminated by resonant right-circularly polarized light at a frequency of 3.844×10^{14} Hz, state $|1\rangle$ couples only to the state $|2\rangle \equiv 5^2P_{3/2}:|F=3, m=3\rangle$, which in turn can decay only to state $|1\rangle$. This cycling transition can thus be used to pump the system into state $|1\rangle$. When a right-circularly polarized microwave eld at 6.683 47 GHz is applied, state $|1\rangle$ couples only to state $|0\rangle$, even when the RWA approximation breaks down. The strong-coupling regime (e.g., η_0 of the order of 0.1) can be reached, for example, by using a superconducting, high-Q (10^{10}) microwave cavity [12]. The theoretical model developed above is then a valid description of the coupling between $|0\rangle$ and $|1\rangle$.

The strong microwave eld is turned on adiabatically with a switching time constant τ_{sw}, starting at $t=0$. After an interaction time of τ, chosen so that $g_0'(\tau)\tau = \pi/2$, the population of state $|1\rangle$ can be determined by coupling this state to the state $|2\rangle$ with a short (faster than $1/\omega$ and $1/g_{0M}$) laser pulse and monitoring the resulting uorescence [13].

We have simulated this process explicitly for the following parameters: $\omega = 2\pi\times 6.683\,47\times 10^9$ sec^{1}, $g_{0M}=0.1$, and $\tau_{sw}=0.1$. These numbers are easily achievable experimentally. The laser pulse width τ_{LP} is chosen to be $10^{1\ 2}$ sec in order to satisfy the constraint that $\tau_L \ll 1/\omega$ and $\tau_L \ll 1/g_{0M}$.

In order to optimize the signal, the laser Rabi frequency Ω_L is chosen to be such that $\Omega_L\tau_L = \pi$, so that all the populations of state $|1\rangle$ are excited to state $|2\rangle$ at the end of the pulse. For the cycling transition (1-2) and a pulse focused to an area of 25 μm^2, the power needed for achieving this Rabi frequency is 1.2 W, which is achievable experimentally. After the laser pulse is turned off, the uorescence is collected for a duration longer than the spontaneous-decay lifetime (32 nsec) of state $|2\rangle$. Under this condition, our simulation veri es that the detector signal is essentially proportional to the population of state $|1\rangle$, as given by Eq. (13), with the proportionality constant determined by the ef ciency of the detection system. If 10^6 atoms are used (a number easily achievable in a dipole trap), the signal-to-noise ratio can be more than 100 for the parameters considered here, assuming a detector solid angle of 0.1π and a quantum ef ciency of 0.8. In Fig. 2(a), we have shown the evolution of the excited-state population as a function of the interaction time τ using the analytical expression of Eq. (12). Under the RWA, this curve would represent the conventional Rabi oscillation. However, we notice here some additional oscillations, which are magni ed and shown separately in Fig. 2(b), produced by subtracting the conventional Rabi oscillation ($\sin^2[g_0'(\tau)\tau/2]$) from Fig. 2(a). That is, Fig. 2(b) corresponds to what we call the Bloch-Siegert oscillation (BSO), given by $\eta\sin[g_0'(\tau)\tau]\sin(2\phi_\tau)$. The dashed curve (c) shows the time dependence of the Rabi frequency. These analytical results agree closely with the results obtained via direct numerical integration of Eq. (7). Consider next a situation where the interaction time τ is xed so that we are at the peak of the BSO envelope. The experiment is now repeated many times, with a different value of ϕ each time. The corresponding population of $|1\rangle$ is given by $\eta\sin(2\phi_\tau)$ and is plotted as a function of ϕ in the inset of Fig. 2. This dependence of the population of $|1\rangle$ on the initial phase ϕ (and, therefore, on the final phase ϕ_τ) makes it possible to measure these quantities.

Note, of course, that the speed of the detection system is limited fundamentally by the spontaneous decay rate γ^{-1} ($\sim$32 nsec in this case) of state $|2\rangle$. As such, it is impossible in this explicit scheme to monitor the phase of the microwave field on a time scale shorter than its period. If one were interested in monitoring the phase of a microwave field of a lower frequency (so that $\omega^{-1} \gg \gamma^{-1}$), it would be possible to track the phase on a time scale much shorter than its period. One possible set of atomic levels that can be used for this purpose is the Zeeman sublevels (e.g., those of the $5^2S_{1/2}:F=1$ hyperfine level of ^{87}Rb atoms), where the energy spacing between the sublevels can be tuned by a dc magnetic field to match the microwave field to be measured. However, the number of sublevels that get coupled is typically more than 2. A simple extension of our theoretical analysis shows that the signature of the phase of the microwave field still appears in the population of any of these levels and can be used to measure the phase. More generally, the phase signature is likely to appear in the population of the atomic levels, no matter how many levels are involved, as long as the Rabi frequency is strong enough for the RWA to break down.

A recent experiment by Martinis *et al.* [5] is an example where a qubit is driven very fast. In this experiment, a qubit is made using the two states of a current-biased Josephson junction, the resonance frequency is ω=6.9 GHz, and the Rabi frequency is g=80 MHz. If this experiment is carried out without keeping track of the phase of the driving field, the degree of qubit excitation will fluctuate due to the BSO, leading to an error which is of the order of g/ω=0.01—i.e., nearly 1%. This error is much larger than the permissible error rate of 10^{-6} for an error-correcting quantum computer that would consist of 10^6 qubits [11]. In order to eliminate the BSO-induced error, one can design the driving system such that the phase is measured, e.g., by using an auxiliary cluster of bits located close to the qubit of interest, at the onset of the qubit excitation, and the measured value of the phase is used to determine the duration of the excitation pulse, in order to ensure the desired degree of excitation of the qubit [14,15]. Finally, we point out that by making use of distant entanglement, the BSO process may enable teleportation of the phase of a field that is encoded in the atomic state amplitude, for potential applications to remote frequency locking [16–19].

In conclusion, we have shown that when a two-level atomic system is driven by a strong periodic field, the Rabi oscillation is accompanied by another oscillation at twice the transition frequency, and this oscillation carries information about the absolute phase of the driving field. One can detect this phase by simply measuring only the population of the excited state. This leads to a phase-correlated fluctuation in the excitation of a qubit and violation of the rule that the degree of excitation depends only on the pulse area. We have shown how the resulting error may be significant and must be controlled for low-energy fast qubit operations.

We thank G. Cardoso for fruitful discussions. We wish to acknowledge support from DARPA Grant No. F30602-01-2-0546 under the QUIST program, ARO Grant No. DAAD19-001-0177 under the MURI program, and NRO Grant No. NRO-000-00-C-0158.

[1] *The Physics of Quantum Information*, edited by D. Bouwmeester, A. Ekert, and A. Zeilinger (Springer, Berlin, 2000).
[2] A. M. Steane, Appl. Phys. B: Lasers Opt. **64**, 623 (1997).
[3] A. M. Steane *et al.*, e-print quant-ph/0003087.
[4] D. Jonathan, M. B. Plenio, and P. L. Knight, Phys. Rev. A **62**, 042307 (2000).
[5] J. M. Martinis *et al.*, Phys. Rev. Lett. **89**, 117901 (2002).
[6] L. Allen and J. Eberly, *Optical Resonance and Two Level Atoms* (Wiley, New York, 1975).
[7] F. Bloch and A. J. F. Siegert, Phys. Rev. **57**, 522 (1940).
[8] J. H. Shirley, Phys. Rev. **138**, B979 (1965).
[9] S. Stenholm, J. Phys. B **6**, 1650 (1973).
[10] R. J. Abraham, J. Fisher, and P. Loftus, *Introduction to NMR Spectroscopy* (Wiley, New York, 1992).
[11] J. Preskill, Proc. R. Soc. London, Ser. A **454**, 469 (1998).
[12] S. Brattke, B. T. H. Varcoe, and H. Walther, Phys. Rev. Lett. **86**, 3534 (2001).
[13] C. Monroe *et al.*, Phys. Rev. Lett. **75**, 4714 (1995).
[14] P. Pradhan, G. C. Cardoso, J. Morzinski, and M. S. Shahriar, e-print quant-ph/0402122.
[15] M. S. Shahriar and P. Pradhan in *Proceedings of the 6th International Conference on Quantum Communication, Measurement and Computing* (Rinton Press, Princeton, NJ, 2002).
[16] R. Jozsa, D. S. Abrams, J. P. Dowling, and C. P. Williams, Phys. Rev. Lett. **85**, 2010 (2000).
[17] S. Lloyd, M. S. Shahriar, J. H. Shapiro, and P. R. Hemmer, Phys. Rev. Lett. **87**, 167903 (2001).
[18] G. S. Levy *et al.*, Acta Astron. **15**, 481 (1987).
[19] M. S. Shahriar, e-print quant-ph/0209064.

Limits to clock synchronization induced by completely dephasing communication channels

V. Giovannetti,[1,*] S. Lloyd,[2,†] L. Maccone,[1,‡] and M. S. Shahriar[1,§]
[1]*Research Laboratory of Electronics, Massachusetts Institute of Technology, 50 Vassar Street, Cambridge, Massachusetts 02139*
[2]*Department of Mechanical Engineering, Massachusetts Institute of Technology, Cambridge, Massachusetts 02139*
(Received 26 October 2001; published 17 June 2002)

Clock synchronization procedures are analyzed in the presence of imperfect communications. In this context we show that there are physical limitations, which prevent one from synchronizing distant clocks when the intervening medium is completely dephasing, as in the case of a rapidly varying dispersive medium.

DOI: 10.1103/PhysRevA.65.062319 PACS number(s): 03.67.Hk, 06.30.Ft, 03.65.Ta

INTRODUCTION

There are two main kinds of protocols for achieving clock synchronization. The rst is the "Einstein synchronization protocol" [1] in which a signal is sent back and forth between one of the clocks (say Alice's clock) and the other clocks. By knowing the signal speed dependence on the intermediate environment, it is possible to synchronize all the clocks with Alice's. The other main protocol is the "Eddington slow clock transfer" [2]: after locally synchronizing it with hers, Alice sends a clock (i.e., a physical system that evolves in time with a known time dependence) to all the other parties. The clock's transfer must of course be perfectly controllable, as one must be able to predict how the clock will react to the physical conditions encountered *en route*, which may shift its time evolution. Moreover, since any acceleration of the transferred clocks introduces a delay because of relativistic effects, one must suppose that the transfer is performed "adiabatically slowly," i.e., such that all accelerations are negligible. Notice that the above protocols can be implemented using only classical resources: peculiar quantum features such as entanglement, squeezing, etc., are not needed. In what follows, such synchronization schemes will be referred to as "classical protocols."

A recently proposed quantum clock synchronization protocol [3] was found [4] to be equivalent to the Eddington slow clock synchronization. The application of entanglement puri cation to improve quantum clock synchronization in the presence of dephasing was attempted without success in [5]. One might think there were other ways to implement a synchronization scheme that employs quantum features such as entanglement and squeezing, but this paper shows that this is not the case. In fact, it will be shown that quantum mechanics does not allow one to synchronize clocks if it would not be possible to also employ one of the classical protocols, which one can always employ if the channel is perfect or if its characteristics are controllable. However, the relevance of quantum mechanics to the clock synchronization procedures should not be underestimated, since there exist schemes that exploit quantum mechanics to achieve a (classically not allowed) increase in the accuracy of classical clock synchronization protocols, such as the one obtainable exploiting entangled systems [6–8].

The presented discussion also takes into account the possibility that the two distant parties who want to synchronize their clocks (say Alice and Bob) and who are localized in space can entangle their systems by exchanging a certain number of quantum states, and the possibility that they may employ the "wave function collapse" [3], through postselection measurements. The intuitive idea behind the proof is as follows. To synchronize clocks, Alice and Bob must exchange physical systems such as clocks or pulses of light that include timing information. But any effect, such as rapidly varying dispersion, that randomizes the relative phases between energy eigenstates of such systems completely destroys the timing information. Any residual information, such as entanglement between states with the same energy, cannot be used to synchronize clocks as shown below.

The paper is organized as follows. In Sec. I the analytic framework is established. In Sec. II the clock synchronization procedure is de ned and the main result is derived. In particular, in Sec. II A the exchange of quantum information between Alice and Bob is analyzed and in Sec. II B the analysis is extended to include partial measurements and postselection schemes in the synchronization process.

I. THE SYSTEM

Assume the following hypotheses that describe the most general situation in which two distant parties communicate through a noisy environment:

(1) Alice and Bob are *separate* entities that initially are *disjoint*. They belong to the same inertial reference frame and communicate by exchanging some physical system.

(2) The environment randomizes the phases between different energy eigenstates of the exchanged system while in transit.

From these hypotheses it will be shown that Alice and Bob cannot synchronize their clocks.

In Sec. I A we explain the rst hypothesis by giving its formal consequences. In Sec. I B we analyze the second hypothesis and explain how it describes a dephasing channel.

A. First hypothesis

The rst hypothesis states the problem and ensures that initially Alice and Bob do not already share any kind of

*Email address: vittorio@mit.edu
†Email address: slloyd@mit.edu
‡Email address: maccone@mit.edu
§Email address: smshahri@mit.edu

system that acts as a synchronized clock. By *separate* we mean that at any given time Alice and Bob cannot gain access to the same degrees of freedom and there is no direct interaction between Alice's and Bob's systems. This can be described by the following properties of the system's Hilbert space and Hamiltonian. At time t the Hilbert space of the global system can be written as

$$\mathcal{H}=\mathcal{H}_A(t)\otimes\mathcal{H}_C(t)\otimes\mathcal{H}_B(t), \tag{1}$$

where the Hilbert space $\mathcal{H}_A(t)$ refers to the system on which Alice can operate at time t, $\mathcal{H}_B(t)$ refers to Bob's system, and $\mathcal{H}_C(t)$ describes the systems on which neither of them can operate. The time dependence in Eq. (1) does not imply that the global Hilbert space changes in time, but it refers to the possibility that a system that was previously under Alice's influence has been transferred to Bob (or vice versa), after a transient time at which it cannot be accessed by any of them. Since information *must* be encoded into a physical system, this mechanism describes any possible communication between them. Moreover, the Hamiltonian of the system can be written as

$$H(t)=H_A(t)+H_B(t)+H_C(t), \tag{2}$$

where the time dependent $H_A(t)$ and $H_B(t)$ evolve the states in $\mathcal{H}_A$ and $\mathcal{H}_B$ under the control of Alice and Bob, respectively, while $H_C(t)$ evolves the system in transit between them when it is not accessible. As a consequence of Eq. (1), at time t the three terms on the right side of Eq. (2) commute, since they act on different Hilbert spaces. For the same reason any operator under the influence of Alice at time t commutes with all Bob's operators at the same time. A simple example may help explain this formalism. Consider the situation in which the system is composed of three 1/2 spin particles (qubits). A possible communication is then modeled by the sequence

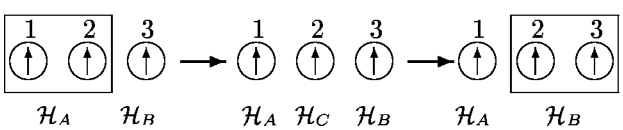

i.e., initially Alice's Hilbert space $\mathcal{H}_A$ contains spins 1 and 2, and Bob owns only spin 3. Alice then encodes some information on spin 2 (eventually entangling it with spin 1), and sends it to Bob. There will be a time interval in which none of them can access spin 2, and this situation corresponds to having spin 2 belonging to $\mathcal{H}_C$. Finally, Bob receives spin 2, and his Hilbert space $\mathcal{H}_B$ describes both spins 2 and 3. Notice that the form of the Hamiltonian in Eq. (2), where no interaction terms are present, allows each of them to act, at a given time t, only on the spins that live in their own Hilbert space at time t. An analogous description applies also to more complicated scenarios, such as the exchange of light pulses. In this case, causality constraints allow Alice and Bob to act only on localized traveling wave modes of the electromagnetic field. Thus, also here, it is possible to define a traveling system Hilbert space $\mathcal{H}_C$ that factorizes as in Eq. (1). From the above example, it is easy to see that in each communication exchange it is possible to define a *departure* time t_s after which the sender cannot act anymore on the system in transit, and an *arrival* time t_r before which the receiver cannot yet act on such system. It is between these two times that the exchanged system belongs to $\mathcal{H}_C$.

In hypothesis 1 by initially *disjoint* we mean that Alice and Bob do not share any information prior to the first communication exchange. In particular this means that, before they start to interact, the state of the system factorizes as

$$|\Psi\rangle=|\phi\rangle_A\otimes|\varphi\rangle_B, \tag{3}$$

i.e., the initial state is not entangled and they do not share any quantum information. Here $|\phi\rangle_A$ is the state of Alice's system evaluated at the time at which she starts to act, while $|\varphi\rangle_B$ is the state of Bob's system evaluated at the time at which *he* starts to act. For ease of notation, the tensor product symbol $\otimes$ will be omitted in the following except when its explicit presence helps comprehension.

B. Second hypothesis

The second hypothesis imposes limitations to the information retrieved from the exchanged signal. The dephasing of the energy eigenstates describes the nondissipative noise present in most nonideal communication channels and implies a certain degree of decoherence in any quantum communication between Alice and Bob. Define $|e,d\rangle$ as the eigenstate relative to the eigenvalue $\hbar\omega_e$ of the free Hamiltonian of the exchanged system C. The label d takes into account possible degeneracy of such eigenstate. We assume that during the travel, when neither Alice nor Bob can control the exchanged system in $\mathcal{H}_C$, the states $|e,d\rangle$ undergo the transformation

$$|e,d\rangle\rightarrow e^{-i\varphi_e}|e,d\rangle, \tag{4}$$

where the random phase $\varphi_e\in[0,2\pi]$ is independent of d. The channel dephasing arises when different energy eigenstates are affected by different phase factors φ_e. For this reason the dephasing is characterized by the joint probability function $p_\epsilon(\varphi_e,\varphi_{e'})$ that weights the probability that the energy levels $|e,d\rangle$ and $|e',d\rangle$ are affected by the phases φ_e and $\varphi_{e'}$, respectively. The parameter $\epsilon\in[0,1]$ measures the degree of decoherence in the channel. In particular, $\epsilon=1$ describes the case of complete decoherence, where the phases relative to different energy eigenstates are completely uncorrelated, namely $p_\epsilon(\varphi_e,\varphi_{e'})$ is a constant. On the other hand, $\epsilon=0$ describes the case of no decoherence, where each energy eigenstate acquires the same phase, namely $p_\epsilon(\varphi_e,\varphi_{e'})\rightarrow\delta(\varphi_e-\varphi_{e'})/2\pi$. Written in the energy representation, the channel density matrix ϱ_c evolves, using Eq. (4), as

$$\varrho_c=\sum_{ee'}P_e\varrho_cP_{e'}\rightarrow\sum_{ee'}e^{-i(\varphi_e-\varphi_{e'})}P_e\varrho_cP_{e'}, \tag{5}$$

where $P_e=\Sigma_d|e,d\rangle\langle e,d|$ is the projection operator on the channel eigenspace of energy $\hbar\omega_e$. Taking into account the stochasticity of the evolution (4), the right-hand term of Eq. (5) must be weighted by the probability distribution $p_\epsilon(\varphi_e,\varphi_{e'})$, resulting in

$$\varrho_c \to \sum_{ee'} \delta^{(\epsilon)}_{ee'} P_e \varrho_c P_{e'}\,, \tag{6}$$

where

$$\delta^{(\epsilon)}_{ee'} = \int_0^{2\pi} d\varphi_e \int_0^{2\pi} d\varphi_{e'} p_\epsilon(\varphi_e,\varphi_{e'}) e^{-i(\varphi_e-\varphi_{e'})}. \tag{7}$$

The width of the function $\delta^{(\epsilon)}_{ee'}$ decreases with ϵ, so that $\delta^{(\epsilon=0)}_{ee'}$ is independent of e and e' and the state is unchanged, while $\delta^{(\epsilon=1)}_{ee'}$ is the Kronecker δ and the state suffers from decoherence in the energy eigenstate basis.

The dephasing process of Eq. (4) can be derived assuming a time dependent Hamiltonian $H_C(t)=H^o_C+H'_C(t)$, where H^o_C is the free evolution of the system with eigenstates $|e,d\rangle$ and $H'_C(t)$ is a stochastic contribution that acts on the system in a small time interval δt by shifting its energy eigenvalues by a random amount ν_e, such that $\nu_e \delta t=\varphi_e$. In fact, in the limit $\delta t \to 0$, the evolution of the exchanged system is described by

$$U_C(t_r,t_s)=\exp\left\{-i\sum_e P_e[\omega_e(t_r-t_s)+\varphi_e]\right\}, \tag{8}$$

where $\hbar\omega_e$ is the energy eigenvalue of the exchanged system relative to the eigenvector $|e,d\rangle$ and t_r and t_s are the exchanged system's arrival and departure times, respectively, introduced in Sec. I A [9]. Notice that for φ_e independent of e (which corresponds to the case $\epsilon=0$), U_C reduces to the deterministic free evolution operator $\exp[-(i/\hbar)H^o_C(t_r-t_s)]$, apart from an overall phase term.

It might be interesting to consider the simpler case in which the random phase φ_e can be written as $\omega_e\theta$ with the random term θ independent of e. In this case, Eq. (8) simplifies to

$$U_C(t_r,t_s)=\exp\left[-\frac{i}{\hbar}H^o_C(t_r-t_s+\theta)\right]. \tag{9}$$

This last situation depicts the case in which all signals exchanged between Alice and Bob are delayed by an amount θ. As an example consider light signals that encounter a medium with unknown (possibly varying) refractive index or a traveling "clock" that acquires an unpredictable delay. The situation described by Eq. (8) is even worse, since not only may such a delay be present, but also the wave function of the system is degraded by dispersion effects. In both cases, the information on the transit time t_r-t_s that may be extracted from $U_C(t_r,t_s)$ depends on the degree of randomness of φ_e. In particular, if φ_e is a completely random quantity (i.e., for $\epsilon=1$), no information on the transit time can be obtained.

This, of course, prevents the possibility of using classical synchronization protocols, where unknown delays in either the signal travel time or in the exchanged clock prove to be fatal. One might think that by exploiting the apparently nonlocal properties of quantum mechanics (e.g., entanglement), these limits can be overcome. In the following sections we will show that this is not the case.

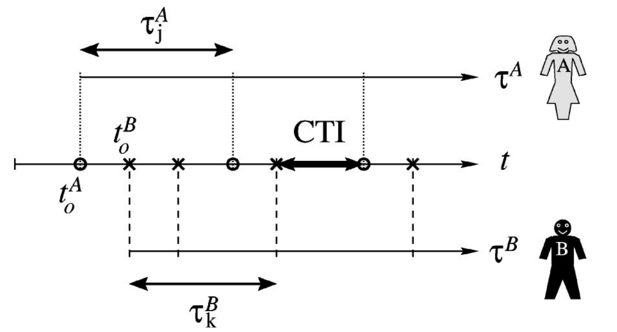

FIG. 1. Comparison between the times τ^A and τ^B of Alice and Bob's clocks. The center line represents the "absolute" time as measured by an external clock. The small circles represent the times of events that take place on Alice's side, while the crosses represent those on Bob's side. The upper line is the time as measured by Alice's clock: she only has direct access to the proper time intervals such as τ^A_j. Analogously, the lower line represents Bob's proper time. To achieve clock synchronization, Alice and Bob need to recover a connecting time interval (CTI) such as the one shown.

II. CLOCK SYNCHRONIZATION

In this section we analyze the clock synchronization schemes in detail and show the effect of a dephasing communication channel.

How does synchronization take place? Define t^A_0 and t^B_0 as the initial times of Alice and Bob's clocks as measured by an external clock. (Of course, since they do not have a synchronized clock to start with, they cannot measure t^A_0 and t^B_0.) Alice and Bob will be able to synchronize their clocks *if and only if* they can recover the quantity $t^A_0-t^B_0$, or any other time interval that connects two events that happen one on Alice's side and the other on Bob's side. Each of them has access to the times at which events on her/his side happen and can measure such events only relative to their own clocks. We will refer to these quantities as "proper time intervals" (PTIs). For Alice such quantities are defined as $\tau^A_j = t^A_j - t^A_0$, where t^A_j is the time at which the jth event took place as measured by the external clock. Analogously for Bob we define his PTI as $\tau^B_k=t^B_k-t^B_0$. If Alice and Bob share the data regarding their own PTIs, they cannot achieve synchronization: they need also a "connecting time interval" (CTI), i.e., a time interval that connects an event that took place on Alice's side with an event that took place on Bob's side as shown in Fig. 1.

Within this framework, consider the case of Einstein's and Eddington's clock synchronizations. In the Einstein clock synchronization the PTIs on Alice's side are the two times at which she sent and received back the signal she sends Bob. Bob's PTI is the time at which he bounces back the signal to Alice. The CTI in this case measures the time difference between the events "Alice sends the signal" and "Bob bounces the signal back." The protocol allows Alice to recover the CTI by simply dividing by two the time difference between her two PTIs. The analysis of Eddington's slow clock transfer is even simpler. In this case Bob's PTI is the time at which Bob looks at the clock Alice has sent him after synchronizing it with hers. The CTI is, for example, the time difference between the event "Bob looks at the clock sent by Alice" and "on Alice's side it is noon": Bob can recover it just looking at the time shown on the clock he received from Alice.

In this paper we show that in the presence of a dephasing communication channel (as described in hypothesis 2), there is no way in which Alice and Bob may achieve a CTI. The best that they can do is to collect a series of PTIs related to different events and a collection of CTI transit times corrupted by the noisy communication line: clock synchronization is thus impossible.

A. Timing information exchange

In this section we analyze the exchange of quantum information between Alice and Bob in the presence of dephasing.

Starting from the state $|\Psi\rangle$ of Eq. (3), Alice's and Bob begin to act on their systems at two times (that are not necessarily the same), in order to get ready for the information transfer. Without loss of generality one can assume that these two times coincide with their own time origins, i.e., t_0^A and t_0^B. This means that, at those two times, they introduce time dependent terms in the system Hamiltonian

$$\begin{aligned} H_A^o &\to H_A(t) \equiv H_A^o + H_A'(t-t_0^A), \\ H_B^o &\to H_B(t) \equiv H_B^o + H_B'(t-t_0^B), \end{aligned} \tag{10}$$

where H_A^o and H_B^o are the free Hamiltonians of Alice's and Bob's systems and $H_A'(t-t_0^A)$ and $H_B'(t-t_0^B)$ characterize the most general unitary transformations that they can apply to their systems. These last terms are null for $t<t_0^A$ and $t<t_0^B$ (when they have not yet started to act on their systems). Notice that according to Eq. (1), also the domains of $H_A(t)$ and $H_B(t)$ may depend on time.

Suppose rst that Alice is going to send a signal to Bob. De ne t_s^A the departure time at which Alice sends a message to Bob encoding it on a system described by the Hilbert space $\mathcal{H}_c$. This implies that the system she has access to will be $\mathcal{H}_a$ up to t_s^A and $\mathcal{H}_{a'}$ afterward, so that $\mathcal{H}_a = \mathcal{H}_{a'} \otimes \mathcal{H}_c$. In the same way, de ning t_r^B as the arrival time on Bob's side, we may introduce a space $\mathcal{H}_{b'} = \mathcal{H}_b \otimes \mathcal{H}_c$ that describes the Hilbert space on which Bob acts after t_r^B. The label A on t_s^A refers to the fact that the event of sending the message happens locally on Alice's side, so in principle she can measure such a quantity as referred to her clock as the PTI $\tau_s^A = t_s^A - t_0^A$. Analogous consideration applies to Bob's receiving time t_r^B and Bob's PTI $\tau_r^B = t_r^B - t_0^B$.

Consider the situation of Fig. 2 in which, for explanatory purposes, $t_0^A < t_0^B < t_s^A < t_r^B$. Start from the group property of the time evolution operators

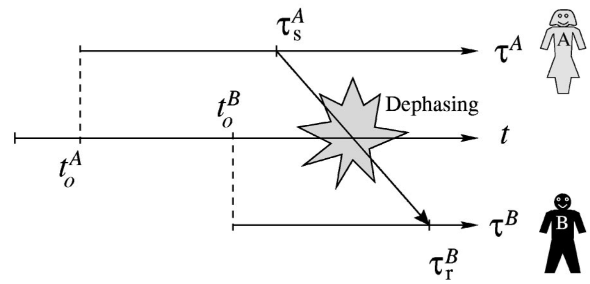

FIG. 2. Alice sends Bob a message encoded into a quantum system C at time t_s^A (her proper time τ_s^A) and Bob receives it at time t_r^B (his proper time τ_r^B). During the travel the system C undergoes dephasing.

$$U(t,0) = U(t,t')U(t',0), \tag{11}$$

and the commutativity of the operators that act on the distinct spaces of Alice and Bob. It is easy to show that for $t_s^A \leq t \leq t_r^B$ the state of the system is given by

$$|\Psi(t)\rangle = U_b(t,t_0^B)U_{a'}(t,t_s^A)U_c(t,t_s^A)U_a(t_s^A,t_0^A)|\Psi\rangle, \tag{12}$$

where $U_x(t,t')$ is the evolution operator in space $\mathcal{H}_x$ and

$$|\Psi\rangle \equiv U_a(t_0^A,0)U_b(t_0^B,0)|\Psi(0)\rangle \tag{13}$$

is the initial state as far as Alice and Bob are concerned, de ned in Eq. (3). By hypothesis 1 this state does not contain any usable information on t_0^A and t_0^B. In Eq. (12) notice that up to time t_s^A the systems $\mathcal{H}_c$ and $\mathcal{H}_{a'}$ are evolved together by U_a. Analogously, for $t \geq t_r^B$ after Bob has received the system Alice sent him, one has

$$|\Psi(t)\rangle = U_{a'}(t,t_r^B)U_{b'}(t,t_r^B)|\Psi(t_r^B)\rangle. \tag{14}$$

Joining Eqs. (12) and (14), it follows

$$\begin{aligned} |\Psi(t)\rangle = &\, U_{b'}(t,t_r^B)U_b(t_r^B,t_0^B)U_{a'}(t,t_s^A)U_c(t_r^B,t_s^A) \\ &\times U_a(t_s^A,t_0^A)|\Psi\rangle. \end{aligned} \tag{15}$$

The time dependence of Alice's and Bob's Hamiltonians (10) allows to write their unitary evolution operators as functions of their PTIs, i.e.,

$$\begin{aligned} U_\alpha(t',t'') &= \overleftarrow{\exp}\left[-\frac{i}{\hbar}\int_{t''}^{t'} dt[H_\alpha^o + H_\alpha'(t-t_0^A)]\right] \\ &= \overleftarrow{\exp}\left[-\frac{i}{\hbar}\int_{t''-t_0^A}^{t'-t_0^A} dt[H_\alpha^o + H_\alpha'(t)]\right] \\ &\equiv \overline{U}_\alpha(\tau'^A,\tau''^A), \end{aligned} \tag{16}$$

where $\alpha = a, a'$ and the arrow indicates time ordering in the expansion of the exponential. Analogously

$$U_\beta(t',t'') \equiv \overline{U}_\beta(\tau'^B,\tau''^B), \tag{17}$$

with $\beta = b, b'$. Now Eq. (15) can be rewritten as

$$|\Psi(t)\rangle = \overline{U}_{b'}(\tau^B,\tau_r^B)\overline{U}_b(\tau_r^B,0)\overline{U}_{a'}(\tau^A,\tau_s^A)U_c(t_r^B,t_s^A) \times \overline{U}_a(\tau_s^A,0)|\Psi\rangle. \tag{18}$$

Notice that the state $|\Psi(t)\rangle$ in Eq. (18) depends on t_0^A, t_s^A, t_0^B, and t_r^B through PTIs and through the term $U_c(t_r^B,t_s^A)$, de ned in Eq. (8). As already discussed in the preceding section, the random phase φ_e present in Eq. (8) prevents Bob from recovering the CTI transit time $t_r^B - t_s^A$.

This example may be easily generalized to the case of multiple exchanges. De ne t_h^A and t_h^B the times at which the last change in Alice and Bob's Hilbert space took place, i.e., the last time at which they either sent or received a signal. Expressing it in terms of the PTIs $\tau_h^A = t_h^A - t_0^A$ and $\tau_h^B = t_h^B - t_0^B$, the state of the system is then

$$|\Psi(t)\rangle = \overline{U}_A(\tau^A,\tau_h^A)\overline{U}_B(\tau^B,\tau_h^B)U_C(t,t_h)|\overline{\Psi}\rangle, \tag{19}$$

where A, B, and C refer, respectively, to the Hilbert spaces of Alice, Bob, and the exchanged system at time t, and t_h is the last time at which the Hilbert space of the exchanged system was modi ed. As can be seen by iterating Eq. (18), the state vector $|\overline{\Psi}\rangle$ in Eq. (19) depends only on PTIs and on the transit times of the systems Alice and Bob have exchanged. To show that the state $|\Psi(t)\rangle$ of Eq. (19) does not contain useful information to synchronize their clocks, suppose that (say) Bob performs a measurement at time t. The state he has access to is given by

$$\rho_B(t) = \mathrm{Tr}_{AC}[|\Psi(t)\rangle\langle\Psi(t)|] = \overline{U}_B(\tau^B,\tau_h^B)\mathrm{Tr}_{AC}[|\overline{\Psi}\rangle\langle\overline{\Psi}|]\overline{U}_B^{\dagger}(\tau^B,\tau_h^B), \tag{20}$$

where Tr_{AC} is the partial trace over $\mathcal{H}_C$ and $\mathcal{H}_A$ and where the cyclic invariance of the trace and the commutativity of operators acting on different Hilbert space has been used. The state $\rho_B(t)$ does not depend on τ^A. The only informations relevant to clock synchronization (that connect events on Alice's side to events on Bob's side) that may be recovered are the CTI transit times of the exchanged systems. However, in the case of complete dephasing ($\epsilon=1$), these quantities are irremediably spoiled by the random phases as discussed previously.

Up to now we have shown that by exchanging physical systems and performing a measurement, Alice and Bob cannot recover suf cient information to synchronize their clocks if the environment is completely dephasing. In other words, Alice can always encode some information on the system she sends Bob, but any operation she does, will always be referred to her PTI and will thus be useless to Bob if he ignores any CTI. That is equivalent to say that Alice may always send Bob some photographs of her clock, but Bob will have no use of them, since he cannot arrange them relative to his own time axis. A better strategy could be to measure only part of their systems and employ postselection schemes. As will be shown in the following section, even in this case all their efforts are in vain if hypothesis 2 applies.

B. Postselection schemes

Allow Alice and Bob to make partial measurements on their systems. The global system evolution is no longer unitary, since the measurements will project part of the Hilbert space into the eigenstates of the measured observable. The communication of the measurement results permits the implementation of postselection schemes. We will show that also in this case, Alice and Bob cannot synchronize their clocks in presence of dephasing in the communication channel.

Using the Naimark extension [10], one can assume the projective-type measurement as the most general. Suppose that Alice performs the rst measurement at time t_m^A on a part of her system. De ne $\mathcal{H}_{A_1}$ the Hilbert space that describes such a system, so that $\mathcal{H}_A = \mathcal{H}_{A_0} \otimes \mathcal{H}_{A_1}$ is the Hilbert space of Alice. The state of the system after the measurement for $t > t_m^A$ (and before any other measurement or system exchange) is

$$|\Psi(t)\rangle = U(t,t_m^A)P(A_1)|\Psi(t_m^A)\rangle, \tag{21}$$

where $|\Psi(t_m^A)\rangle$ is given in Eq. (19) and the global evolution operator is

$$U(t,t_m^A) = \overline{U}_A(\tau^A,\tau_m^A)\overline{U}_B(\tau^B,t_m^A - t_0^B)U_C(t,t_m^A) \tag{22}$$

with $\tau_m^A = t_m^A - t_0^A$. In Eq. (21) the measurement performed by Alice on $|\Psi(t_1^A)\rangle$ is described by the projection operator

$$P(A_1)|\psi\rangle \equiv \frac{1}{||\langle\psi|\phi\rangle_{A_1}||}(|\phi\rangle_{A_1}\langle\phi|\otimes \mathbb{1}_{A_0})|\psi\rangle, \tag{23}$$

where $\mathbb{1}_{A_0}$ is the identity on $\mathcal{H}_{A_0}$, $|\phi\rangle_{A_1} \in \mathcal{H}_{A_1}$ is the eigenstate relative to Alice's measurement result ϕ. Notice that Eqs. (21–23) take into account the postselection scheme in which Alice communicates her measurement result to Bob, since the operator $U(t,t_m^A)$ can depend on Alice's measurement result ϕ. Using again the commutation properties between operators that act on different spaces, Eq. (21) simpli es to

$$|\Psi(t)\rangle = \overline{U}_B(\tau^B,\tau_h^B)U_C(t,t_h)\overline{U}_A(\tau^A,\tau_m^A) \times P(A_1)\overline{U}_A(\tau_m^A,\tau_h^A)|\overline{\Psi}\rangle. \tag{24}$$

Equation (24) shows that even though the partial measurement introduces a nonunitary evolution term, this allows Alice to encode in the state only information about her PTI τ_m^A and nothing on the absolute time t_m^A (as measured by an external clock) or on any CTI. In fact, the same considerations of Eq. (20) apply and no information relevant to clock synchronization can be extracted from the state (24). The formalism introduced also allows one to consider the situation in which Alice does not look at her results (or does not communicate them to Bob): in this case, in Eq. (24) one must perform the sum on all the possible measurement results weighted by their outcome probability.

In the most general scenario Alice and Bob will perform multiple partial measurements, communicate by exchanging physical systems (as analyzed in the preceding section), and again perform partial measurements. By iterating Eq. (24) one can show that none of these efforts allows them to extract any CTI.

Before concluding, it is worth commenting on how the quantum clock synchronization scheme proposed in Ref. [3] is related to our analysis. In Ref. [3], the authors assume as a starting point that Alice and Bob share an entangled state of the form

$$|\chi\rangle=\sum_{a,b}\chi_{ab}|a\rangle|b\rangle, \tag{25}$$

where $|a\rangle$ and $|b\rangle$ are energy eigenstates of Alice's and Bob's systems, respectively, and where the sum on the indexes a and b runs over nondegenerate eigenstates. From the considerations given in the present section, one can show that, in the presence of a dephasing channel, such a state cannot be obtained starting from the initial state given in Eq. (3) without introducing some stochastic phases in it. For this reason, it cannot be obtained without relaxing hypothesis 2: such a protocol is then equivalent to classical protocols [4]. In fact, if one relaxes the hypotheses of channel dephasing, then it is possible to also achieve classical clock synchronization.

CONCLUSION

In conclusion, a de nition of clock synchronization was given and it was shown that, under some very general hypotheses that preclude the possibility of employing classical protocols, such a synchronization is not possible. This does not imply that quantum mechanics may not be exploited in the clock synchronization procedures, but it may be limited only to enhancing classical clock synchronization protocols [6–8]. Indeed, we have shown elsewhere [8] that quantum mechanics may be used to cancel the effect of dispersion in clock synchronization.

ACKNOWLEDGMENTS

We wish to acknowledge support from DARPA Grant No. F30602-01-2-0546 under the QUIST program, ARO Grant No. DAAD19-001-0177 under the MURI program, and NRO Grant No. NRO-000-00-C-0158.

[1] A. Einstein, Ann. Phys. (Leipzig) **17**, 891 (1905).

[2] A. S. Eddington, *The Mathematical Theory of Relativity*, 2nd ed. (Cambridge University Press, Cambridge, UK, 1924).

[3] R. Jozsa, D.S. Abrams, J.P. Dowling, and C.P. Williams, Phys. Rev. Lett. **85**, 2010 (2000).

[4] E.A. Burt, C.R. Ekstrom, and T.B. Swanson, e-print quant-ph/0007030.

[5] J. Preskill, e-print quant-ph/0010098; U. Yurtsever and J. P. Dowling, Phys. Rev. A **65**, 052317 (2002).

[6] I.L. Chuang, Phys. Rev. Lett. **85**, 2006 (2000).

[7] V. Giovannetti, S. Lloyd, and L. Maccone, Nature (London) **412**, 417 (2001); V. Giovannetti, S. Lloyd, and L. Maccone, Phys. Rev. A **65**, 022309 (2002).

[8] V. Giovannetti, S. Lloyd, L. Maccone, and F.N.C. Wong, Phys. Rev. Lett. **87**, 117902 (2001).

[9] Consider, for example, a time dependent perturbation $H'_C(t)$ that acts on the system for a time δt during the interval $[t_s, t_r]$, taking the value $\hbar\Sigma_e P_e \nu_e$. Since $H'_C(t)$ is diagonal in the energy basis of H^o_C, then it is easy to derive the evolution dynamics (8).

[10] M.A. Naimark, Izv. Akad. Nauk USSR, Ser. Mat. **4**, 277 (1940); A. Peres, *Quantum Theory: Concepts and Methods*, Vol. 57 of *Fundamental Theories of Physics* (Kluwer Academic Publishers, Dordrecht, 1993).

Appendix E:

Super efficient absorption filter for quantum memory using atomic ensembles in a vapor

Alexander Heifetz [a,*], Ashish Agarwal [a], George C. Cardoso [a], Venkatesh Gopal [a], Prem Kumar [a,b], M.S. Shahriar [a,c]

[a] *Center for Photonic Communication and Computing, Department of Electrical and Computer Engineering, Robert R. McCormick School of Engineering and Applied Science, Northwestern University, Evanston, IL 60208, USA*
[b] *Department of Physics and Astronomy, North-Western University, Evanston, IL 60208, USA*
[c] *Research Laboratory of Electronics, Massachussets Institute of Technology, Cambridge, MA 02139, USA*

Received 31 October 2003; received in revised form 6 January 2004; accepted 8 January 2004

Abstract

We demonstrate how a natural rubidium vapor cell can efficiently filter out a pump beam that produces an Raman gain in the stimulated Raman process at the D2 line of ^{85}Rb. We observe a Raman gain of at least 12 dB in ^{85}Rb when the pump beam is detuned below the first transition in ^{85}Rb, while being exactly on-resonance with the first transition in ^{87}Rb. With a single pass through a second cell, we observe an attenuation of at least 30 dB of the incoming pump at 2 mW, while the probe remained unaffected. This filtering process is critical to the realization of a single photon quantum memory based on vapor cells.

PACS: 03.67.−a; 32.30.−r; 03.75.F; 32.10.B

Keywords: Quantum; Memory; Atomic; Vapor; Ensambles; Raman

Recently, proposed experimental realizations of quantum memories using halted light can be divided into three categories. They use either Bose–Einstein condensates [1,2], cryogenic solids [3] or vapor ensembles [4]. Similar processes in vapor ensembles have also been proposed to be used for quantum teleportation [5–9]. For the BEC-based memories, the main physical limitation is that the density is too low. In the case of the solid-state experiments, a potentially important constraint is the imprecision in the selection rules. The atomic vapor may be the best compromise, since it does not suffer from these two inconveniences. A possible quantum memory using an atomic vapor would involve sending one probe photon from an entangled photon pair [10] through a vapor cell, and another photon from the same pair through a different path. A pump pulse temporally

* Corresponding author. Tel.: +1-84-74913055; fax: +1-84-74914455.

E-mail address: a-heifetz@northwestern.edu (A. Heifetz).

superposed with the probe photon is sent through the memory cell to perform a Raman transition in a Λ system, and store the single photon information in the atomic coherence of the two lower levels of the Λ system. The retrieval operation can be performed by applying a reverse pump pulse. To test the photon storage, the second photon that goes through the second path is sent through a delay line to be compared later with the retrieved photon. We have been investigating the realization of such a quantum memory using rubidium. Our setup is designed to pursue this approach using two natural rubidium vapor cells (25.75% ^{87}Rb and 74.25% ^{85}Rb isotopic concentrations). Our goal is to use the Raman effect in ^{85}Rb vapor to store a single photon [8,12–14] and then to retrieve the photon in a manner that validates the quantum nature of the storage process. In order to detect single photons at the Raman-shifted frequency, one needs to suppress the pump while leaving the Raman-shifted signal intact. The problem of pump suppression is particularly formidable since pump power on the order several hundreds of milliwatts is typically used to produce the Raman effect in the inhomogeneously broadened atomic vapor. Consider for example the case where the stored photon has a temporal duration of 100 ns. For a pump power of 100 mW at 780 nm we need an extinction ratio of about 130 dB. Typically, the pump and probe polarizations are orthogonal, so that a polarizing beam splitter is used to separate them. But the extinction ratio for this process is not good enough. Another potential source of problem is that the pump polarization is modified due to optical activity in the vapor cell [7]. A usual way to filter out one of two very closely separated frequencies is by means of gratings or Fabry–Perot cavities. Gratings are not well suited, because they produce signal scattering. For a filter based on a Fabry–Perot cavity, in order to prevent the concomitant attenuation of the weak field, one would need a very high finesse, such as in the scheme used in [9–11]. Such a cavity requires complicated electronics for stabilization [15]. Furthermore, the transmitted signal is still attenuated significantly, which is highly undesirable in single photon experiments, since it decreases the fidelity of the measurement.

In this letter, we show a serendipitous method to suppress the pump beam very efficiently. In order to illustrate this method it is useful to describe the transitions used in the system. Specifically, we use the hyperfine sublevels of ^{85}Rb for the Λ system. The transitions are illustrated in

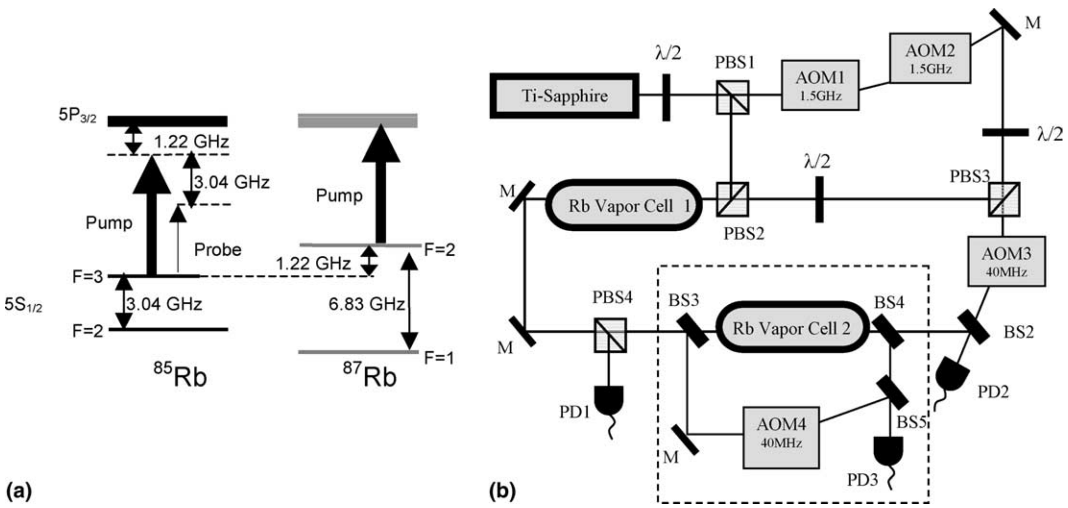

Fig. 1. (a) Energy diagrams in ^{85}Rb and ^{87}Rb isotopes and stimulated Raman process on ^{85}Rb. Notice that the pump field is coincidentally resonant with the ^{87}Rb transition $5S_{1/2}$, $F = 2 \rightarrow 5P_{3/2}$. (b) Experimental Setup. The pump and probe beams are combined at PBS2. The Fabry–Perot cavity is not shown.

Fig. 1(a). Notice that while the probe frequency is always detuned by more than 1 GHz for both rubidium isotopes, the pump frequency happens to coincide with an absorption line of ^{87}Rb. Ordinarily, this is a concern, since this would cause undesirable pump attenuation. However, as described later, we have found that it is possible to observe strong Raman gain under this condition. On the other hand, the presence of this absorption line gives us a naturally occurring filter for the pump, to be realized by a separate cell. In what follows, first we show that the presence of pump absorption does not prevent the Raman gain. Then we show the efficiency of the filter effect.

The use of a vapor cell in general or neighboring isotopic transitions in rubidium in particular for filtering is not new by itself. However, for the objective at hand, the efficiency of the process is not obvious a priori. This is because there is potentially a wide range of detunings that can be employed for the Raman gain process. For example, if one were to use ^{87}Rb transitions, with the pump detuned below the first resonance or above the second resonance, the pump would not be on resonance with any transitions. While absorptive filtering using another cell would still be possible, the attenuation per pass would be rather small, requiring so many passes through the cell that residual scattering and attenuation from the cell windows would become a dominant source of loss for the probe. Even for ^{85}Rb, there are many potential choices of the pump frequency for which the filtering process would be inefficient and ineffective. For example, if trapped atoms were used instead of a vapor cell, the optimal detuning of the pump below the first resonance, which depends on the inhomogeneous broadening of the ensemble, is likely to be less than 1 GHz due to the comparatively negligible Doppler width of the cold atoms. Even for the hot atoms in the vapor, there is no apparent reason to expect that the optimum Raman gain should occur for a pump frequency that is on resonance with the first ^{87}Rb transition. In our experiment, it is accidentally the case that the optimum Raman gain occurs – for a wide range of pump intensities – under precisely this condition. This result also shows that all else being equal (which may not necessarily be the case), one would benefit from using ^{85}Rb as the medium for the quantum memory, as opposed to ^{87}Rb.

The experiment was performed using a Ti:Sapphire laser pumped by an argon-ion laser. Each vapor cell is a heat-pipe oven with a 5-cm active length and a 0.5-cm diameter, containing natural rubidium under a 30-mTorr vacuum maintained by a mechanical pump. As shown in Fig. 1(b), the Ti:Sapphire laser beam is divided by a polarizing beam splitter (PBS1) into two orthogonally polarized beams. We produce the probe beam by redshifting a part of the pump beam by about 3.04 GHz (corresponding to the ground state hyperfine splitting of ^{85}Rb), using two cascaded 1.52 GHz acousto-optical modulators (AOM), as shown in Fig. 1(b). For diagnostic purposes, part of the probe beam undergoes an additional frequency shift with a 40-MHz AOM (the choice of 40 MHz is due simply to the availability of an efficient AOM at this frequency, and has nothing to do with the fact that the hyperfine splitting frequency happens to be about 40 MHz higher than 3 GHz, of course). The remaining part of the probe is recombined with the pump on PBS2, so that the two co-propagating beams are orthogonally polarized, as required for efficient Raman transitions in this medium. The collimated pump and probe beams are then focused onto the middle of the first rubidium vapor cell with a 50-cm focusing lens. Assuming that the pump beam is Gaussian, its beam spot size is estimated to be 68 μm, and maximum intensity is about 16 kW/cm^2. At the vapor cell output, PBS4 transmits the probe beam and reflects the pump beam. Thus PBS4 filters out most of the pump beam from the transmitted signal, and allows for monitoring the linear absorption in the vapor cell with the photo-detector 1 (PD1). A small amount of the pump that leaks through PBS4 is higher than expected for this PBS. This happens because the pump beam undergoes polarization rotation in the vapor cell due to intensity-induced birefringence in the rubidium atomic vapor. While determining the Raman gain in the first cell, the second cell is kept cold, so that the part of the optical circuit enclosed in the dashed square in Fig. 1(b) does not participate actively in this part of the process. The oven of the first vapor cell is kept at 170 °C. The Raman-amplified probe is mixed with the 40 MHz-shifted probe on a 50/50 non-polarizing beam splitter (BS2) to give a 40MHz beat signal on PD2. The signal level with the pump blocked is recorded on the spectrum analyzer (Fig. 2(a)). Unblocking the pump increases the beat signal amplitude by 12 dB (Fig. 2(b)). Maximum gain occurs when the Ti:Sapphire laser frequency is detuned 1.22 GHz away from the first ^{85}Rb transition line ($F = 3 \rightarrow 5S_{3/2}$), which coincides with the ^{87}Rb $F = 2 \rightarrow 5S_{3/2}$ transition (Fig. 1(a)). The gain is maximum at the peak pump power mentioned above, and is still observable even when the pump is attenuated by 15 dB. Significantly, the location of the peak gain as a function of pump frequency remains the same over this range of pump powers. The Raman gain decreases gradually when the Ti:Sapphire laser frequency is tuned away from the ^{87}Rb, $F = 2 \rightarrow 5S_{3/2}$ transition. The gain profile as a function of frequency is asymmetric around the peak, as documented previously for the Raman gain process [12–14].

The second cell, operated with its oven at 160 °C, acts as the frequency filter to suppress the residual pump co-propagating with the Raman signal (dashed line inset in Fig. 1(b)). The pump beam is seen to be strongly absorbed in the second vapor cell because it is on-resonance with the ^{87}Rb $F = 2 \rightarrow 5P_{3/2}$ transition line. To verify the absorption levels in spectrally resolved probe and pump, we installed a Fabry–Perot cavity (not shown in the figure) with 95% reflectivity mirrors after the second vapor cell. When the pump frequency is red-detuned by several GHz below the ^{87}Rb $5S_{1/2}$, $F = 2 \rightarrow 5P_{3/2}$ transition, we observe both the pump and the probe in the Fabry–Perot spectrum (Fig. 3(a)). As the laser frequency approaches the ^{87}Rb $5S_{1/2}$, $F = 2 \rightarrow 5P_{3/2}$ transition frequency, the pump signal gradually decreases in the Fabry–Perot spectrum. When the laser is exactly on-resonance with the ^{87}Rb transition, the pump signals is strongly suppressed, while the

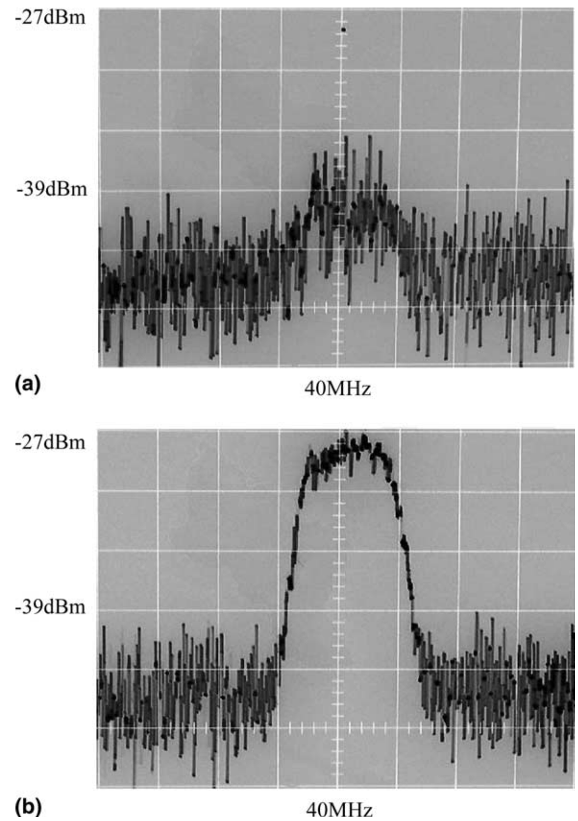

Fig. 2. Stimulated Raman gain. The vertical axis (4 dB/div scale) represents the amplitude of the beat signal of the probe beam going through the cell with the 40 MHz-shifted reference probe. The horizontal axis is on a 5 kHz/div frequency scale. (a) Pump is off. The beating signal peak of 40 MHz is at −39 dBm, or 6 dB above the noise level. (b) Pump is on. The beating signal peak shows a Raman gain of 12 dB as compared to (a).

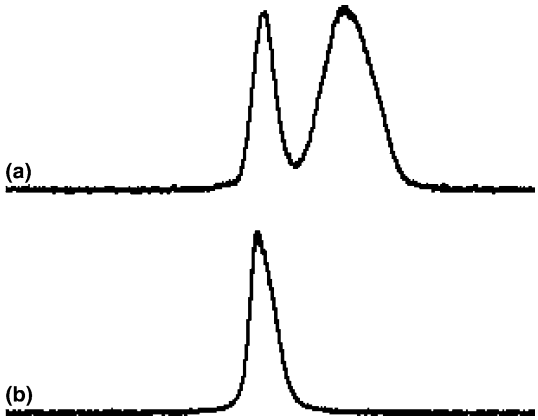

Fig. 3. (a) Pump and probe are spectrally resolved in the Fabry–Perot cavity when the pump is far detuned from the ^{87}Rb $5S_{1/2}$, $F = 2 \rightarrow 5P_{3/2}$ transition. (b) Pump disappears from the Fabry–Perot spectrum when it is on resonance with ^{87}Rb $5S_{1/2}$, $F = 2 \rightarrow 5P_{3/2}$ transition.

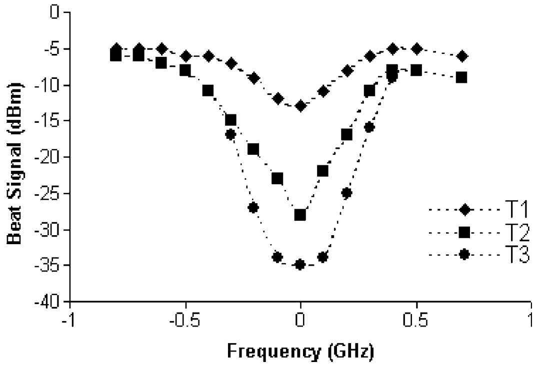

Fig. 4. Absorption increases with increasing oven temperatures ($T_1 = 110$ °C, $T_2 = 150$ °C, $T_3 = 160$ °C). Maximum signal attenuation of 30 dB is observed at the zero frequency, which corresponds to the ^{87}Rb $5S_{1/2}$, $F = 2 \rightarrow 5P_{3/2}$ transition.

probe signal remains unchanged (Fig. 3(b)). Next, we blocked the probe beam (by turning off the 1.52 GHz AOMs), removed the Fabry–Perot cavity and set up a detection scheme to quantify the pump absorption level, starting with the temperature dependence of the absorption (Fig. 4). We split the pump on a 50/50 non-polarizing beam splitter (BS3) just before the entrance to the second vapor cell. Half of the pump beam passes through the second Rb vapor cell, while the other half is frequency-shifted by 40 MHz by AOM4. The beams are recombined on a 50/50 non-polarizing beam splitter (BS5), and the 40 MHz beating signal detected by PD3 is displayed on the spectrum analyzer. When the laser frequency is on-resonance with the first ^{87}Rb transition, the incident pump beam at 2mW is absorbed down to the noise level, or at least by 30 dB. In Fig. 4, we show the absorption profiles as functions of the pump detuning around the ^{87}Rb $5S_{1/2}$, $F = 2 \rightarrow 5P_{3/2}$ transition for different oven temperatures. The maximum pump absorption increases with temperature as expected. We could attain further attenuation by multiple passes through the cell because absorption in this regime is a linear process. The number of passes necessary would be only a few (say 4), so that degradation of the probe from the AR-coated windows would be negligible.

We have demonstrated that the pump beam that produces Raman amplification of the probe of up to 12 dB in ^{85}Rb of a natural Rb vapor cell can be attenuated on a single pass by at least 30 dB with ^{87}Rb of another natural Rb vapor cell, while the probe/signal is not affected. This makes a super-efficient frequency selective filter that may be very useful to simplify single photon experiments involving Raman gains in rubidium vapor.

Acknowledgements

This work was supported by DARPA Grant #F30602-01-2-0546 under the QUIST program, and ARO Grant #DAAD19-001-0177 under the MURI program.

References

[1] L.V. Hau, S.E. Harris, Z. Dutton, C.H. Behroozi, Nature 397 (1999) 594.
[2] C. Liu, Z. Dutton, C.H. Behroozi, L.V. Hau, Nature 409 (2001) 490.
[3] A.V. Turukhin, V.S. Sudarshanam, M.S. Shahriar, J.A. Musser, B.S. Ham, P.R. Hemmer, Phys. Rev. Lett. 88 (2002) 023602.
[4] M.M. Kash et al., Phys. Rev. Lett. 82 (1999) 5229; D.F. Phillips et al., Phys. Rev. Lett. 86 (2001) 783.
[5] L.-M. Duan, M.D. Lukin, J.I. Cirac, P. Zoeller, Nature 414 (2001) 413.
[6] L.-M. Duan, J.I. Cirac, P. Zoller, Phys. Rev. A 66 (2002) 023818.
[7] W. Happer, Rev. Mod. Phys. 44 (1972) 169.
[8] C.H. van der Wal, M.D. Eisman, A. Andre, R.L. Walsworth, D.F. Phillips, A.S. Zibrov, M.D. Lukin, Science 301 (2003) 196.
[9] M.D. Lukin, Rev. Mod. Phys. 75 (2003) 457.
[10] P.G. Kwiat, E. Waks, A.G. White, I. Appelbaum, P.H. Eberhard, Phys. Rev. A 60 (1999) 773.
[11] P.G. Kwiat, K. Mattle, H. Weinfurter, A. Zeilinger, A.V. Sergienko, Y. Shih, Phys. Rev. Lett. 75 (1995) 4337.
[12] P. Kumar, J.H. Shapiro, Opt. Lett. 10 (1985) 226.
[13] M. Poelker, P. Kumar, S.-T. Ho, Opt. Lett. 16 (1991) 1853.
[14] M. Poelker, P. Kumar, Opt. Lett. 17 (1991) 399.
[15] H. Mabuchi, J. Ye, H.J. Kimble, Appl. Phys. B 68 (1999) 1095.

Appendix F:

Lorentz-invariant look at quantum clock-synchronization protocols based on distributed entanglement

Ulvi Yurtsever and Jonathan P. Dowling
Quantum Computing Technologies Group, Jet Propulsion Laboratory, California Institute of Technology, 4800 Oak Grove Drive, Pasadena, California 91109-8099
(Received 20 November 2000; published 6 May 2002)

Recent work has raised the possibility that quantum-information-theory techniques can be used to synchronize atomic clocks nonlocally. One of the proposed algorithms for quantum clock synchronization (QCS) requires distribution of entangled pure singlets to the synchronizing parties [R. Jozsa *et al.*, Phys. Rev. Lett. **85** 2010 (2000)]. Such remote entanglement distribution normally creates a relative phase error in the distributed singlet state, which then needs to be puri ed asynchronously. We present a relativistic analysis of the QCS protocol that shows that asynchronous entanglement puri cation is not possible, and, therefore, the proposed QCS scheme remains incomplete. We discuss possible directions of research in quantum-information theory, which may lead to a complete, working QCS protocol.

I. INTRODUCTION: A QUANTUM PROTOCOL FOR CLOCK SYNCHRONIZATION

Suppose a supply of identical but distinguishable two-state systems (e.g., atoms) is available whose between-state transitions can be manipulated (e.g., by laser pulses). Let $|1\rangle$ and $|0\rangle$ denote, respectively, the excited and ground states of the prototype two-state system (which span the internal Hilbert space $\mathcal{H}$), and let the energy difference between the two states be Ω (we will use units in which $\hbar=c=1$ throughout this paper). Without loss of generality, we can assume

$$\hat{H}_0|0\rangle=0, \quad \hat{H}_0|1\rangle=\Omega|1\rangle, \tag{1}$$

where $\hat{H}_0$ denotes the internal Hamiltonian operator. Suppose pairs of these two-state systems are distributed to two spatially separated observers Alice and Bob. The Hilbert space of each pair can be written as $\mathcal{H}_A\otimes\mathcal{H}_B$, where $\otimes$ denotes the tensor product of the two vector spaces. A ("perfect") singlet is the speci c entangled quantum state in this product Hilbert space given by

$$\Psi=\frac{1}{\sqrt{2}}(|0\rangle_A\otimes|1\rangle_B-|1\rangle_A\otimes|0\rangle_B). \tag{2}$$

[In what follows, we will omit tensor-product signs in expressions of the kind of Eq. (2) unless required for clarity.] Two important properties of the singlet state Ψ are as follows. (i) It is a "dark" state (invariant up to a multiplicative phase factor) under the time evolution $\hat{U}_t\equiv\exp(it\hat{H}_0)$, i.e., $(\hat{U}_t\otimes\hat{U}_t)\Psi=e^{i\phi}\Psi$, where $e^{i\phi}$ is an overall phase, and (ii) it is similarly invariant under all unitary transformations of the form $\hat{U}\otimes\hat{U}$, where $\hat{U}$ is any arbitrary unitary map on $\mathcal{H}$ (not necessarily equal to $\hat{U}_t$). Both properties are needed for the quantum clock-synchronization (QCS) protocol of Jozsa *et al.* [1], which assumes a supply of such pure singlet states shared as a resource between the synchronizing parties Alice and Bob (in addition, Bob and Alice are assumed to be stationary with respect to a common reference frame). Speci -cally, consider the unitary (Hadamard) transformation ($\pi/2$ pulse followed by the spin operator $\hat{\sigma}_z$) on $\mathcal{H}$ given by

$$|0\rangle\mapsto|+\rangle\equiv\frac{1}{\sqrt{2}}(|0\rangle+|1\rangle),$$

$$|1\rangle\mapsto|-\rangle\equiv\frac{1}{\sqrt{2}}(|0\rangle-|1\rangle). \tag{3}$$

Unlike the states $|0\rangle$ and $|1\rangle$, which are dark under time evolution (they only pick up an overall phase under $\hat{U}_t$), the states $|+\rangle$ and $|-\rangle$ are "clock states" (in other words, they accumulate an observable relative phase under $\hat{U}_t$) because of the energy difference Ω as speci ed in Eq. (1). Such states can be used to "drive" precision clocks in the following way: Start, for example, with an ensemble of atoms in the state $|+\rangle$ produced by an initial Hadamard pulse at time t_0, and apply a second Hadamard pulse at a later time t_0+T. This leads to a nal state at t_0+T equivalent, up to an overall phase factor, to the state

$$\cos\left(\frac{\Omega}{2}T\right)|0\rangle+i\sin\left(\frac{\Omega}{2}T\right)|1\rangle. \tag{4}$$

Measurement of the statistics (relative populations) of ground vs excited atoms in the state Eq. (4) then yields a precision measurement of the time interval T; hence clock functionality for $|+\rangle$. [In practice, such measurements are used to stabilize the frequency of a relatively noisy local oscillator (typically a maser), whose (stabilized) oscillations then drive the ultimate clock readout.] Now, the invariance of the pure singlet Ψ [Eq. (2)] under the Hadamard transformation Eq. (3) can be seen explicitly in the alternative representation

$$\Psi = \frac{1}{\sqrt{2}}(|-\rangle_A \otimes |+\rangle_B - |+\rangle_A \otimes |-\rangle_B). \tag{5}$$

Here, in Eq. (5), we have the crux of the QCS algorithm of Ref. [1]: The dark, invariant state Ψ, shared between Alice and Bob, contains two clock states, one for each observer, entangled in such a way as to "freeze" their time evolution. As soon as Bob or Alice performs a measurement on Ψ in the basis $\{|+\rangle, |-\rangle\}$, thereby destroying the entanglement, he or she starts these two dormant clocks "simultaneously" in both reference frames. Classical communications are then necessary to sort out which party has the $|+\rangle$ clock and which party has $|-\rangle$. When used to stabilize identical quantum clocks at each party's location, these correlated clock states then provide precise time synchrony between Bob and Alice [2].

It is important to emphasize that the nondegenerate nature of the singlet state Ψ [Eq. (2)] is crucial for the QCS protocol to work. This is in complete contrast with other quantum-information-theory protocols (such as teleportation [3], quantum cryptographic key distribution [4], and others) all of which will work equally well with degenerate ($\Omega = 0$) singlets.

What is the significance of entanglement in the above protocol? As has been pointed out by a number of authors [5,6] following the original publication [1], the QCS protocol is completely equivalent to slow clock transport as long as the entanglement in the singlet state Eq. (2) is distributed by transporting the entangled pairs kinematically to the synchronizing parties Alice and Bob (see also the discussion in Sec. II below). The potentially far-reaching consequences of the QCS algorithm become clear when we realize that the physical transport of entangled constituents is by no means the only way to distribute entanglement, though it is by far the most obvious.

Notice that *provided* such a "nonlocal" method of entanglement distribution is available to practically create pure singlets of the form Eq. (2), the QCS algorithm gives a way of synchronizing clocks across arbitrarily large distances, independent of the medium that separates the two atomic clocks to be synchronized—so long as a classical communications link exists between the two synchronizing parties. Since the synchrony transfer takes place instantaneously over the quantum channel, no timing information needs to be passed over the classical channel. This allows the protocol to bypass a number of noise sources present on the classical link (such as an interceding medium with fluctuating index of refraction), which currently limit the accuracy of satellite-to-satellite and satellite-to-ground synchronization protocols.

There are a number of "nonlocal" entanglement transfer protocols that have been discussed in the theory literature, and some of these are briefly considered in Sec. VI below. Most of the rest of this paper, however, is devoted to the analysis of what is perhaps the next most obvious method of entanglement transfer: entanglement purification. The idea of entanglement purification is to distribute the entangled state, Eq. (2), to the synchronizing parties in some noisy manner (possibly via simple kinematical transport), and then to purify the resulting imperfect singlet state by using some sort of asynchronous purification protocol (i.e., one that does not rely on preestablished time synchrony between the local clocks of Alice and Bob) which may involve (asynchronous) classical communication between the parties (as well as the loss of some fraction of the noisy singlets depending on the fidelity of the original transport and the yield of the purification protocol). In this paper we will give an answer to the fundamental question: Is asynchronous entanglement purification possible?

II. THE PRESKILL PHASE OFFSET

In principle, the QCS protocol as outlined in Sec. I is rigorously correct and self-contained. If our Universe somehow possessed primordial nondegenerate singlet states Ψ (leftover as "relics" from the Big Bang), the protocol just described would be perfectly sufficient to implement ultraprecise clock synchronization between comoving distant observers. In practice, however, the QCS algorithm can reasonably be viewed as simply reducing the problem of clock synchronization to the problem of distributing pure entanglement to spatially separated regions of space-time. To see that the latter is a nontrivial problem, consider the simplest way one would attempt to distribute entanglement to remote regions: start with locally created pairs of two-level systems (atoms) in pure singlet states Ψ of the form Eq. (2), and transport the two subsystems separately to the locations of Bob and Alice. The internal Hamiltonians of the two subsystems while in transport can be written in the form

$$\hat{H}_A = \hat{H}_0 + \hat{H}_A{}^{\mathrm{ext}}, \quad \hat{H}_B = \hat{H}_0 + \hat{H}_B{}^{\mathrm{ext}}, \tag{6}$$

where $\hat{H}_A{}^{\mathrm{ext}}$ and $\hat{H}_B{}^{\mathrm{ext}}$ denote interaction Hamiltonians arising from the coupling of each subsystem to its external environment, and, unless the environment, which each subsystem is subject to during transport is precisely controlled, $\hat{H}_A{}^{\mathrm{ext}} \neq \hat{H}_B{}^{\mathrm{ext}}$ in general, leading to a relative phase offset in the final entangled state. Furthermore, unless the world lines of the transported subsystems are arranged to have precisely the same Lorentz length (proper time), a further contribution to this phase offset would occur due to the proper-time delay between the two world-lines (see also the discussion in Sec. IV below). The end result is an imperfect singlet state

$$\Psi_\delta = \frac{1}{\sqrt{2}}(|0\rangle_A |1\rangle_B - e^{i\delta}|1\rangle_A |0\rangle_B), \tag{7}$$

where δ is a real phase offset that is fixed but entirely unknown, which we call "the Preskill phase" in honor of its original discoverer [6]. In general, coupling to the environment will lead to other errors such as bit flips and decoherence, resulting in a mixed state at the end of the transport process. These kinds of errors, however, are correctable (after restoring energy degeneracy to the qubit basis $\{|0\rangle, |1\rangle\}$ if necessary) by using standard entanglement purification techniques [7]. The phase error in Eq. (7), however, is inextricably mixed with the synchronization offset between Alice and Bob, as we will argue below, and it cannot be puri ed asynchronously.

Although Ψ_δ is still a dark state under time evolution, it no longer has the key property of invariance under arbitrary unitary transformations $\hat{U}\otimes\hat{U}$. In particular, an equivalent form in terms of entangled clock states [such as in Eq. (5)] is not available for Ψ_δ [8]. Instead,

$$\Psi_\delta=\left(\frac{1+e^{i\delta}}{2\sqrt{2}}\right)(|-\rangle_A|+\rangle_B-|+\rangle_A|-\rangle_B) + \left(\frac{1-e^{i\delta}}{2\sqrt{2}}\right)(|+\rangle_A|+\rangle_B-|-\rangle_A|-\rangle_B), \tag{8}$$

and a measurement by Bob or Alice in the $\{|+\rangle,|-\rangle\}$ basis will leave the other party's clock in a superposition of clock states $|+\rangle$ and $|-\rangle$, which, if Bob and Alice were to follow the above QCS protocol blindly, effectively introduces an (unknown) synchronization offset of $-\delta/\Omega$ between them.

III. QCS AS TELEPORTATION OF CLOCKS

This connection between δ and the time-synchronization offset is much easier to understand by adopting a different point of view for the QCS protocol: one which is based on teleportation [3]. Accordingly, the essence of the QCS protocol can be viewed as the teleportation of clock states between Bob and Alice using the singlet states Ψ (or, in the present case, the imperfect singlets Ψ_δ). More explicitly, suppose Bob and Alice arrange, through prior classical communications, the teleportation of a known quantum state $\alpha|0\rangle_{B'}+\beta|1\rangle_{B'}\in\mathcal{H}_{B'}$ from Bob to Alice via the singlet Ψ_δ. Since the teleported state, as well as Bob's Bell-basis states [3]

$$\Psi^\pm\equiv\frac{1}{\sqrt{2}}(|0\rangle_B|1\rangle_{B'}\pm|1\rangle_B|0\rangle_{B'}),$$

$$\Phi^\pm\equiv\frac{1}{\sqrt{2}}(|0\rangle_B|0\rangle_{B'}\pm|1\rangle_B|1\rangle_{B'}) \tag{9}$$

are, in general, time dependent, the standard teleportation protocol needs to be slightly modi ed in the following way. The parties need to agree on a time, which we may take without loss of generality to be $t_B=0$ as measured by Bob's local clock, at which the following three actions will be performed instantaneously by Bob.

(i) Prepare an ancillary two-state system B' in the known quantum state $\alpha|0\rangle_{B'}+\beta|1\rangle_{B'}$, where α and β are complex numbers previously agreed on by the two parties.

(ii) Select a speci c singlet Ψ_δ as in Eq. (7), and construct a Bell basis for $\mathcal{H}_B\otimes\mathcal{H}_{B'}$ that has the form Eq. (9) at $t_B=0$.

(iii) Perform a measurement in this basis and communicate its outcome to Alice through a classical channel. Upon receipt of this outcome, Alice is then to rotate the (collapsed) quantum state of her half of the singlet Ψ_δ (now a vector in the Hilbert space $\mathcal{H}_A$) by one of the four unitary operators

$$\hat{M}_{\Psi^\pm}=\begin{pmatrix}\pm1 & 0\\ 0 & -e^{-i\Omega t_A}\end{pmatrix},$$

$$\hat{M}_{\Phi^\pm}=\begin{pmatrix}-e^{-i\Omega t_A} & 0\\ 0 & \pm1\end{pmatrix}, \tag{10}$$

depending on whether the transmitted outcome of Bob's measurement is one of Ψ^+,Ψ^-,Φ^+ or Φ^-. Here t_A denotes Alice's proper time (as measured by her local clock) at the moment she performs her unitary rotation. Now let the (unknown) synchronization offset between Bob and Alice be τ, so that $t_B=t_A+\tau$. It is easy to show that the state teleported to Alice under this arrangement will have the form

$$\alpha|0\rangle_A+e^{i(-\Omega\tau+\delta)}\beta|1\rangle_A, \tag{11}$$

as obtained by Alice immediately following her unitary operation (one of $\hat{M}_{\Psi^\pm}$, $\hat{M}_{\Phi^\pm}$ [Eqs. (10)]) on $\mathcal{H}_A$.

A number of key results can now be easily read out from Eq. (11).

(1) If $\delta=0$, i.e., under the same assumption as in the original QCS protocol [1] that the shared singlet states are pure, the time-synchronization offset τ can be immediately determined by Alice (recall that α and β are known to both parties). Hence, the synchronization result of the QCS protocol can equivalently be achieved through teleportation.

(2) Conversely, if $\tau=0$, i.e., if Bob and Alice have their clocks synchronized to begin with, or if $\Omega=0$, i.e., if the qubits spanning the local Hilbert spaces $\mathcal{H}_A$ and $\mathcal{H}_B$ are degenerate, then δ can be immediately determined by Alice. Hence, puri cation of the phase-offset singlet Ψ_δ is possible under either of these two conditions.

(3) If, on the other hand, none of the quantities Ω,τ, and δ vanish, then the two unknowns τ and δ are inextricably mixed in the only phase observable $-\Omega\tau+\delta$, and asynchronous puri cation cannot be achieved via teleportation.

This last conclusion can be greatly clari ed and strengthened by a Lorentz-invariant formulation of the above teleportation protocol (which, as we just argued, is equivalent to the original QCS), and it is this formulation we will turn to next.

IV. LORENTZ-INVARIANT ANALYSIS OF QCS

The key ingredient in any relativistic discussion of quantum-information theory is the space-time dependence of the qubit states. The "true" Hilbert space to which the quantum state of a singlet belongs is, accordingly, $L^2(\mathbf{R}^4)\otimes\mathcal{H}_A\otimes L^2(\mathbf{R}^4)\otimes\mathcal{H}_B$, where each $L^2(\mathbf{R}^4)$ is supposed to account for the space-time wave function of each two-state system in the entangled pair [for simplicity (but without any loss of generality), we consider only scalar (as opposed to spinor) qubits]. We will assume in what follows that background space-time is at (Minkowski), and that the space-time dependence of each system's wave function can be approximated by that of a plane wave. In a more careful treatment, plane waves should be replaced by localized, normalizable wave packets.

We emphasize that a fully relativistic theory of quantum information would have to be formulated in the framework of relativistic quantum eld theory. Since such a full- edged formalism does not yet exist, we will con ne our attention to a naive, " rst-quantized' ' analysis, which is adequate for a qualitative understanding of the role of Lorentz invariance in QCS.

Denote the four-velocities of Alice and Bob by u_A and u_B, respectively, so that $u_A \cdot u_A = u_B \cdot u_B = -1$ [we will adopt the sign convention in which Minkowski metric on $\mathbf{R}^4$ has the form $\eta = -dt \otimes dt + dx \otimes dx + dy \otimes dy + dz \otimes dz$, and use the abbreviation $a \cdot b$ to denote $\eta(a,b)$ for any two four-vectors a and b]. The wave four-vectors of Alice's and Bob's atoms then have the form

$$k^0{}_J = m_0 u_J, \quad k^1{}_J = (m_0 + \Omega) u_J, \tag{12}$$

where m_0 is the ground-state rest mass of each (identical) two-level atom, and $k^0{}_J$ and $k^1{}_J$ denote the wave vectors corresponding to the ground and excited states of the atoms, respectively, where $J = A,B$. The plane-wave space-time dependence of the wave functions corresponding to the ground and excited states of each of the atoms can then be written in the form

$$|0\rangle_J \rightarrow e^{ik^0{}_J \cdot x}|0\rangle_J, \quad |1\rangle_J \rightarrow e^{ik^1{}_J \cdot x}|1\rangle_J, \tag{13}$$

where $J = A,B$, and x denote an arbitrary point (event) in space-time (a four-vector). Simple algebra then shows that, up to an overall phase factor (which can always be ignored), the wave function corresponding to the singlet state Eq. (7) can be expressed as a two-point space-time function of the form

$$\Psi_\delta(x_1,x_2) = |0\rangle_A |1\rangle_B - e^{i\Phi_\delta(x_1,x_2)}|1\rangle_A |0\rangle_B, \tag{14}$$

where x_1 and x_2 denote space-time points along the world lines of Alice and Bob, respectively, and $\Phi_\delta(x_1,x_2)$ is the Lorentz-invariant two-point phase function

$$\Phi_\delta(x_1,x_2) \equiv \Omega(u_A \cdot x_1 - u_B \cdot x_2) + \delta. \tag{15}$$

In the important special case where $u_A = u_B = u$, i.e., when Alice and Bob are comoving (and it makes sense to synchronize their clocks), Φ_δ takes the simpler form

$$\Phi_\delta(x_1,x_2) = \Omega u(x_1 - x_2) + \delta. \tag{16}$$

In the comoving case, Eq. (16), (when $u_A = u_B$), the singlet wave function $\Psi_\delta(x_1,x_2)$ is invariant under arbitrary Lorentz transformations including translations. This is in contrast with the general case, where the phase function $\Phi_\delta(x_1,x_2)$ [Eq. (15)] does not have translation invariance. This dependence on the choice of origin of coordinates is a manifestation of the fact that Ψ_δ is not a dark state unless $u_A = u_B$.

V. DISCUSSION: IS ASYNCHRONOUS ENTANGLEMENT PURIFICATION POSSIBLE?

The teleportation protocol of Sec. III (which is equivalent to the original QCS protocol of [1]) demonstrates that as long as x_1 and x_2 are timelike separated events in space time, the relative phase $\Phi_\delta(x_1,x_2)$ can be directly observed by Alice and Bob via quantum measurements followed by classical communication of the outcomes. An observation of $\Phi_\delta(x_1,x_2)$ would commence by the selection by Alice and Bob of space-time points x_1 and x_2 along their respective world lines at which they wish to measure this invariant phase function. Bob then would carry out his part of the teleportation protocol of Sec. III at his proper time corresponding to the event x_2, and broadcast the outcome to Alice along a nonspacelike communication path that reaches Alice before x_1. Alice would subsequently apply her unitary rotation [Eqs. (10)] sharp at her proper time corresponding to the event x_1. The resulting teleported state then has the form Eq. (11), where the relative phase is precisely $\Phi_\delta(x_1,x_2)$. Conversely, since the wave function contains all knowledge that can ever be obtained about a quantum system, the *only* (classical) observable associated with the singlet state Ψ_δ that contains any information about δ is $\Phi_\delta(x_1,x_2)$.

Focusing now on the comoving case $u_A = u_B$, the above fact implies that the phase offset δ *cannot* be observed in isolation; only the combination two-point function $\delta + \Omega u(x_1 - x_2)$ [Eq. (16)] is accessible to direct measurement. On the other hand, clock synchronization between Bob and Alice is equivalent to identi cation of pairs of events $(x_1^{(i)},x_2^{(i)})$ such that $u(x_1^{(i)} - x_2^{(i)}) = 0$. Therefore, by making a sequence of measurements of the relative phase function $\Phi_\delta(x_1,x_2)$, Alice and Bob can use the singlets Ψ_δ as a shared quantum-information resource to (i) synchronize their clocks if $\delta = 0$, and (ii) measure and purify δ if they have synchronized clocks to start with. In the general case of an unknown δ and an unknown time-synchronization offset, however, δ by itself is not observable, and, consequently, Ψ_δ cannot be puri ed without rst establishing time synchrony between the two parties.

Note that this argument is *completely independent* of the particular protocol that may be used to purify the entanglement Eq. (7). Instead, the argument relies entirely on the nature of the space-time wave function describing an entangled pair, and this "universality" is its primary signi cance. The crucial observation is that the invariant two-point phase function $\Phi_\delta(x_1,x_2)$ is the *only* observable in the singlet state Eq. (7), and this function depends not only on the *a priori* relative phase δ, but also, through its dependence, on *both* x_1 and x_2, on the *a priori* time-synchrony information between Alice and Bob. Since the relative-phase information cannot be separated from time-synchrony information as long as the qubits remain nondegenerate, no protocol that does not rely on prior time synchrony in an essential way can purify the entanglement so as to distill pure ($\delta = 0$) entangled pairs.

VI. CONCLUSIONS AND FUTURE WORK

By using entangled (nondegenerate) qubits as a resource shared between spatially separated observers, the QCS protocol as reformulated above in Secs. III–V allows the direct measurement of certain nonlocal, covariant phase functions on space-time. Moreover, this functionality of the protocol is straightforward to generalize to many-particle entanglement [9]. While these results give hints of a profound connection between quantum information and space-time structure, they fall just short of providing a practical clock-synchronization algorithm because of the uncontrolled phase offsets [e.g, δ in Eq. (7)] that arise inevitably during the distribution of entanglement. Since, as we showed above, these phase offsets cannot be puri ed asynchronously after they are already in place, a successful completion of the (singlet based) QCS algorithm would need some method of entanglement distribution that avoids the accumulation of relative phase offsets. We believe a complete clock-synchronization algorithm based on quantum information theory will likely result from one of the following approaches.

"Phase-locked" entanglement distribution. It may be possible to use the inherent nonlocal (Bell) correlations of the singlet states (which remain untapped in the current QCS protocol), and implement a "quantum feedback loop," which, during entanglement transport, will help keep the phase offset δ vanishing to within a small tolerance of error. For example, states of the form

$$\frac{1}{\sqrt{2}}(|0\rangle_A|1\rangle_{A'}|1\rangle_B|0\rangle_{B'}-|1\rangle_A|0\rangle_{A'}|0\rangle_B|1\rangle_{B'}), \quad (17)$$

where two pairs of atoms (the primed and the unprimed pair) are entangled together, are not only dark but also immune to phase offsets during transport of the pairs to Alice and Bob (provided both pairs are transported along a common world line through the same external environment). Can such phase-offset-free states be used to control the purity of singlets during transport?

Entanglement distribution without transport. Physically moving each prior-entangled subsystem to its separate spatial location is not the only way to distribute entanglement. An intriguing idea, recently discussed by Cabrillo *et al.* [10], proposes preparing two spatially separated atoms in their long-lived excited states $|1\rangle_A|1\rangle_B$. A single-photon detector, which cannot (even in principle) distinguish the direction from which a detected photon arrives, is placed halfway between the atoms. When one of the atoms makes a transition to its ground state, and the detector registers the emitted photon, the result of its measurement is to put the combined two-atom system into the entangled state

$$\frac{1}{\sqrt{2}}(|0\rangle_A|1\rangle_B+e^{i\phi}|1\rangle_A|0\rangle_B), \quad (18)$$

where ϕ is a random phase. Is there a similar procedure (based on quantum measurements rather than physical transport) that creates entanglement with a controlled rather than random phase offset ϕ?

Another method of entanglement distribution without transport, recently investigated in detail by Haroche and coworkers [11] is (in very rough outline) the following: Start with a single-mode cavity whose excitation frequency is tuned to Ω. Send the pair of atoms A and B into the cavity one after the other, with atom B rst. Initially, both atoms and the cavity are in their ground states

$$|0\rangle_A\otimes|0\rangle_B\otimes|0\rangle_{EM}, \quad (19)$$

where $|0\rangle_{EM}$ denotes the vacuum state of the cavity. After atom B is in the cavity, apply a $\pi/2$ pulse on it, which transforms the state Eq. (19) into

$$\frac{1}{\sqrt{2}}|0\rangle_A\otimes(|0\rangle_B\otimes|1\rangle_{EM}-|1\rangle_B\otimes|0\rangle_{EM}). \quad (20)$$

When both atoms are in the cavity, apply a second, π pulse, this time on the atom A, thereby transforming the state Eq. (20) into

$$\frac{1}{\sqrt{2}}(|1\rangle_A\otimes|0\rangle_B-|0\rangle_A\otimes|1\rangle_B)\otimes|0\rangle_{EM}, \quad (21)$$

which, for the atom pair A and B, is in the desired form Eq. (2) up to an overall phase factor. Since at each step the overall quantum state (of atoms and the electromagnetic eld) is dark, no relative phase errors can creep in, and pure entanglement distribution is achieved between atoms A and B. Can this method be adapted to design a practical entanglement transfer protocol between distant pairs of atoms using a controlled cavity environment?

Avoiding entanglement distribution altogether. Can classical techniques of clock synchronization be improved in accuracy and noise performance by combining them with techniques from quantum-information theory, which do not necessarily involve (nondegenerate) entanglement distribution? A recent proposal in this direction was made by Chuang in [12].

After this paper was submitted for publication, further ideas utilizing quantum entanglement *without* entanglement distribution to improve the accuracy of classical Einstein synchronization have been proposed in Refs. [13–15] (see also [16] for an overview).

ACKNOWLEDGMENTS

We would like to acknowledge valuable discussions with Daniel Abrams, George Hockney, and Colin Williams of the JPL Quantum Computing Technologies group. The research was carried out at the Jet Propulsion Laboratory, California Institute of Technology, under a contract with the National Aeronautics and Space Administration, and was supported by a contract with ARDA, the Department of Defense.

[1] R. Jozsa, D.S. Abrams, J.P. Dowling, and C.P. Williams, Phys. Rev. Lett. **85**, 2010 (2000).

[2] There is one additional complication in the QCS protocol, having to do with making sure that the Hadamard transforms [Eqs. (3)] performed by Alice and Bob are phase matched. This matching is equivalent to setting up a canonical isomorphism between the Hilbert spaces $\mathcal{H}_A$ and $\mathcal{H}_B$, and is relatively straightforward to implement as discussed in detail in [1]. Throughout the rest of this paper, we will assume without further comment that such an isomorphism has been set up by Alice and Bob prior to the operations under discussion; Ref. [1] should be consulted for further details.

[3] C.H. Bennett, G. Brassard, C. Crépeau, R. Jozsa, A. Peres, and W.K. Wootters, Phys. Rev. Lett. **70**, 1895 (1993).

[4] A.K. Ekert, Phys. Rev. Lett. **67**, 661 (1991).

[5] E.A. Burt, C.R. Ekstrom, and T.B. Swanson, e-print quant-ph/0007030; Phys. Rev. Lett. **87**, 129801 (2001).

[6] J. Preskill, e-print quant-ph/0010098.

[7] C.H. Bennett, D.P. DiVincenzo, J.A. Smolin, and W.K. Wootters, Phys. Rev. A **54**, 3824 (1996).

[8] If the phase offset δ were known, such an equivalent entangled-clock expression for Ψ_δ would be available in terms of modi ed clock states $|\pm_\delta\rangle_A \equiv (|0\rangle_A \pm e^{i\delta/2}|1\rangle_A)/\sqrt{2}$ and $|\pm_\delta\rangle_B \equiv (|0\rangle_B \pm e^{-i\delta/2}|1\rangle_B)/\sqrt{2}$; but if δ is unknown, Alice and Bob can instead simply purify Ψ_δ by agreeing to rotate Bob's $|0\rangle$ basis state by $e^{i\delta}$.

[9] For example, to states of the form

$$\Psi_N = \frac{1}{\sqrt{N!}} \sum_\sigma (-1)^\sigma |0\rangle_{A\sigma(1)} |1\rangle_{A\sigma(2)} \cdots |N-1\rangle_{A\sigma(N)},$$

where $A1, A2, \ldots, AN$ denote N observers who have, distributed to them, N identical atoms with N distinct internal energy levels, and the sum σ is over all permutations of $\{1,2,\ldots,N\}$. The state Ψ_N is a generalization of the singlet Ψ [Eq. (2)] in that it is invariant under $U \otimes U \otimes \cdots \otimes U$ for arbitrary unitary U.

[10] C. Cabrillo, J.I. Cirac, P. Garcia-Fernandez, and P. Zoller, Phys. Rev. A **59**, 1025 (1999).

[11] E. Hagley, X. Maˆtre, G. Nogues, C. Wunderlich, M. Brune, J.M. Raimond, and S. Haroche, Phys. Rev. Lett. **79**, 1 (1997); A. Jabs, e-print quant-ph/9811042; A. Rauschenbeutel, P. Bertet, S. Osnaghi, G. Nogues, M. Brune, J.M. Raimond, and S. Haroche, Phys. Rev. A **64**, 050301 (2001).

[12] I.L. Chuang, Phys. Rev. Lett. **85**, 2006 (2000).

[13] V. Giovannetti, S. Lloyd, and L. Maccone, e-print quant-ph/0103006.

[14] V. Giovannetti, S. Lloyd, L. Maccone, and F.N.C. Wong, Phys. Rev. Lett. **87**, 117902 (2001).

[15] V. Giovannetti, S. Lloyd, and L. Maccone, Phys. Rev. A **65**, 022309 (2002).

[16] V. Giovannetti, S. Lloyd, L. Maccone, and S.M. Shahriar, e-print quant-ph/0110156.

Appendix G:

Quantum Entanglement of Moving Bodies

Robert M. Gingrich and Christoph Adami
Quantum Computing Technologies Group, Jet Propulsion Laboratory 126-347, California Institute of Technology, Pasadena, California 91109-8099
(Received 21 June 2002; revised manuscript received 3 September 2002; published 16 December 2002)

We study the properties of quantum entanglement in moving frames, and show that, because spin and momentum become mixed when viewed by a moving observer, the entanglement between the spins of a pair of particles is not invariant. We give an example of a pair, fully spin entangled in the rest frame, which has its spin entanglement reduced in all other frames. Similarly, we show that there are pairs whose spin entanglement increases from zero to maximal entanglement when boosted. While spin and momentum entanglement separately are not Lorentz invariant, the joint entanglement of the wave function is.

Mostly, theories in physics are born out of necessity, but not always. The thermodynamics of moving bodies, for example (relativistic thermodynamics), was a hotly contested topic without resolution [1–4] (but see [5]) mostly because no experiment required it. As a side effect, it was learned that the temperature concept in relativistic thermodynamics is ambiguous simply because radiation that is perfectly blackbody in an inertial frame is *not* thermal if viewed from a moving frame [5,6]. This is an interesting result for information theory [7], however, since if probability distributions can depend on the inertial frame, then so can Shannon entropy and information. Even more interesting are the consequences for quantum information theory, where quantum entanglement plays the role of the primary resource in quantum computation and communication [8]. Relativistic quantum information theory may become a necessary theory in the near future, with possible applications to quantum teleportation [9], entanglement-enhanced communication [10], quantum clock synchronization, and quantum-enhanced global positioning [11].

Entanglement is a property unique to quantum systems. Two systems (microscopic particles or even macroscopic bodies [12]) are said to be quantum entangled if they are described by a joint wave function that cannot be written as a product of wave functions of each of the subsystems (or, for mixed states, if a density matrix cannot be written as a weighted sum of product density matrices). The subsystems can be said *not* to have a state of their own, even though they may be arbitrarily far apart. The entanglement produces correlations between the subsystems that go beyond what is classically possible [13]. It is this feature that enables quantum communication protocols such as teleportation and superdense coding. However, the preparation, sharing, and purification of entanglement is usually a complicated and expensive process that requires great care. It is therefore of some importance to understand all those processes that might affect quantum entanglement (in particular, those processes that lead to decoherence). It was shown recently that Lorentz boosts can affect the marginal entropy of a single quantum spin [14]. Here, we determine that the entanglement between *two* systems depends on the frame in which this entanglement is measured. We show that a fully entangled spin-1/2 system (a Bell state) loses entanglement if observed by a Lorentz-boosted observer. Thus, Lorentz boosts introduce a transfer of entanglement *between* degrees of freedom, that could be used for entanglement manipulation. While the entanglement between spin or momentum alone may change due to Lorentz boosts, the entanglement of the *entire* wave function (spin and momentum) is invariant.

In order to define the momentum eigenstates for a massive particle with spin, we start by defining the rest frame eigenstates,

$$P^{\mu}|\mathbf{0}\lambda\rangle = |\mathbf{0}\lambda\rangle p_0^{\mu}, \tag{1}$$

$$\mathbf{J}^2|\mathbf{0}\lambda\rangle = |\mathbf{0}\lambda\rangle s(s+1), \tag{2}$$

$$J_z|\mathbf{0}\lambda\rangle = |\mathbf{0}\lambda\rangle \lambda, \tag{3}$$

where $p_0^{\mu} = (m, \mathbf{0})$, s is the total angular momentum of the particle, and λ is the z component of angular momentum. Since the particle is at rest, s and λ are the spin and the z component of the spin for the particle, respectively.

We define a momentum state by acting on the rest frame state with a pure Lorentz boost

$$|\mathbf{p}\lambda\rangle \equiv L(\boldsymbol{\xi}_{\mathbf{p}})|\mathbf{0}\lambda\rangle, \tag{4}$$

where $L(\boldsymbol{\xi}_{\mathbf{p}})$ is a boost such that

$$L(\boldsymbol{\xi}_{\mathbf{p}})(m, \mathbf{0}) = (\sqrt{\mathbf{p}^2 + m^2}, \mathbf{p}), \tag{5}$$

where the rapidity, $\boldsymbol{\xi}_{\mathbf{p}}$, is given by

$$\sinh|\boldsymbol{\xi}_{\mathbf{p}}| = \frac{|\mathbf{p}|}{m} \tag{6}$$

$$\frac{\boldsymbol{\xi}_{\mathbf{p}}}{|\boldsymbol{\xi}_{\mathbf{p}}|} = \frac{\mathbf{p}}{|\mathbf{p}|}. \tag{7}$$

In what follows, we use $\mathbf{p}$ to represent the 4-vector $(\sqrt{\mathbf{p}^2 + m^2}, \mathbf{p})$ unless it is ambiguous.

The effect of an arbitrary Lorentz transformation Λ (rotation and boost) on a momentum eigenstate is

$$\Lambda|\mathbf{p}\lambda\rangle = \Lambda L(\boldsymbol{\xi}_{\mathbf{p}})|\mathbf{0}\boldsymbol{\lambda}\rangle \tag{8}$$

$$= L(\boldsymbol{\xi}_{\Lambda\mathbf{p}})L(\boldsymbol{\xi}_{\Lambda\mathbf{p}})^{-1}\Lambda L(\boldsymbol{\xi}_{\mathbf{p}})|\mathbf{0}\boldsymbol{\lambda}\rangle. \tag{9}$$

Since $L(\boldsymbol{\xi}_{\Lambda\mathbf{p}})^{-1}\Lambda L(\boldsymbol{\xi}_{\mathbf{p}})$ leaves $\mathbf{0}$ invariant, it must be a rotation. These rotations are called the Wigner rotations $R(\Lambda, \mathbf{p})$, and they act only on the rest frame spin component λ. Hence, we can write

$$\Lambda|\mathbf{p}\lambda\rangle = \sum_{\lambda'} |\Lambda\mathbf{p}\lambda'\rangle D^{(s)}_{\lambda',\lambda}(R(\Lambda, \mathbf{p})), \tag{10}$$

where $D^{(s)}_{\lambda',\lambda}(R)$ is the spin s representation of the rotation R. Here, we restrict ourselves to $s = 1/2$, but the generalization to larger spins is straightforward. For a review of momentum eigenstates and spin, see [15]. Since a local unitary transformation will not affect any measure of entanglement [16,17], the unitary transformation Λ on the infinite dimensional space of momentum and rest frame spin will not change the entanglement between two particles, provided we do not trace out a part of the wave function. However, in looking at the entanglement between spins, tracing out over the momentum is implied.

The wave function for two massive spin-1/2 particles can be written as

$$|\Psi_{AA'BB'}\rangle = \iint \sum_{\lambda\sigma} g_{\lambda\sigma}(\mathbf{p}, \mathbf{q})|\mathbf{p}\lambda\rangle_{AA'}|\mathbf{q}\sigma\rangle_{BB'}\tilde{\mathrm{d}}\mathbf{p}\tilde{\mathrm{d}}\mathbf{q}, \tag{11}$$

where $\tilde{\mathrm{d}}\mathbf{p}$ and $\tilde{\mathrm{d}}\mathbf{q}$ are the Lorentz-invariant momentum integration measures given by

$$\tilde{\mathrm{d}}\mathbf{p} \equiv \frac{\mathrm{d}^3\mathbf{p}}{2\sqrt{\mathbf{p}^2 + m^2}}, \tag{12}$$

and the functions $g_{\lambda\sigma}(\mathbf{p}, \mathbf{q})$ must satisfy

$$\sum_{\lambda\sigma} \iint |g_{\lambda\sigma}(\mathbf{p}, \mathbf{q})|^2\tilde{\mathrm{d}}\mathbf{p}\tilde{\mathrm{d}}\mathbf{q} = 1. \tag{13}$$

To an observer in a frame Lorentz transformed by Λ^{-1}, the state $|\Psi_{AA'BB'}\rangle$ appears to be transformed by $\Lambda \otimes \Lambda$. Using Eq. (10), and a change of variables for $\mathbf{p}$, $\mathbf{q}$, λ, and σ, $g_{\lambda\sigma}(\mathbf{p}, \mathbf{q})$ goes through the following transformation:

$$g_{\lambda\sigma}(\mathbf{p}, \mathbf{q}) \rightarrow \sum_{\lambda'\sigma'} U^{(\Lambda^{-1}\mathbf{p})}_{\lambda,\lambda'} U^{(\Lambda^{-1}\mathbf{q})}_{\sigma,\sigma'} g_{\lambda'\sigma'}(\Lambda^{-1}\mathbf{p}, \Lambda^{-1}\mathbf{q}), \tag{14}$$

where we defined

$$U^{(\mathbf{p})}_{\lambda,\lambda'} \equiv D^{(1/2)}_{\lambda,\lambda'}(R(\Lambda, \mathbf{p})) \tag{15}$$

for compactness of notation. The Lorentz transformation can be viewed as a unitary operation, $R(\Lambda, \mathbf{p})$, conditioned on $\mathbf{p}$ acting on the spin, followed by a boost $\mathbf{p} \rightarrow \Lambda\mathbf{p}$ on the momentum represented by the circuit diagram in Fig. 1.

By writing $|\Psi_{AA'BB'}\rangle$ as a density matrix and tracing over the momentum degrees of freedom, the entanglement between A and B (that is, between the spin degrees of freedom) can be obtained by calculating Wootters's concurrence [18,19]

$$C(\rho_{AB}) = \max\{\lambda_1 - \lambda_2 - \lambda_3 - \lambda_4, 0\}, \tag{16}$$

where $\{\lambda_1, \lambda_2, \lambda_3, \lambda_4\}$ are the square roots of the eigenvalues of the matrix $\rho_{AB}\tilde{\rho}_{AB}$, and $\tilde{\rho}_{AB}$ is the "time-reversed" matrix [18]

$$\tilde{\rho}_{AB} = (\sigma_y \otimes \sigma_y)\rho^{\star}_{AB}(\sigma_y \otimes \sigma_y). \tag{17}$$

The first step in calculating the Lorentz-transformed concurrence is to find an explicit form for $U^{(\mathbf{p})}_{\lambda,\lambda'}$. Since any Lorentz transformation Λ can be written as a rotation $R(\boldsymbol{\Theta})$ followed by a boost $L(\boldsymbol{\xi})$ [see also Eq. (8)], it is clear that, for a pure rotation, $U^{(\mathbf{p})}_{\lambda,\lambda'}$ does not depend on $\mathbf{p}$. Hence, tracing over the momentum after a rotation will not change the concurrence. Therefore, we can look only at pure boosts, and without loss of generality we may choose boosts in the z direction. Writing the momentum 4-vector in polar coordinates as

$$\mathbf{p} = [E, p\cos(\theta)\sin(\phi), p\sin(\theta)\sin(\phi), p\cos(\phi)], \tag{18}$$

we obtain

$$U^{(\mathbf{p})} = \begin{bmatrix} \alpha & \beta e^{-i\theta} \\ -\beta e^{i\theta} & \alpha \end{bmatrix}, \tag{19}$$

where

$$\alpha = \sqrt{\frac{E + m}{E' + m}}\left[\cosh\left(\frac{\xi}{2}\right) + \frac{p\cos(\phi)}{(E + m)}\sinh\left(\frac{\xi}{2}\right)\right], \tag{20}$$

$$\beta = \frac{p\sin(\phi)}{\sqrt{(E + m)(E' + m)}}\sinh\left(\frac{\xi}{2}\right), \tag{21}$$

and

$$E' = E\cosh(\xi) + p\cos(\phi)\sinh(\xi). \tag{22}$$

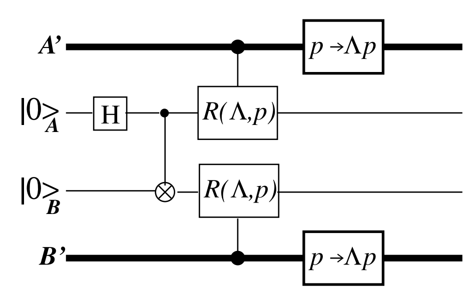

FIG. 1. Circuit diagram for a Lorentz boost on a state with spins in a $|\phi^+\rangle$ state. Lines representing momentum degrees of freedom are bold.

Here we use $\xi = |\boldsymbol{\xi}|$ as the rapidity of the boost in the z direction.

For momentum distributions in this Letter, we use a "relativistic Gaussian" with width σ_r,

$$f(\mathbf{p}) = \sqrt{\frac{1}{N(\sigma_r)} \exp-\left(\frac{p^2}{2\sigma_r^2}\right)}, \tag{23}$$

which differs from the standard Gaussian only in the normalization $N(\sigma_r)$, chosen in accordance with (12).

For a spin Bell state $|\phi^+\rangle$ with momenta in a product Gaussian, we have

$$g_{\lambda\sigma}(\mathbf{p}, \mathbf{q}) = \frac{1}{\sqrt{2}} \delta_{\lambda\sigma} f(\mathbf{p}) f(\mathbf{q}). \tag{24}$$

Boosting this state, we move some of the spin entanglement to the momentum. Tracing out the momentum from the Lorentz-transformed density matrix destroys some of the entanglement, and, hence, the concurrence in the moving frame diminishes. The change in concurrence depends only on the ratio σ_r/m and ξ. Figure 2 shows the concurrence vs rapidity ξ, for $\sigma_r/m = 1$ and 4. The decrease from the maximum value (the concurrence is one for Bell states) documents the boost-induced decoherence of the spin entanglement.

In the limit $\xi \to \infty$ (boost to the speed of light), the concurrence saturates, i.e., it reaches a constant value that depends on the mass of the particles and the shape of the momentum distribution. In this particular example, it depends on the ratio σ_r/m. The saturation level decreases as σ_r/m increases until $\sigma_r/m \simeq 3.377$ when the saturation level becomes zero. Note that in the limit of "pure" momentum states (plane waves), the spins undergo local unitary rotations but entanglement transfer does not occur, as was observed in [20,21]. The reason for the saturation can be seen by examining (19) in the limit $\xi \to \infty$,

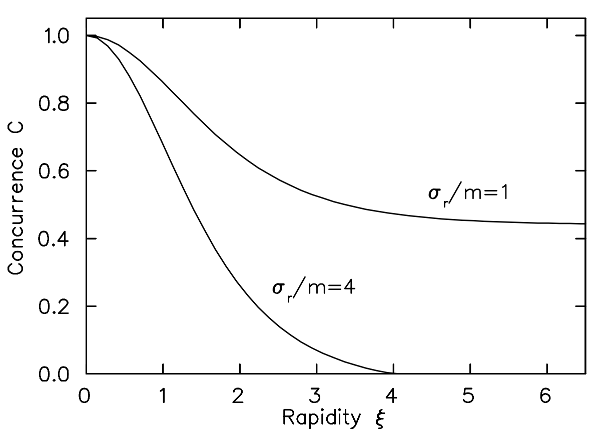

FIG. 2. Spin concurrence as a function of rapidity, for an initial Bell state with momenta in a product Gaussian. Data is shown for $\sigma_r/m = 1$ and $\sigma_r/m = 4$.

$$\lim_{\xi\to\infty} \alpha = \sqrt{\frac{E + m}{2[E + p\cos(\phi)]}}\left(1 + \frac{p\cos(\phi)}{E + m}\right), \tag{25}$$

$$\lim_{\xi\to\infty} \beta = \frac{p\sin(\phi)}{\sqrt{2(E + m)[E + p\cos(\phi)]}}. \tag{26}$$

The parameter β represents the amount of rotation due to the boost. If we maximize β with respect to ϕ, we obtain

$$\beta \to \frac{p/m}{1 + \sqrt{1 + (p/m)^2}}, \tag{27}$$

which is a monotonically increasing function of p/m. For a particle of mass m and magnitude of momentum p, Eq. (27) represents the maximal amount of rotation due to a boost. By increasing σ_r/m in our example, we effectively increase this limit for β, and, hence, how much we can alter the concurrence. Note that since for large p/m the rotation β tends to one, the Lorentz transformation is equivalent to a conditional spin flip in this regime.

If boosts can disentangle spins, can they transfer entanglement from the momentum degrees of freedom to an unentangled spin wave function? Indeed this is possible. One way to achieve this is to take any of the resulting states after boosting the state in Eq. (24) and apply the inverse boost to increase concurrence to one. Note that the increase in spin entanglement comes at the expense of a loss of momentum entanglement, since the entanglement between all degrees of freedom (spin and momentum) is constant under Lorentz transformations.

Simply reversing a previously applied Lorentz transformation as in the last example is not a very satisfying way to create entanglement. Is there a way we could create an unentangled state in the laboratory frame that would appear entangled to a moving observer? Consider the state

$$|\Psi_{AA'BB'}\rangle = \frac{1}{\sqrt{2}}(|\mathbf{p}, -\mathbf{p}\rangle|\phi^+\rangle + |\mathbf{p}_\perp, -\mathbf{p}_\perp\rangle|\phi^-\rangle), \tag{28}$$

where $\mathbf{p}$ and $\mathbf{p}_\perp$ are both in the x, y plane, have the same magnitude p, and are perpendicular. We could imagine such a state arising from a particle decay where the products are restricted to movement in the x or y axes with a conditional σ_z gate on the perpendicular direction. The reduced density matrix ρ_{AB} for this wave function is separable, and its concurrence vanishes. However, taking the large p limit in Eqs. (25) and (26) and choosing ϕ and θ appropriate for $\mathbf{p}$ and $\mathbf{p}_\perp$ in the x and y directions, respectively, one can show that for a large boost in the z direction both $|\phi^+\rangle$ and $|\phi^-\rangle$ are transformed into the $|\psi^-\rangle$ state and, hence, the spins are maximally entangled in this reference frame. In fact, the concurrence as a function of $\mathbf{p}$ and ξ is given by

$$C(\rho_{AB}) = \frac{p^2[\cosh^2(\xi) - 1]}{[\sqrt{1 + p^2}\cosh(\xi) + 1]^2}, \tag{29}$$

when choosing $m = 1$. Note that the concurrence is greater than zero whenever p and ξ are nonzero, and as p and ξ become large the concurrence tends to one. So, if we restrict ourselves to spin measurements, an observer in the rest frame of the decay particle cannot use entanglement as a resource (e.g., for teleportation, superdense coding, etc.) while the moving observer *can.* Such a purification of spin entanglement is not always possible, however, and the following theorem characterizes the limitations.

Theorem.—The entanglement *between* the spin and momentum parts of a pure state wave function, $|\Psi_{AA'BB'}\rangle$, must be nonzero to allow the spin entanglement to increase under Lorentz transformations.

Proving the contrapositive, starting with a product state of the form

$$|\Psi_{AA'BB'}\rangle = |\psi\rangle_{A'B'}|\phi\rangle_{AB}, \tag{30}$$

and applying boosts of the form $\Lambda \otimes \Lambda$ or even $\Lambda \otimes \Lambda'$, we obtain

$$\rho_{AB} = \sum_i p_i U_A^i \otimes V_B^i |\phi\rangle\langle\phi| U_A^{i\dagger} \otimes V_B^{i\dagger}, \tag{31}$$

where U_A^i and V_B^i are unitary operators and the sum $\sum_i p_i$ will be an integral for certain states $|\psi\rangle$. We can now plug Eq. (31) into any entanglement monotone $E(\rho)$ and obtain the inequality,

$$E(\rho_{AB}) \leq \sum_i p_i E(U_A^i \otimes V_B^i |\phi\rangle) \tag{32}$$

$$= \sum_i p_i E(|\phi\rangle) \tag{33}$$

$$= E(|\phi\rangle), \tag{34}$$

where inequality (32) comes from the definition of an entanglement monotone [22]. Hence, for states of the form Eq. (30), the spin entanglement can only *decrease* after a Lorentz transformation. □

Note that this theorem does not hold if arbitrary unitary operations are applied to a particle's spin and momentum degrees of freedom (for instance, a swap gate), but it does hold for the entire class of unitaries realized by Lorentz transformations.

We have investigated the properties of moving entangled pairs of massive particles. Because Lorentz boosts entangle the spin and momentum degrees of freedom, entanglement can be transferred between them. This is true for single particles [14], and we have shown here that it is true for pairs, where the Lorentz boost affects the entanglement *between* spins. Quite generally, we can say that fully entangled spin states will (depending on the initial momentum wave function) most likely decohere due to the mixing with momentum degrees of freedom. We also note, however, that such mixing can *purify* spin entanglement if the momentum degrees are entangled with the spin. The physics of creating entanglement between spins and between momenta is very different. Thus, the possibility of entanglement transfer via Lorentz boosts could conceivably, in special situations, lead to simplified state preparation and purification protocols.

We thank Jonathan Dowling, and the members of the JPL Quantum Computing Group, for useful discussions and encouragement. We also acknowledge Daniel Terno for valuable suggestions. This work was carried out at the Jet Propulsion Laboratory (California Institute of Technology) under a contract with the National Aeronautics and Space Administration, with support from the National Security Agency, the Advanced Research and Development Activity, the Defense Advanced Research Projects Agency, the National Reconnaissance Office, and the Office of Naval Research.

[1] A. Einstein, Jahrb. Radioakt. Elektron. **4**, 411 (1907); M. Planck, Ann. Phys. (Leipzig) **26**, 1 (1908).
[2] H. Ott, Z. Phys. **175**, 70 (1963); H. Arzeliès, Nuovo Cimento **35**, 792 (1964).
[3] R. Aldrovandi and J. Gariel, Phys. Lett. A **170**, 5 (1992).
[4] K. P. Trout and A. J. Greiner, Nuovo Cimento **113**, 1439 (1998).
[5] P. T. Landsberg and G. E. A. Matsas, Phys. Lett. A **223**, 401 (1996).
[6] P. J. B. Peebles and D. T. Wilkinson, Phys. Rev. **174**, 2168 (1968).
[7] C. E. Shannon, Bell Syst. Tech. J. **27**, 379 (1948); **27**, 623 (1948).
[8] M. A. Nielsen and I. L. Chuang, *Quantum Computation and Quantum Communication* (Cambridge University Press, Cambridge, England, 2000).
[9] C. H. Bennett *et al.*, Phys. Rev. Lett. **70**, 1895 (1993).
[10] C. H. Bennett and S. J. Wiesner, Phys. Rev. Lett. **69**, 2881 (1992).
[11] R. Josza, D. S. Abrams, J. P. Dowling, and C. P. Williams, Phys. Rev. Lett. **85**, 2010 (2000); V. Giovanetti, S. Lloyd, and L. Maccone, Nature (London) **412**, 417 (2001).
[12] B. Julsgaard, A. Kozhekin, and E. S. Polzik, Nature (London) **413**, 400 (2001).
[13] N. J. Cerf and C. Adami, Phys. Rev. Lett. **79**, 5194 (1997).
[14] A. Peres, P. F. Scudo, and D. R. Terno, Phys. Rev. Lett. **88**, 230402 (2002).
[15] W. Tung, *Group Theory in Physics* (World Scientific, New York, 1985).
[16] G. Vidal, J. Mod. Opt. **47**, 355 (2000).
[17] S. Parker, S. Bose, and M. B. Plenio, Phys. Rev. A **61**, 032305 (2000).
[18] W. K. Wootters, Phys. Rev. Lett. **80**, 2245 (1998).
[19] After the Lorentz transform the spins are in a mixed state; entanglement measures based on pure states cannot be used.
[20] M. Czachor, Phys. Rev. A **55**, 72 (1997).
[21] P. M. Alsing and G. J. Milburn, Quantum Inf. Comput. **2**, 487 (2002).
[22] G. Vidal, J. Mod. Opt. **47**, 355 (2000).

Appendix H:

Entangled light in moving frames

Robert M. Gingrich, Attila J. Bergou, and Christoph Adami
Quantum Computing Technologies Group, Jet Propulsion Laboratory, 126-347 California Institute of Technology, Pasadena, California 91109-8099, USA

(Received 17 March 2003; published 7 October 2003)

We calculate the entanglement between a pair of polarization-entangled photon beams as a function of the reference frame, in a fully relativistic framework. We nd the transformation law for helicity basis states and show that, while it is frequency independent, a Lorentz transformation on a momentum-helicity eigenstate produces a momentum-dependent phase. This phase leads to changes in the reduced polarization density matrix, such that entanglement is either decreased or increased, depending on the boost direction, the rapidity, and the spread of the beam.

The second quantum revolution [1] is changing the ways in which we think about quantum systems. Rather than just describing and predicting their behavior, we now use new tools such as quantum information theory to organize and control quantum systems, and turn their nonclassical features to our advantage in creating *quantum technology*. The central feature that makes quantum technology possible is quantum *entanglement*, which implies that particles or elds that have once interacted are connected by an overall wave function even if they are detected arbitrarily far away from each other. Such *entangled pairs*, rst discussed after their introduction by Einstein, Podolsky, and Rosen [2], are crucial in technology such as quantum teleportation [3] and superdense coding [4]. Furthermore, quantum entanglement is critical in applications such as quantum optical interferometry, where quantum entangled N-photon pairs can increase the shot-noise limited sensitivity up to the Heisenberg limit [5].

While quantum entanglement as a resource has been studied extensively within the last decade [6], it was realized only recently that this resource is frame dependent, and changes nontrivially under Lorentz transformations [7–12]. In particular, Gingrich and Adami showed that the entanglement between the spins of a pair of massive spin-1/2 particles depends on the reference frame, and can either decrease or increase depending on the wave function of the pair [11]. A consequence of this nding is that the entanglement resource could be manipulated by applying frame changes only. Many applications of quantum technology, however, involve entangled photons rather than massive spin-1/2 particles, to which the massive theory does not apply. In this paper, we work out the consequences of Lorentz transformations on photon beams that are entangled in polarization. Each photon beam is described by a Gaussian wave packet with a particular angular spread in momentum, and for the sake of being de nite we discuss a state whose polarization entanglement can be thought of as being produced by downconversion. Because both spin-1/2 particles and photons can be used as quantum information carriers (qubits), the present calculation also contributes to the nascent eld of relativistic quantum information theory [13].

In order to calculate how a polarization-entangled photon state transforms under Lorentz transformations, we need to discuss the behavior of the photon basis sates. Because there is no rest frame for a massless particle, the analysis of the spin (polarization) properties is quite distinct from the massive case. For instance, instead of using $p^\mu=(m,\mathbf{0})$ as the standard four-vector (see Ref. [11]), we have to de ne the massless analog $k^\mu=(1,\hat{\mathbf{z}})$. Note that k^μ has no parameter m and is no longer invariant under all rotations. In fact, the *little group* of k^μ is isomorphic to the noncompact two-dimensional Euclidean group E(2) (the set of transformations that map a two-dimensional Euclidean plane onto itself). For a massless spin-1 particle the standard vector allows us to de ne the eigenstate

$$P^\mu|\hat{\mathbf{z}}\lambda\rangle=k^\mu|\hat{\mathbf{z}}\lambda\rangle, \tag{1}$$

$$J_z|\hat{\mathbf{z}}\lambda\rangle=\lambda|\hat{\mathbf{z}}\lambda\rangle, \tag{2}$$

where $\hat{\mathbf{z}}$ is a unit vector pointing in the z direction. Since the particle is massless, λ is restricted to ± 1 [14].

The momentum-helicity eigenstates are de ned as

$$|\mathbf{p}\lambda\rangle=H(\mathbf{p})|\hat{\mathbf{z}}\lambda\rangle, \tag{3}$$

where $H(\mathbf{p})$ is a Lorentz transformation that takes $\hat{\mathbf{z}}$ to $\mathbf{p}$. The choice of $H(\mathbf{p})$ is not unique, and different choices lead to different interpretations of the parameter λ. For instance, in the massive case the choice of $H(\mathbf{p})$ can lead to λ being either the rest-frame spin or the helicity. In the present case it is convenient to choose

$$H(\mathbf{p})=R(\hat{\mathbf{p}})L_z(\xi_{\mathbf{p}}), \tag{4}$$

where $L_z(\xi_{\mathbf{p}})$ is a Lorentz boost along $\hat{\mathbf{z}}$ that takes $\hat{\mathbf{z}}$ to $|\mathbf{p}|\hat{\mathbf{z}}$ and $R(\mathbf{p})$ is a rotation that takes $\hat{\mathbf{z}}$ to $\hat{\mathbf{p}}$, while $\xi_{\mathbf{p}}$ is the rapidity of the moving frame,

$$\xi_{\mathbf{p}}=\ln|\mathbf{p}|. \tag{5}$$

For a parametrization in polar coordinates, we can write $\hat{\mathbf{p}}=(\sin\theta\cos\phi,\sin\theta\sin\phi,\cos\theta)$:

$$R(\hat{\mathbf{p}})\equiv R_z(\phi)R_y(\theta). \tag{6}$$

Again, this choice of $R(\hat{\mathbf{p}})$ is not unique (see, for example, Ref. [17]) but particularly easy to deal with in this context. An arbitrary two-particle state in this formalism can be written as

$$|\Psi_{AA'BB'}\rangle = \int\int \sum_{\lambda\sigma} g_{\lambda\sigma}(\mathbf{p},\mathbf{q}) |\mathbf{p}\lambda\rangle_{AA'} |\mathbf{q}\sigma\rangle_{BB'} \widetilde{d}\mathbf{p} \widetilde{d}\mathbf{q}, \tag{7}$$

where $|\mathbf{p}\lambda\rangle_{AA'}$ and $|\mathbf{q}\sigma\rangle_{BB'}$ correspond to the momentum and helicity states, as de ned in Eq. (3), of photons A and B. Furthermore, $\widetilde{d}\mathbf{p}$ and $\widetilde{d}\mathbf{q}$ are the Lorentz-invariant momentum integration measures:

$$\widetilde{d}\mathbf{p} \equiv \frac{d^3\mathbf{p}}{2|\mathbf{p}|} \tag{8}$$

and the functions $g_{\lambda\sigma}(\mathbf{p},\mathbf{q})$ must satisfy

$$\int\int \sum_{\lambda\sigma} |g_{\lambda\sigma}(\mathbf{p},\mathbf{q})|^2, \widetilde{d}\mathbf{p} \widetilde{d}\mathbf{q} = 1. \tag{9}$$

To work out how a Lorentz boost affects an entangled state, we must understand how the basis states $|\mathbf{p}\lambda\rangle$ transform. Following Refs. [14,15], we apply a boost Λ to $|\mathbf{p}\lambda\rangle$,

$$\Lambda|\mathbf{p}\lambda\rangle = H(\Lambda\mathbf{p}) H(\Lambda\mathbf{p})^{-1} \Lambda H(\mathbf{p}) |\hat{\mathbf{z}}\lambda\rangle, \tag{10}$$

where $H(\Lambda\mathbf{p})^{-1}\Lambda H(\mathbf{p})$ is a member of the little group of $\hat{\mathbf{z}}$ (leaves $\hat{\mathbf{z}}$ invariant), and hence is a rotation and/or translation in the x-y plane. The translations can be shown [14] not to affect the spin/helicity, and we are thus left with just a rotation by an angle $\Theta(\Lambda,\mathbf{p})$. Using the parametrization $\mathbf{p} = p(\sin\theta\cos\phi, \sin\theta\sin\phi, \cos\theta)$ and solving for $\Theta(\Lambda,\mathbf{p})$ we obtain

$$\Theta(\Lambda,\mathbf{p}) = \begin{cases} 0 & : \quad \Lambda = L_z(\xi) \\ 0 & : \quad \Lambda = R_z(\gamma), \quad \hat{\mathbf{p}} \neq \hat{\mathbf{z}} \\ \gamma & : \quad \Lambda = R_z(\gamma), \quad \hat{\mathbf{p}} = \hat{\mathbf{z}} \\ \arg(B+iA) & : \quad \Lambda = R_y(\gamma) \end{cases} \tag{11}$$

for different Lorentz transformations and momenta, where

$$A = \sin\gamma\sin\phi, \tag{12}$$

$$B = \sin\gamma\cos\theta\cos\phi + \cos\gamma\sin\theta. \tag{13}$$

Noting that

$$R_z(\Theta(\Lambda'\Lambda,\mathbf{p})) = R_z(\Theta(\Lambda',\Lambda\mathbf{p})) R_z(\Theta(\Lambda,\mathbf{p})) \tag{14}$$

and taking advantage of the fact that all Lorentz boosts can be constructed using L_z, R_z and R_y, Eq. (11) allows us to nd $\Theta(\Lambda,\mathbf{p})$ for any Λ, and any momentum $\mathbf{p}$. Applying this rotation to the momentum-helicity eigenstate of a massless particle we obtain

$$\Lambda|\mathbf{p}\lambda\rangle = e^{-i\lambda\Theta(\Lambda,\mathbf{p})} |\Lambda\mathbf{p}\lambda\rangle. \tag{15}$$

At this point one may be tempted to use the two helicity states as a basis for the polarization density matrix. However, because helicity states for different momentum eigenstates reside in different Hilbert spaces, tracing out the momentum degree of freedom produces unphysical results. For example, we would nd that a spatial rotation can change the entanglement between two particles. Instead, we shall use the photon's polarization four-vectors as basis states.

The polarization four-vectors for positive and negative helicity states are given by

$$\epsilon^{\mu}_{\pm}(\hat{\mathbf{p}}) = \frac{R(\hat{\mathbf{p}})}{\sqrt{2}} \begin{bmatrix} 0 \\ 1 \\ \pm i \\ 0 \end{bmatrix}. \tag{16}$$

A general polarization vector is, of course, formed by the superposition of the two basis vectors. According Refs. [9,18], for a given four-momentum p^{μ} and associated polarization ϵ^{μ}, a Lorentz boost has the following effect:

$$D(\Lambda)\epsilon^{\mu} = R(\Lambda\hat{\mathbf{p}}) R(\hat{\mathbf{p}})^{-1} \epsilon^{\mu}. \tag{17}$$

However, this transformation is only correct for pure boosts in the z direction, or rotations around the z axis if this axis is not the momentum axis [as for those cases the angle $\Theta(\Lambda,\mathbf{p})$ in Eq. (11) vanishes]. In general, the four-vector ϵ^{μ} transforms as

$$D(\Lambda)\epsilon^{\mu} = R(\Lambda\hat{\mathbf{p}}) R_z(\Theta(\Lambda,\mathbf{p})) R(\hat{\mathbf{p}})^{-1} \epsilon^{\mu}. \tag{18}$$

It is helpful to write $D(\Lambda)$ in an alternative form

$$D(\Lambda)\epsilon^{\mu} = \Lambda\epsilon^{\mu} - \frac{(\Lambda\epsilon^{\mu})^0}{(\Lambda p^{\mu})^0} \Lambda p^{\mu}, \tag{19}$$

where $(\Lambda\epsilon^{\mu})^0$ and $(\Lambda p^{\mu})^0$ denote the timelike component of the transformed polarization and momentum four-vectors, respectively. The form, Eq. (19), agrees with the general law described in Ref. [16]. Note that from Eq. (19) we can see that $D(\Lambda)$ is independent of our choice of $R(\hat{\mathbf{p}})$. The proof that Eqs. (18) and (19) are equivalent is nontrivial, but an outline is as follows. Note that both forms of $D(\Lambda)$ obey

$$D(\Lambda')D(\Lambda)\epsilon^{\mu} = D(\Lambda'\Lambda)\epsilon^{\mu} \tag{20}$$

and both forms have the property

$$D(R)\epsilon^{\mu} = R\epsilon^{\mu}, \tag{21}$$

where R is a rotation. An explicit calculation of $D(L_z(\xi))$ then shows that they are equivalent.

The second term on the right-hand side of Eq. (19) is just a momentum-dependent gauge transformation. It must be different for each momentum in order to keep a consistent overall (Coulomb) gauge. To see that this term leads to measurable consequences consider the polarization vector for classical electromagnetic waves. The polarization vector points along the *gauge-invariant* electric eld, and the direc-

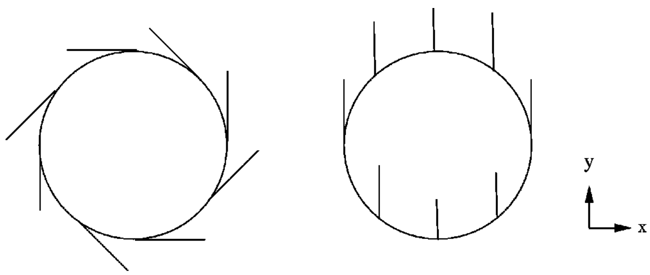

FIG. 1. (a) "Standard" vertical polarization vectors $|v'_{\mathbf{p}}\rangle$ point in azimuthal directions. (b) "True" vertical polarization vectors $|v_{\mathbf{p}}\rangle$ remain mostly in the x-y plane.

tion of this vector undergoes the same transformation as in Eq. (19) [or Eq. (18)] when acted on by a Lorentz transformation. In fact, the magnitude of the electric eld undergoes the same transformation as the diameter of an in nitesimal circle centered at the momentum. This holds for any Lorentz transformation and momentum. A detailed study of this transformation will be published elsewhere.

In the following, we investigate two entangled photon beams moving along the z axis. The beams are in a momentum product state, and fully entangled in polarization,

$$g_{\lambda\sigma}(\mathbf{p},\mathbf{q})=\frac{1}{\sqrt{2}}\delta_{\lambda\sigma}e^{\mathrm{i}\lambda\phi_{\mathbf{p}}}e^{\mathrm{i}\sigma\phi_{\mathbf{q}}}f(\mathbf{p})f(\mathbf{q}). \tag{22}$$

In Eq. (22), $\phi_{\mathbf{p}}$ and $\phi_{\mathbf{q}}$ are the azimuthal angles of $\mathbf{p}$ and $\mathbf{q}$, respectively. The phase factors $e^{\mathrm{i}\lambda\phi_{\mathbf{p}}}e^{\mathrm{i}\sigma\phi_{\mathbf{q}}}$ allow us to write the state as

$$|\Psi\rangle=\int\int\frac{1}{\sqrt{2}}(|h_{\mathbf{p}}\rangle|h_{\mathbf{q}}\rangle-|v_{\mathbf{p}}\rangle|v_{\mathbf{q}}\rangle)f(\mathbf{p})|\mathbf{p}\rangle f(\mathbf{q})|\mathbf{q}\rangle\widetilde{d}\mathbf{p}\widetilde{d}\mathbf{q}, \tag{23}$$

where $|h_{\mathbf{p}}\rangle$ and $|v_{\mathbf{p}}\rangle$ are approximations of horizontal polarizatoion and vertical polarization given by [19]

$$|h_{\mathbf{p}}\rangle\equiv\frac{1}{\sqrt{2}}[e^{\mathrm{i}\phi_{\mathbf{p}}}\epsilon_{+}^{\mu}(\hat{\mathbf{p}})+e^{-\mathrm{i}\phi_{\mathbf{p}}}\epsilon_{-}^{\mu}(\hat{\mathbf{p}})] \tag{24}$$

$$|v_{\mathbf{p}}\rangle\equiv\frac{-i}{\sqrt{2}}[e^{\mathrm{i}\phi_{\mathbf{p}}}\epsilon_{+}^{\mu}(\hat{\mathbf{p}})-e^{-\mathrm{i}\phi_{\mathbf{p}}}\epsilon_{-}^{\mu}(\hat{\mathbf{p}})]. \tag{25}$$

So, for small θ (small spread of the momentum distribution) we have

$$|h_{\mathbf{p}}\rangle\simeq\hat{\mathbf{x}}, \tag{26}$$

$$|v_{\mathbf{p}}\rangle\simeq\hat{\mathbf{y}}, \tag{27}$$

and Eq. (23) is a close approximation to a polarization Bell state. Omitting the phase factors in Eqs. (22) and (24) instead describes a photon beam where horizontal and vertical polarizations point in the $\hat{r}$ and $\hat{\phi}$ directions, respectively (see Fig. 1).

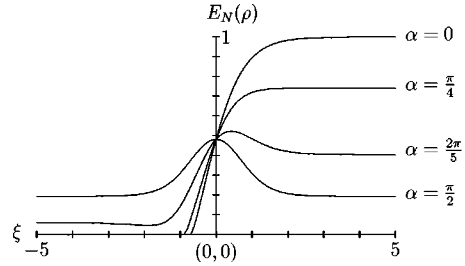

FIG. 2. Log negativity of the spin as a function of rapidity shown for various boost directions. α is the boost angle. For all of the curves the angular spread is the same, $\sigma=1.0$.

We speci cally consider the beams to have a Gaussian spread in the θ direction,

$$f(\mathbf{p})=\frac{1}{N(\sigma)}\exp\left[-\frac{1}{2}\left(\frac{\theta}{\sigma_\theta}\right)^2\right]\delta(|\mathbf{p}|-p_0), \tag{28}$$

where σ_θ is a parameter which controls the spread of the beam, θ is the polar angle of the momentum vector, and p_0 is the magnitude of the momentum of the photon beam, which we arbitrarily set to unity. We do not take into account a spread in the *magnitude* of the momentum because the magnitude ω is just a constant multiplying the momentum four-vector and so

$$\Lambda p^\mu=\Lambda(\omega,\omega\hat{\mathbf{p}})=\Lambda\omega(1,\hat{\mathbf{p}})=\omega\Lambda(1,\hat{\mathbf{p}}). \tag{29}$$

Inserting this result into Eq. (19), we see that the ω dependence cancels. We now boost state (23) and trace out the momentum degrees of freedom to construct the polarization density matrix [20].

Even though photons are constrained to be transverse for any particular momentum, states that are *not* momentum eigenstates must, because they are spin-1 particles, be treated as three-level systems. In order to calculate the entanglement present in the quantum state, we therefore cannot use Wootters' concurrence [21], as it is only a measure of entanglement for two-state quantum entangled systems. Instead, we use here "log negativity," an entanglement measure introduced by Vidal and Werner [22]. This measure is de ned as

$$E_N(\rho)=\log_2\|\rho^{T_A}\|, \tag{30}$$

where $\|\rho\|$ is the trace norm and ρ^{T_A} is the partial transpose of ρ. $E_N(\rho)$ is a measure of the entanglement but is unable to detect bound entanglement. We can now calculate the change in log negativity explicitly for a Lorentz boost with rapidity ξ at an angle α with respect to the photon momentum, i.e., a Lorentz transformation

$$\Lambda=R_y(\alpha)L_z(\xi)R_y(\alpha)^{-1}, \tag{31}$$

applied to Eq. (23). Figure 2 summarizes the results of varying the boost direction α for a given spread σ_θ, and shows that the entanglement can increase or decrease, depending on boost direction. For $\alpha=0$, positive ξ corresponds to boosting the photon in the direction of the detector. Note that the entanglement at zero rapidity is only about half its maximal

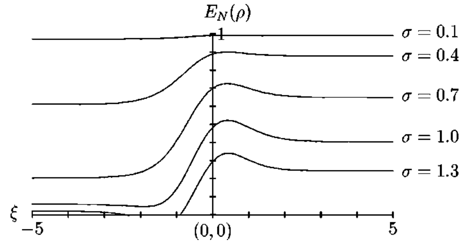

FIG. 3. Log negativity as a function of rapidity shown for beams of various angular spreads, σ. For all of the above curves the boost direction $\alpha = 2\pi/5$.

value, because the angular spread of the momentum leaves the spin degrees of freedom in a mixed state after tracing out momentum.

In general, boosts in the direction of motion tend to increase the entanglement to saturation, while boosts away from it decrease it. As α approaches $\pi/2$, the effect on entanglement becomes symmetric.

Figure 3 summarizes the effect of applying the boost in Eq. (31) for varying spreads in the momentum distribution, for a boost direction given by $\alpha = 2\pi/5$.

Distributions with small spread $\sigma_\theta \leqslant 0.1$ tend to change entanglement only imperceptively, while for larger spread the entanglement changes become more pronounced. Note that for $\sigma_\theta = 1.3$ the entanglement becomes zero (for boosts of negative rapidity) and then increases. This appears to happen because the momentum spread becomes so large that a signi cant portion of the beam is in fact moving in the $-\hat{\mathbf{z}}$ direction. Because of the collimating effect that a Lorentz boost has on the beam, the entanglement can actually increase in such a situation.

We have derived the relativistic transformation law for photon polarizations, and shown that the entanglement of polarization-entangled pairs of photon beams depends on the reference frame. Boosting a detector (even at an angle) towards the beams increases this entanglement because the momentum distribution is shrunk by the boost (see also Ref. [12]). The type of entangled beams that we have investigated in this paper are idealizations of realistic states that can be created using parametric down-conversion. In principle, therefore, the effects discussed here should become relevant as soon as linear-optics based quantum technology is created that is placed on systems that move with respect to a detector (or when the detector moves with respect to such a system).

We would like to thank Jonathan Dowling, and the members of the JPL Quantum Computing Group, for useful discussions and encouragement. We also acknowledge János Bergou for helpful suggestions. This work was carried out at the Jet Propulsion Laboratory (California Institute of Technology) under a contract with the National Aeronautics and Space Administration Code Y, with support from the Army Research Of ce, the National Security Agency, the Advanced Research and Development Activity, the Defense Advanced Research Projects Agency, the National Reconnaissance Of ce, and the Of ce of Naval Research.

[1] J.P. Dowling and G.J. Milburn, Philos. Trans. R. Soc. London **361**, 1 (2003).
[2] A. Einstein, B. Podolsky, and N. Rosen, Phys. Rev. **47**, 777 (1935).
[3] C.H. Bennett *et al.*, Phys. Rev. Lett. **70**, 1895 (1993).
[4] C.H. Bennett and S.J. Wiesner, Phys. Rev. Lett. **69**, 2881 (1992).
[5] J.P. Dowling, Phys. Rev. A **57**, 4736 (1998).
[6] M. A. Nielsen and I. L. Chuang, *Quantum Computation and Quantum Communication* (Cambridge University Press, Cambridge, 2000).
[7] A. Peres, P.F. Scudo, and D.R. Terno, Phys. Rev. Lett. **88**, 230402 (2002).
[8] M. Czachor, Phys. Rev. A **55**, 72 (1997).
[9] P.A. Alsing and G.J. Milburn, Quantum Inf. Comput. **2**, 487 (2002).
[10] H. Terashima and M. Ueda, Int. J. Quant. Inf. **1**, 93 (2003).
[11] R.M. Gingrich and C. Adami, Phys. Rev. Lett. **89**, 270402 (2002).
[12] A. Peres and D.R. Terno, J. Mod. Opt. **50**, 1165 (2003).
[13] A. Peres and D.R. Terno, Rev. Mod. Phys. (to be published).
[14] E.P. Wigner, Ann. Math. **40**, 149 (1939).
[15] W. K. Tung, *Group Theory in Physics* (World Scienti c, Singapore, 1985).
[16] S. Weinberg, *The Quantum Theory of Fields* (Cambridge University Press, Cambridge, 1995), Vol. I.
[17] F. J. Yndurain, *Relativistic Quantum Mechanics and Introduction to Field Theory* (Springer-Verlag, Berlin, 1996).
[18] D. Han, Y.S. Kim, and D. Son, Phys. Rev. D **31**, 328 (1985).
[19] The choice of basis vectors $|h_{\mathbf{p}}\rangle$ and $|v_{\mathbf{p}}\rangle$ that guarantees polarization vectors as close as possible to the laboratory $\hat{\mathbf{x}}, \hat{\mathbf{y}}$ directions is obtained instead by replacing $\phi_{\mathbf{p}}$ by $\psi_{\mathbf{p}}$, where $\psi_{\mathbf{p}}$ is such that

$$\tan(2\psi_{\mathbf{p}}) = \tan(2\phi)\frac{2\cos(\theta)}{1+\cos^2(\theta)}.$$

However, we used $\phi_{\mathbf{p}}$ in the present calculations because it is approximately equal to $\psi_{\mathbf{p}}$ except when θ is large, and much more convienient for our numerical simulations. We carried out a subset of the calculations displayed in Figs. 2 and 3 using the optimal angle $\psi_{\mathbf{p}}$, and found essentially unchanged results.
[20] Note that because a Lorentz transformation on the combined momentum-polarization space is unitary, the *overall* momentum-polarization entanglement between the beams is unchanged by a Lorentz transformation. However, in the laboratory, usually only polarization is measured, which effectively traces out the momentum part of the wave function.
[21] W.K. Wootters, Phys. Rev. Lett. **80**, 2245 (1998).
[22] G. Vidal and R.F. Werner, Phys. Rev. A **65**, 032314 (2002).

Appendix I:

Quantum-enhanced positioning and clock synchronization

Vittorio Giovannetti*, Seth Lloyd† & Lorenzo Maccone*

* *Massachusetts Institute of Technology, Research Laboratory of Electronics, MIT36-497, Cambridge, Massachusetts 02139, USA*
† *Massachusetts Institute of Technology, Department of Mechanical Engineering, MIT3-160, Cambridge, Massachusetts 02139, USA*

A wide variety of positioning and ranging procedures are based on repeatedly sending electromagnetic pulses through space and measuring their time of arrival. The accuracy of such procedures is classically limited by the available power and bandwidth. Quantum entanglement and squeezing have been exploited in the context of interferometry[1–5], frequency measurements[6], lithography[7] and algorithms[8]. Here we report that quantum entanglement and squeezing can also be employed to overcome the classical limits in procedures such as positioning systems, clock synchronization and ranging. Our use of frequency-entangled pulses to construct quantum versions of these protocols results in enhanced accuracy compared with their classical analogues. We describe in detail the problem of establishing a position with respect to a fixed array of reference points.

Any position (say, that of Alice) may be obtained simply by sending pulses that originate from that position and measuring the time it takes for each pulse to reach the reference points. The time of flight, the speed of the pulses and the arrangement of the reference points determine Alice's position. The accuracy of such a procedure depends on the number of pulses, their bandwidth and the number of photons per pulse. Here we show that, by measuring the correlations between the times of arrival of M pulses which are frequency-entangled, it is in principle possible to increase the accuracy of such a positioning procedure by a factor $\sqrt{M}$ as compared to positioning using unentangled pulses with the same bandwidth. Moreover, if number-squeezed pulses can be produced[9], it is possible to obtain a further increase in accuracy of $\sqrt{N}$ by employing squeezed pulses of N quanta, rather than employing 'classical' coherent states with a mean number of quanta N. Combining entanglement with squeezing gives an overall enhancement of $\sqrt{MN}$. In addition, the procedure exhibits improved security: because the timing information resides in the entanglement between pulses, it is possible to implement quantum cryptographic schemes that do not allow an eavesdropper to obtain information on the position of Alice (V.G., S.L. and L.M., unpublished results). The primary drawbacks of this scheme are the difficulty of creating the requisite entanglement and the sensitivity to loss. On the other hand, the frequency entanglement allows similar schemes to be highly robust against pulse broadening due to transit through dispersive media[10].

The clock synchronization problem can be treated using the same method. In refs 11 and 12 two techniques for clock synchronization using entangled states were presented. However, the authors of ref. 11 themselves point out that the resources needed by their scheme could be used to perform conventional clock synchronization without entanglement. Similarly, all the enhancement reported in ref. 12 arises from employing high-frequency atoms, which themselves could be used for clock synchronization to the same degree of accuracy without any entanglement. In neither case do these proposals give an obvious enhancement over classical procedures that use the same resources. Here, by contrast, we show that quantum features such as entanglement and squeezing could in principle be used to supply a significant enhancement of the accuracy of clock synchronization as compared with classical protocols using light of the same frequency and power. In fact, the clock synchronization could be accomplished by sending pulses back and forth between the parties whose clocks are to be synchronized, and measuring the times of arrival of the pulses (Einstein's protocol). In this way synchronization may be treated on the same basis as positioning, and the same accuracy enhancements may be achieved through entanglement and squeezing. Here we will address in detail only the enhancement of positioning accuracy.

In order to introduce the formalism, we present the simple case of position measurement with classical coherent pulses. As each dimension can be treated independently, the analysis will be limited to the one-dimensional case. For the sake of simplicity, consider the situation in which Alice wants to measure her position x by sending a pulse to each of M detectors placed in a known position (Fig. 1). This can be easily generalized to different set-ups, such as the case in which the detectors are not all in the same location, the case in which only one detector is employed with M time-separated pulses, the case in which the pulses originate from the reference points and are measured by Alice (as in GPS, the global positioning system), and so on. Alice's estimate of her position is given by $x = (c/M)\Sigma_{i=1}^{M} t_i$, where t_i is the travel time of the ith pulse and c is the speed of light. The variable t_i has an intrinsic indeterminacy dependent on the spectral characteristics and mean number of photons N of the ith pulse. For example, given a gaussian pulse of frequency spread $\Delta\omega$, then, according to the central limit theorem, t_i cannot be measured with an accuracy better than $1/(\Delta\omega\sqrt{N})$ as it is estimated at most from N data points (that is, the times of arrival of the single photons, each having an indeterminacy $1/\Delta\omega$). Thus, if Alice uses M gaussian pulses of equal frequency spread, the accuracy in the measurement of the average time of arrival is:

$$\Delta t = \frac{1}{\Delta\omega\sqrt{MN}} \tag{1}$$

Quantum mechanics allows us to do much better. In order to demonstrate the gain in accuracy afforded by quantum mechanics, we provide first a fully quantum analysis of the problem of determining the average time of arrival of a set of M classical pulses, each having a mean number of photons N. Such a quantum treatment for a classical problem may seem excessive, but once the quantum formalism is presented, the speed-up attainable in the fully quantum case can be derived directly. In addition, it is important to verify that no improvement over equation (1) is obtainable using classical pulses. The M coherent pulses are described by a state of the radiation field of the form

$$|\Psi\rangle_{\rm cl} \equiv \bigotimes_{i=1}^{M} \bigotimes_{\omega} \left|\alpha\left(\phi_\omega\sqrt{N}\right)\right\rangle_i \tag{2}$$

where ϕ_ω is the pulses' spectral function, $|\alpha(\lambda_\omega)\rangle_i$ is a coherent state of amplitude λ_ω in the mode at frequency ω directed towards the ith detector, and N is the mean number of photons in each pulse. The pulse spectrum $|\phi_\omega|^2$ has been normalized so that $\int d\omega|\phi_\omega|^2 = 1$. For detectors with perfect time resolution, the joint probability for the

ith detector to detect N_i photons in the ith pulse at times $t_{i,k}$ is given by[13]

$$p(\{t_{i,k}\}) \propto \left\langle : \prod_{i=1}^{M} \prod_{k=1}^{N_i} E_i^{(-)}(t_{i,k}) E_i^{(+)}(t_{i,k}) : \right\rangle \tag{3}$$

where $t_{i,k}$ is the time of arrival of the kth photon in the ith pulse, shifted by the position of the detectors $t_{i,k} \rightarrow t_{i,k} + x/c$. The signal field at the position of the ith detector at time t is given by $E_i^{(-)}(t) \equiv \int \mathrm{d}\omega\, a_i^\dagger(\omega) e^{i\omega t}$ and $E_i^{(+)} \equiv (E_i^{(-)})^\dagger$, where $a_i(\omega)$ is the field annihilator of a quantum of frequency ω at the ith detector, which satisfies $[a_i(\omega), a_j^\dagger(\omega')] = \delta_{ij}\delta(\omega - \omega')$. The estimation of the ensemble average in equation (3) on the state $|\Psi\rangle_{\mathrm{cl}}$, using the property $a(\omega')\bigotimes_\omega |\alpha(\lambda_\omega)\rangle = \lambda_{\omega'}\bigotimes_\omega |\alpha(\lambda_\omega)\rangle$, gives

$$p(\{t_{i,k}\}) \propto \prod_{i=1}^{M} \prod_{k=1}^{N_i} \left| g(t_{i,k}) \right|^2 \tag{4}$$

where $g(t)$ is the Fourier transform of the spectral function ϕ_ω. Averaging over the times of arrival $t_{i,k}$ and over the number of photons N_i detected in each pulse, we have:

$$\langle t \rangle = \left\langle \frac{1}{M} \sum_{i=1}^{M} \frac{1}{N_i} \sum_{k=1}^{N_i} t_{i,k} \right\rangle = \bar{\tau};\ \Delta t \geq \frac{\Delta\tau}{\sqrt{MN}} \tag{5}$$

with approximate equality for $N \gg 1$. Here $\bar{\tau} \equiv \int \mathrm{d}t |g(t)|^2 t$ and $\Delta\tau^2 \equiv \int \mathrm{d}t |g(t)|^2 (t - \bar{\tau})^2$ are independent of i and k as all the photons have the same spectrum. Equation (5) is the generalization of (1) for non-gaussian pulses.

Quantum light can exhibit phenomena that are not possible classically, such as entanglement and squeezing, which, as will now be seen, can give significant enhancement for determining the average time of arrival. We first consider entanglement. The framework just established allows the direct comparison between frequency-entangled pulses and unentangled ones. For the sake of clarity, we consider initially single-photon entangled pulses.

We define the 'frequency state' $|\omega\rangle$ for the electromagnetic field as the state in which all modes are in the vacuum state, except for the mode at frequency ω which is populated by one photon. Thus the state $\int \mathrm{d}\omega \phi_\omega |\omega\rangle$ represents a single-photon wave packet with spectrum $|\phi_\omega|^2$. We consider the M-photon frequency-entangled state given by

$$|\Psi\rangle_{\mathrm{en}} \equiv \int \mathrm{d}\omega\, \phi_\omega |\omega\rangle_1 |\omega\rangle_2 \cdots |\omega\rangle_M \tag{6}$$

where the subscripts 1, 2, M indicate the detector each photon is travelling to. Inserting $|\Psi\rangle_{\mathrm{en}}$ in equation (3), and specializing to the case $N_i = 1$, it follows that

$$p(t_1, \ldots, t_M) \propto \left| g\left(\sum_{i=1}^{M} t_i \right) \right|^2 \tag{7}$$

That is, the entanglement in frequency translates into the bunching of the times of arrival of the photons of different pulses: although their individual times of arrival are random, the average $t \equiv (1/M)\Sigma_{i=1}^{M} t_i$ of these times is highly peaked. (The measurement of t follows from the correlations in the times of arrival at the different detectors.) Indeed, from equation (7) it turns out that the probability distribution of t is $|g(Mt)|^2$. This immediately implies that the average time of arrival is determined to an accuracy

$$\Delta t = \frac{\Delta\tau}{M} \tag{8}$$

where $\Delta\tau$ is the same as in equation (5). This result shows a $\sqrt{M}$ improvement over the classical case of equation (5).

To emphasize the importance of entanglement, equation (8) should be compared to the result that would be obtained from an unentangled state analogous to $|\Psi\rangle_{\mathrm{en}}$. To this end, we consider the state defined as

$$|\Psi\rangle_{\mathrm{un}} \equiv \bigotimes_{i=1}^{M} \int \mathrm{d}\omega_i \phi_{\omega_i} |\omega_i\rangle_i \tag{9}$$

which describes M uncorrelated single-photon pulses each with spectral function ϕ_ω. By looking at the spectrum of the state obtained by tracing away all but one of the modes in equation (6), each of the photons in equation (9) can be shown to have the same spectral characteristics as the photons in the entangled state $|\Psi\rangle_{\mathrm{en}}$. Now, using equation (3) for the uncorrelated M photon pulses $|\Psi\rangle_{\mathrm{un}}$, it follows that

$$p(t_1, \ldots, t_M) \propto \prod_{i=1}^{M} |g(t_i)|^2 \tag{10}$$

which is the same result that was obtained for the classical state $|\Psi\rangle_{\mathrm{cl}}$. Thus equation (5) holds, with $N = 1$, also for $|\Psi\rangle_{\mathrm{un}}$. From the comparison of equation (5) and (8), we see that employing frequency-entangled pulses gives an increase in accuracy by a factor $\sqrt{M}$ in the measurement of t with respect to the case of unentangled photons.

As $|\Psi\rangle_{\mathrm{en}}$ is tailored to give the least indetermination in the quantity t, it is appropriate for the geometry of the case given in Fig. 1, where the sum of the times of arrival is needed. Other entangled states can be tailored for different geometric dispositions of the detectors, as will be shown through some examples.

How can we create the needed entangled states? In the case $M = 2$, the twin beam state at the output of a continuous-wave pumped parametric down-converter will be shown to be appropriate. It is a two-photon frequency-entangled state of the form $\int \mathrm{d}\omega\, \phi_\omega |\omega\rangle_{\mathrm{s}} |\omega_0 - \omega\rangle_i$, where ω_0 is the pump frequency and s and i refer to the signal and idler modes respectively. This state is similar to $|\Psi\rangle_{\mathrm{en}}$, and can be employed for position measurements when the two reference points are in opposite directions—for example, one to the left and one to the right of Alice. In fact, it can be seen that

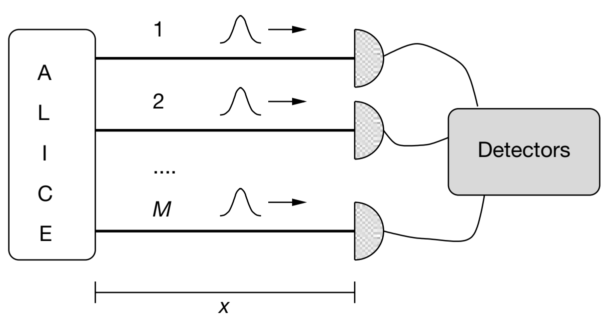

Figure 1 Sketch of the idealized experimental configuration. Alice sends M light pulses to the M detectors. She averages the times of arrival t_i of the pulses to recover her unknown position x.

$p(t_1, t_2) \propto |g(t_1 - t_2)|^2$, and hence such a state is optimized for measurements of differences in the times of arrival, as experimentally reported in ref. 14. In the case of $M = 3$, a suitable state can be obtained starting from a three-photon generation process that creates a state of the form $\int d\omega d\omega' f(\omega, \omega')|\omega\rangle|\omega'\rangle|\omega_0 - \omega - \omega'\rangle$, and then performing a non-demolition (or a post-selection) measurement of the frequency difference of two of the photons. This would create a maximally entangled three-photon state, tailored for the case in which Alice has one detector on one side and two detectors on the other side. However, for $M > 2$, the creation of such frequency-entangled states represents a continuous variable generalization of the Greenberger–Horne–Zeilinger state, and, as such, is a considerable experimental challenge.

Now we turn to the use of number-squeezed states to enhance positioning. Quantum effects in the propagation of multi-photon states are well known (see, for example, ref. 15). The Nth excitation of a quantum system (that is, the state $|N\rangle$ of exactly N quanta) has a de Broglie frequency N times the fundamental frequency of the state. Its shorter wavelength makes such a state appealing for positioning protocols. In this case, the needed 'frequency state' is given by $|N_\omega\rangle$, defined as the state where all modes are in the vacuum except for the mode at frequency ω, which is in the Fock state $|N\rangle$. The probability of measurement of N quanta in a single pulse at times $t_1, \ldots, t_N$ is given by equation (3) with $M = 1$ detectors. We see that, for a state of the form $\int d\omega\, \phi_\omega |N_\omega\rangle$, the time of arrival probability is given by:

$$p(t_1, \ldots, t_N) \propto \left| g\left(\sum_{k=1}^{N} t_k \right) \right|^2 \tag{11}$$

Such a result must be compared to what one would obtain employing a classical pulse $|\Psi\rangle_{cl}$ of mean number of photons N, that is, the state equation (2) with $M = 1$. Its probability (equation (4)) shows that employing the N-photon Fock state gives an accuracy increase of $\sqrt{N}$ compared to the coherent state with mean number of photons N. The similarity of this result (equation (11)) to that obtained in equation (7) stems from the fact that the Fock state $|N_\omega\rangle$ can be interpreted as composed of N one-photon pulses of identical frequency. Hence, all the results and considerations obtained previously apply here. An experiment that involves such a state for $N = 2$ is reported in ref. 16.

Entangled pulses of number-squeezed states combine both these enhancements. By replacing $|\omega\rangle$ with the number-squeezed states $|N_\omega\rangle$ in the M-fold entangled state of equation (6), one immediately obtains an improvement of $\sqrt{MN}$ over the accuracy obtainable by using M classical pulses of N photons each.

The enhanced accuracy achieved comes at the cost of an enhanced sensitivity to loss. If one or more of the photons fails to arrive, the time of arrival of the remaining photons do not convey any timing information. The simplest way to solve this problem is to ignore all trials where one or more photons is lost. A more sophisticated method is to use partially entangled states: these states provide a lower level of accuracy than fully entangled states, but are more tolerant to loss. As shown in Fig. 2, even the simple protocol of ignoring trials with loss still surpasses the unentangled-state accuracy limit even for significant loss levels. The use of intrinsically loss-tolerant, partially entangled states does even better (V.G., S.L. and L.M., unpublished results).

It is useful to consider the following intuitive picture of quantum measurements of timing. A quantum system such as a pulse of photons or a measuring apparatus with spread in energy ΔE can evolve from one state to an orthogonal state in time Δt no less than $h/(4\Delta E)$ (ref. 17). Accordingly, to make more accurate timing measurements, we require states with sharp time dependence, and hence high spreads in energy. Classically, combining M systems each with spread in energy ΔE results in a joint system with spread in energy $\sqrt{M}\Delta E$. Quantum-mechanically, however, M systems can be put in entangled states in which the spread in energy is proportional to $M\Delta E$. Similarly, N photons can be joined in a squeezed state with spread in energy $N\Delta E$. The Margolus–Levitin theorem[18] limits the time Δt it takes for a quantum system to evolve from one state to an orthogonal one by $\Delta t \geq h/(4E)$, where E is the average energy of a system (taking the ground state energy to be 0). This result implies that the $\sqrt{MN}$ enhancement presented here is the best possible. □

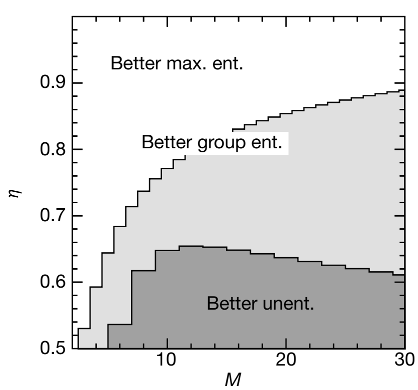

Figure 2 Sensitivity to loss. The quantum efficiency η needed to have an accuracy increase over the unentangled state $|\Psi\rangle_{un}$ is plotted versus the number M of pulses (here the number of photons per pulse is $N = 1$). The upper unshaded region is where the maximally entangled state $|\Psi\rangle_{en}$ does better than the unentangled state $|\Psi\rangle_{un}$. This unshaded region and the light grey region are where a partially entangled state, which exploits a configuration where one partially entangles subgroups of two maximally entangled photons (group entanglement), does better than $|\Psi\rangle_{un}$. The lower dark region is where the unentangled state $|\Psi\rangle_{un}$ does better.

Received 5 March; accepted 11 June 2001.

1. Caves, C. M. Quantum-mechanical noise in an interferometer. *Phys. Rev. D* **23,** 1693–1708 (1981).
2. Bondurant, R. S. & Shapiro, J. H. Squeezed states in phase-sensing interferometers. *Phys. Rev. D* **30,** 2548–2556 (1984).
3. Yurke, B., McCall, S. L. & Klauder, J. R. SU(2) and SU(1,1) interferometers. *Phys. Rev. A* **33,** 4033–4054 (1986).
4. Holland, M. J. & Burnett, K. Interferometric detection of optical phase shifts at the Heisenberg limit. *Phys. Rev. Lett.* **71,** 1355–1358 (1993).
5. Dowling, J P. Correlated input-port, matter-wave interferometer: Quantum-noise limits to the atom-laser gyroscope. *Phys. Rev. A* **57,** 4736–4746 (1998).
6. Bollinger, J. J., Itano, W. M., Wineland, D. J. & Heinzen, D. J. Optimal frequency measurements with maximally correlated states. *Phys. Rev. A* **54,** R4649–R4652 (1996).
7. Boto, A. N. *et al.* Quantum interferometric optical lithography: exploiting entanglement to beat the diffraction limit. *Phys. Rev. Lett.* **85,** 2733–2736 (2000).
8. Grover, L. K. Quantum mechanics helps in searching for a needle in a haystack. *Phys. Rev. Lett.* **79,** 325–328 (1997).
9. Jacobson, J., Björk, G., Chuang, I. & Yamamoto, Y. Photonic de Broglie waves. *Phys. Rev. Lett.* **74,** 4853–4838 (1995).
10. Steinberg, A. M., Kwiat, P. G. & Chiao, R. Y. Dispersion cancellation in a measurement of the single-photon propagation velocity in glass. *Phys. Rev. Lett.* **68,** 2421–2424 (1992).
11. Jozsa, R., Abrams, D. S., Dowling, J. P. & Williams, C. P. Quantum clock synchronization based on shared prior entanglement. *Phys. Rev. Lett.* **85,** 2010–2013 (2000).
12. Chuang, I. L. Quantum algorithm for distributed clock synchronization. *Phys. Rev. Lett.* **85,** 2006–2009 (2000).
13. Mandel, L. & Wolf, E. *Optical Coherence and Quantum Optics* (Cambridge Univ. Press, Cambridge, 1995).
14. Hong, C. K., Ou, Z. Y. & Mandel, L. Measurement of subpicosecond time intervals between two photons by interference. *Phys. Rev. Lett.* **59,** 2044–2046 (1987).
15. Hagelstein, P. L. Application of a photon configuration space model to soliton propagation in a fiber. *Phys. Rev. A* **54,** 2426–2438 (1996).
16. Fonseca, E. J. S., Monken, C. H. & Pádua, S. Measurement of the de Broglie wavelength of a multiphoton wave packet. *Phys. Rev. Lett.* **82,** 2868–2871 (1999).
17. Peres, A. *Quantum Theory: Concepts and methods* (Kluwer Academic, Dordrecht, 1993).
18. Margolus, N. & Levitin, L. B. The maximum speed of dynamical evolution. *Physica D* **120,** 188–195 (1998).

Acknowledgements

This work was funded by the ARDA, NRO, and by ARO under a MURI program.

Correspondence and requests for materials should be addressed to S.L.
(e-mail: slloyd@mit.edu).

Appendix J:

Efficient generation of tunable photon pairs at 0.8 and 1.6 μm

Elliott J. Mason, Marius A. Albota, Friedrich König, and Franco N. C. Wong

Research Laboratory of Electronics, Massachusetts Institute of Technology, Cambridge, Massachusetts 02139

Received July 9, 2002

We demonstrate efficient generation of collinearly propagating, highly nondegenerate photon pairs in a periodically poled lithium niobate cw parametric downconverter with an inferred pair generation rate of 1.4×10^7/s/mW of pump power. Detection of an 800-nm signal photon triggers a thermoelectrically cooled 20%-efficient InGaAs avalanche photodiode for the detection of the 1600-nm conjugate idler photon. Using single-mode fibers as spatial mode filters, we obtain a signal-conditioned idler-detection probability of ~3.1%.

OCIS codes: 270.0270, 030.5260, 190.4410, 270.5570.

Efficient generation of entangled photons is essential for realizing practical quantum information processing applications such as quantum cryptography and quantum teleportation. Entangled photons are routinely generated by spontaneous parametric downconversion (SPDC) in a nonlinear crystal.[1] More recently, nonlinear waveguides were used for photon pair generation with high efficiency[2–4] and better control of the spatial modes. So far, these entangled photon sources have large bandwidths. Recently, a narrowband application was suggested in a singlet-based quantum teleportation system[5] in which narrowband (tens of megahertz) polarization-entangled photons are needed for loading quantum memories that are composed of trapped Rb in optical cavities.[6] Such a narrowband source is most conveniently produced with a resonant cavity such as an optical parametric amplifier (OPA).[7,8] In addition to being narrowband, the OPA outputs have well-defined spatial modes that allow efficient coupling into trapped-Rb cavities. The requirements for efficient generation in an OPA and in SPDC are different. In an OPA, collinearly propagating signal and idler beams are necessary to minimize walk-off, and intracavity losses must be small compared with the cavity's output coupling. A desirable configuration consists of a long crystal with light propagation along one of its principal axes. In contrast, a nonlinear waveguide is an excellent choice for SPDC but is ill suited for intracavity use because of high waveguide propagation losses.

As a precursor to an OPA configuration, we have studied the generation of collinearly propagating tunable outputs at ~800 and ~1600 nm in a quasi-phase-matched periodically poled lithium niobate parametric downconverter. Unlike most other SPDC sources, our periodically poled lithium niobate source utilizes a long bulk crystal, which results in a small bandwidth, and the two output wavelengths are widely separated. The choice of wavelengths is designed for loading local Rb-based quantum memories at 795 nm and for low-loss fiber-optic transmission of the conjugate photons at ~1.6 μm. The 1600-nm photon can be upconverted via quantum frequency translation[9] for remote quantum memory loading. For the current work, we constructed a compact all-solid-state InGaAs single-photon counter for detecting the 1.6-μm photons.

We tested three fiber-pigtailed InGaAs avalanche photodiodes (APDs) from JDS Uniphase (EPM239BA) as passively quenched, gated single-photon counters.[10–12] Each APD was mounted in a small copper block that was attached to a four-stage thermoelectric cooler, which in turn was in contact with a brass heat sink. We placed this thermoelectric-cooled APD assembly in a sealed box mounted on top of four additional TE coolers for improved temperature control of the APD box. Using this all-solid-state cooling apparatus, we were able to adjust the APD temperature down to $-60\,°$C without the use of liquid nitrogen. Typically we biased the APDs at 0.2–1.0 V below the breakdown voltage of the selected APD device, and we applied a gating pulse of 2–4 V to overbias the APDs for single-photon detection. The gate pulses had rise and fall times of 3–4 ns with subnanosecond timing jitters, and the adjustable pulse length was set at 20 ns. The avalanche output pulses were then amplified by 40 dB with resultant pulse amplitudes of 1–2 V and rise times of less than 2 ns.

In general, dark counts increase exponentially with increasing device temperatures, and hence a lower operating temperature is preferred. However, afterpulsing due to trapped charge carriers increases with lower temperatures and also with longer gate durations and higher gate repetition rates. We have found that at an operating temperature of $-50\,°$C there was negligible afterpulsing for gating frequencies of 100 kHz or less, and the dark counts were low enough to yield a high signal-to-noise ratio (see Fig. 3, below). Figure 1

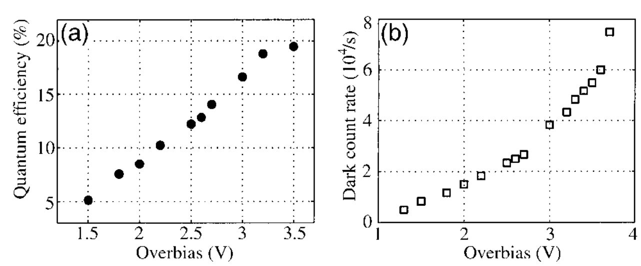

Fig. 1. (a) Quantum efficiency (filled circles) and (b) dark count rate (open squares) of an InGaAs APD with a 20-ns gate at $-50\,°$C as a function of overbias voltage.

shows the quantum efficiencies (filled circles) and dark count rates (open squares) of one of the three APDs at an operating temperature of −50 °C as a function of the overbias voltage. We measured the quantum efficiency of the APD device with a 1.56-μm fiber-pigtailed cw laser. The laser power was attenuated with variable fiber-optic attenuators to 0.13 photon per 20-ns gate (~0.85 pW), and the power was monitored with fiber-optic tap couplers and a high-accuracy optical powermeter with a large dynamic range. For our coincidence measurements, we chose the best of the three APDs and operated it at −50 °C with an overbias of 3.7 V. Under these operating conditions, we achieved a quantum efficiency of ~20% with negligible afterpulses and a dark count probability of 1.1×10^{-3} per 20-ns gate.

We fabricated a 20-mm-long, 0.5-mm-thick periodically poled $LiNbO_3$ (PPLN) crystal with a grating period of 21.6 μm for type I third-order quasi-phase matching. The PPLN was antireflection coated on both facets at 800 and 1600 nm (with ~8% reflection per surface at 532 nm) and was housed in a temperature-stabilized oven with a stability of ±0.1 °C. We first characterized the PPLN by performing difference frequency generation (DFG) with a strong pump at 532 nm and a weak tunable (1580–1610 nm) external-cavity diode laser. We also used a distributed feedback laser at 1559 nm to generate DFG light at 808 nm. We achieved tunable outputs by changing the oven temperature between 140 and 185 °C with a measured tuning coefficient of ~1.3 nm/°C for the 1600-nm light. At a fixed temperature the DFG bandwidth in the probe wavelength was 1.26 nm (~150 GHz), in good agreement with the expected value for a 20-mm-long PPLN. From the DFG output powers we estimate that the effective nonlinear coefficient was 3.8 pm/V for the third-order quasi-phase matching, which is lower than expected because of nonuniformity and the suboptimal duty cycle of the PPLN grating and also because of pump–probe mode mismatch.

For coincidence measurements, we set the PPLN oven at 142 °C, which centered the signal and idler outputs at 808 and 1559 nm, respectively. The cw pump at 532 nm was focused at the center of the crystal with a waist of ~90 μm. The copolarized, collinearly propagating SPDC outputs were spatially separated with a prism at the Brewster angle for detection by a commercial Si single-photon counting module for the 808-nm signal photons and by the InGaAs APD single-photon counter for the 1559-nm idler photons. The single-photon counting module (Perkin-Elmer SPCM-AQR-14) had a quantum efficiency of ~54% at 800 nm with a dark count rate below 100/s. We first measured the singles rate by collecting the freely propagating signal photons to obtain an inferred pair generation rate of 1.4×10^7/s/mW of pump power. The signal was also tuned to other wavelengths within the temperature tuning range, and we obtained similar singles rates. With the ~150-GHz signal bandwidth, the spectral brightness of the output was 9×10^4 pairs/s/GHz/mW of pump power, indicating that the long bulk PPLN crystal was very efficient even though only third-order quasi-phase matching was used.

Spatial mode matching between the signal and idler is a problem with SPDC because of its spontaneous nature and hence its lack of spatial mode selection. Often an interference filter and a small aperture are used to select a narrow spectral width and a small number of spatial modes of a multimode field to yield high visibility in a Hong–Ou–Mandel interferometric measurement. Even SPDC in a waveguide does not necessarily eliminate the spatial mode-matching problem.[4] We took a different approach by coupling the SPDC outputs into single-mode fibers[13] without interference filters. By using a probe laser we measured a fiber coupling efficiency of a well-defined single transverse mode to be ~50%. For the SPDC signal at 808 nm we measured a singles rate of 3×10^4/s/mW of pump power (typical pump powers of 1–2 mW were used). For a measured propagation efficiency of ~85%, a Si detector efficiency of ~54%, and a fiber coupling efficiency of ~50%, we obtain an inferred generation rate of ~1.3×10^5/s/mW for the single-mode signal photons, which is a factor of 100 smaller than that inferred from our multimode free-space detection rate. The challenge in our coincidence measurements was to match the single spatial modes of the highly nondegenerate signal and idler to their respective fibers.

Figure 2 shows the experimental setup for signal–idler coincidence measurements. The signal photon was coupled into an 800-nm single-mode optical fiber and was detected by the single-photon counting module, whose electrical output pulse was used to trigger the gate for the InGaAs detector. We set up the idler collection optics to select the spatial mode that was conjugate to the fiber-coupled signal mode. The idler mode was coupled into a 70-m-long 1550-nm single-mode fiber that provided a 345-ns time delay to allow the gating pulse to turn the InGaAs detector on shortly before the arrival of the idler photon. We limited the maximum trigger and detection rate to 10 kHz to avoid any afterpulsing effect. The outputs of the two detectors were recorded on a two-channel digitizing oscilloscope and stored for analysis. Figure 3 shows a histogram of the conditional detection probability, η_c, of a 1609-nm photon per detected 808-nm photon. The figure clearly shows that the dark count noise was quite small and the photon pairs were time coincident within a 4-ns window. The timing accuracy was limited by the 2-ns digitizing time

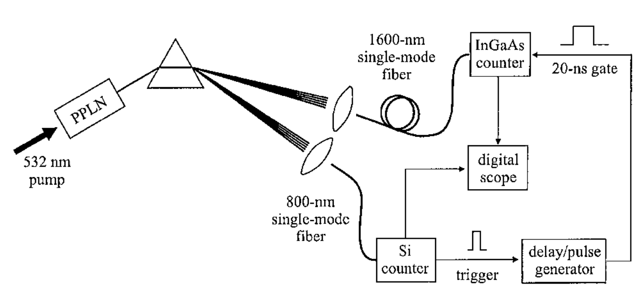

Fig. 2. Schematic of the experimental setup for coincidence measurements.

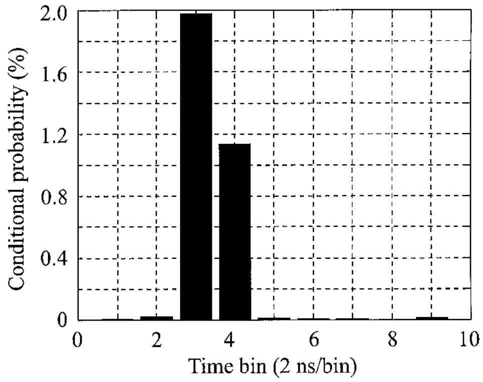

Fig. 3. Histograms of idler photon detection probability conditional on signal photon detection in 2-ns time bins over a 20-ns window. Accidental coincidences due to dark counts are barely noticeable outside the 4-ns coincidence window.

bin and the rise time of the InGaAs detector output pulse (~2 ns). We measured $\eta_c \approx 3.1\%$, limited by the InGaAs detector quantum efficiency of 20%, the propagation efficiency of 85%, and the single-mode fiber-coupling and the signal–idler mode-matching efficiency, which we infer to be ~18%. This inferred coupling and mode-matching efficiency of 18% and our single-mode fiber-coupling efficiency of ~50% of a probe laser suggest that the signal–idler mode matching was ~36%.

In comparison, Banaszek *et al.*[4] reported a measured η_c of 18.5% for a waveguide SPDC and trigger-photon collection (at ~700 nm) with a multimode fiber. If we adjust our results to assume a Si-type detection efficiency of ~70% and no propagation losses, we infer $\eta_c \approx 12.8\%$ for our single-mode fiber collection system. Kurtsiefer *et al.*[13] used single-mode fibers for collecting the degenerate outputs of a type II phase-matched SPDC and obtained an impressive η_c of 28.6%. Our lower η_c was probably a result of suboptimal collection optics, made more difficult by the widely different signal and idler wavelengths.

In summary, we have demonstrated an efficient cw source of highly nondegenerate photon pairs at ~800 and ~1600 nm that uses a long bulk PPLN crystal. Coincidence measurements were made with a home-built all-solid-state InGaAs single-photon counter for 1.6-μm detection. Bidirectional pumping and judicious combining of the outputs[7] should allow us to efficiently generate nondegenerate polarization-entangled photons. Efforts are also under way to use the PPLN crystal in an OPA cavity configuration for generating high-flux narrowband photon pairs.

This work was supported by the U.S. Department of Defense Multidisciplinary University Research Initiative program administered by the U.S. Army Research Office under grant DAAD-19-00-1-0177 and by the National Reconnaissance Office. F. N. C. Wong thanks D. S. Bethune for fruitful discussions on detector bias circuitry.

References

1. P. G. Kwiat, L. Mattle, H. Weinfurter, Z. Zeilinger, A. V. Sergienko, and Y. Shih, Phys. Rev. Lett. **75,** 4337 (1995).
2. S. Tanzilli, H. De Riedmatten, W. Tittel, H. Zbinden, P. Baldi, M. De Micheli, D. B. Ostrowsky, and N. Gisin, Electron. Lett. **37,** 26 (2001).
3. K. Sanaka, K. Kawahara, and T. Kuga, Phys. Rev. Lett. **86,** 5620 (2001).
4. K. Banaszek, A. B. U'Ren, and I. A. Walmsley, Opt. Lett. **26,** 1367 (2001).
5. J. H. Shapiro, New J. Phys. **4,** 47 (2002).
6. S. Lloyd, M. S. Shahriar, J. H. Shapiro, and P. R. Hemmer, Phys. Rev. Lett. **87,** 167903 (2001).
7. J. H. Shapiro and N. C. Wong, J. Opt. B Quantum Semiclass. Opt. **2,** L1 (2000).
8. Y. J. Lu and Z. Y. Ou, Phys. Rev. A **62,** 033804 (2000).
9. J. Huang and P. Kumar, Phys. Rev. Lett. **68,** 2153 (1992).
10. G. Ribordy, J.-D. Gautier, H. Zbinden, and N. Gisin, Appl. Opt. **37,** 2272 (1998).
11. D. S. Bethune and W. P. Risk, IEEE J. Quantum Electron. **36,** 340 (2000).
12. D. Stucki, G. Ribordy, A. Stefanov, H. Zbinden, J. G. Rarity, and T. Wall, J. Mod. Opt. **48,** 1967 (2001).
13. C. Kurtsiefer, M. Oberparleiter, and H. Weinfurter, Phys. Rev. A **64,** 023802 (2001).

Generation of ultrabright tunable polarization entanglement without spatial, spectral, or temporal constraints

Marco Fiorentino,* Gaétan Messin, Christopher E. Kuklewicz, Franco N. C. Wong, and Jeffrey H. Shapiro
Research Laboratory of Electronics, Massachusetts Institute of Technology, Cambridge, Massachusetts 02139, USA
(Received 8 September 2003; published 5 April 2004)

The need for spatial and spectral ltering in the generation of polarization entanglement is eliminated by combining two coherently driven type-II spontaneous parametric down-converters. The resulting ultrabright source emits photon pairs that are polarization entangled over the entire spatial cone and spectrum of emission. We detect a ux of ~12 000 polarization-entangled pairs/s per mW of pump power at 90% quantum-interference visibility, and the source can be temperature tuned for 5 nm around frequency degeneracy. The output state is actively controlled by precisely adjusting the relative phase of the two coherent pumps.

DOI: 10.1103/PhysRevA.69.041801 PACS number(s): 42.65.Lm, 03.65.Ud, 03.67.Mn, 42.50.Dv

Polarization entanglement has been used to demonstrate a variety of quantum effects from quantum teleportation [1] to quantum cryptographic protocols [2]. The quality of polarization-entangled photon sources can be characterized by their pair ux and the purity of the entangled state they generate [3–7]. For the existing sources the requirements of high ux and high purity are often in con ict. Consider, for example, type-II spontaneous parametric down-conversion (SPDC) in a noncollinearly phase-matched β-barium borate (BBO) crystal. Here [4] spatial and spectral ltering are necessary to eliminate nonentangled photons that would reduce the purity of the output state. A source of polarization-entangled photons has been proposed [3] and demonstrated [6] in which the outputs of two different SPDC crystals are combined interferometrically. It was recognized that such a setup would generate entangled photons independent of their wavelengths and angles of emission [3]. The two-crystal interferometer, however, did not show the promised high ux and high visibilities [6]; this was attributed to technical dif- culties in the alignment.

Our group has investigated the use of a collinearly propagating geometry and long periodically poled crystals to simplify alignment and to increase the output ux in both type-I [8] and type-II SPDC [9]. In the case of type-II SPDC in periodically poled potassium titanyl phosphate (PPKTP) [9], we have obtained *post selected* polarization-entangled photons. However, spatial and spectral ltering are still required to obtain a high-purity entangled state and the postselection process involves a 3-dB loss. In this Rapid Communication we report on a robust implementation of the coherent addition of two SPDC sources based on a single PPKTP crystal. Our scheme fully exploits, for the rst time to our knowledge, the properties of interferometric combining of two coherent SPDC sources [3] to yield an ultrabright source of polarization entanglement that has no spatial or spectral constraints. Moreover, collinear operation allows us to control the output state by locking the pump phase of the same interferometer. This setup produces approximately ten times more polarization-entangled pairs/s per mW of pump than any other continuous-wave (cw) source in the literature [5,7].

Figure 1 illustrates a source that coherently combines the outputs of two SPDC crystals. A laser is split by a 50-50 beam splitter (BS) and pumps the two crystals that are phase matched for collinear type-II SPDC. In the low-gain regime, the biphoton state just after the crystals is given by

$$|\Psi\rangle = \frac{1}{\sqrt{2}}(|H_A(\omega_s)V_A(\omega_i)\rangle + e^{i\phi_p}|H_B(\omega_s)V_B(\omega_i)\rangle), \quad (1)$$

where A and B refer to the two arms of the interferometer, ω_s and ω_i are the signal and idler frequencies, respectively, and $\phi_p = k_p(L_B \ \ L_A)$ is the difference of the delays accumulated by the pump (with wave vector k_p) in the paths L_A and L_B between the 50-50 BS and the crystals. A half-wave plate (HWP) is used to rotate the polarizations by 90° in arm B, so that the output state after the polarizing beam splitter (PBS) is

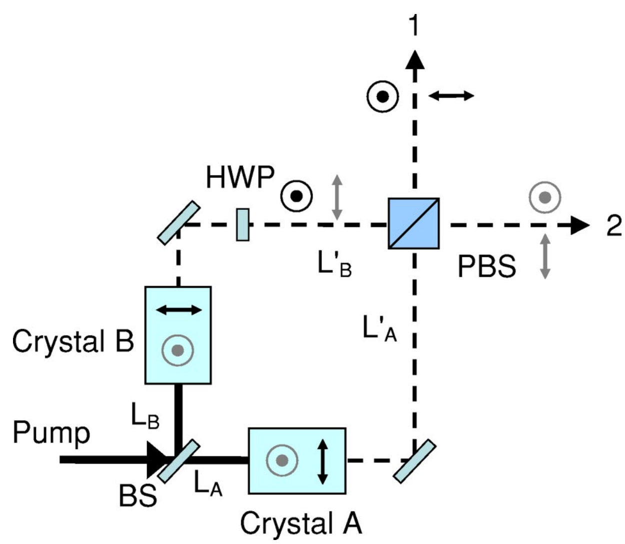

FIG. 1. Schematic of the two-crystal source of polarization-entangled photons. Black (gray) refers to the signal (idler) eld amplitude at ω_s (ω_i). Horizontal (vertical) polarization: ↕ (⊙). BS, beam splitter; HWP, half-wave plate; PBS, polarizing beam splitter.

*Electronic address: m ore@mit.edu

$$|\Psi\rangle = \frac{1}{\sqrt{2}}(|H_1(\omega_s)V_2(\omega_i)\rangle + e^{i\phi}|V_1(\omega_s)H_2(\omega_i)\rangle), \qquad (2)$$

where 1 and 2 refer to the two PBS output ports. The overall phase $\phi=\phi_p+\phi_s+\phi_i$ is determined by the pump phase ϕ_p and the phase delays accumulated by the signal and idler, respectively, with $\phi_{s,i}=k_{s,i}(L'_B \ L'_A) \ \Delta\phi_{\lambda/2}(\omega_{s,i})$. The first term of $\phi_{s,i}$ is the delay due to the arm lengths L'_A and L'_B between the crystals and the PBS, and the second term is the phase difference introduced by the HWP. Note that the phase delays introduced by the identical crystals in the two arms cancel. Under collinear phase matching $k_p=k_s+k_i$, and ϕ is equal to the phase difference accumulated by the pump in the Mach-Zehnder interferometer formed between the 50-50 BS and the PBS except for a fixed offset due to the HWP. The phase of the output biphoton state in Eq. (2) can therefore be precisely controlled by locking the Mach-Zehnder interferometer as seen by the pump alone: one can generate the triplet (for $\phi=0$) or the singlet state ($\phi=\pi$), as well as intermediate states that are linear combinations thereof.

The HWP constrains the signal (idler) elds from the two crystals to exit at output 1 (2) in Fig. 1, ensuring [3,10] that the two sources are indistinguishable so that all the photons are polarization entangled regardless of their wavelengths and directions of emission. Spatial and spectral ltering is unnecessary in this two-crystal con guration, thus promising a source that has a much higher photon-pair ux, plus a larger bandwidth and spatial extension than BBO sources. Due to energy and momentum conservation, one expects the emitted photon pairs from this broadband spatially extended source to show spectral and spatial entanglement. Additional advantages of this scheme include automatic erasure of timing distinguishability, nondegenerate operation, and source tunability.

To implement the interferometric source described above it is crucial that the two SPDC sources be identical. Source differences introduce an element of distinguishability between the two paths that would lead to a mixed state output. We therefore implemented the scheme based on a single crystal with counterpropagating pump beams derived from a single laser. The single-crystal approach is particularly useful with periodically poled crystals, as it mitigates imperfections in the pro les of the periodic gratings.

We used a 10-mm-long (X crystallographic axis), 1-mm-thick (Z axis), and 4-mm-wide (Y axis) hydrothermally grown PPKTP crystal with a grating period of 9.0 μm. At a temperature of $\simeq 32\,^\circ\mathrm{C}$ this grating period phase matches type-II collinear frequency-degenerate downconversion of a 398.5-nm pump polarized along the Y axis and propagating along the crystal's X axis. The crystal was housed in an oven and was maintained at its operating temperature with $\pm 0.1\,^\circ\mathrm{C}$ precision. This crystal was previously characterized and used in type-II collinear SPDC to yield single-beam quantum interference with a 99% visibility [9]. We used second-harmonic generation to measure the temperature and wavelength tuning behavior in PPKTP using a cw tunable laser centered around 797 nm. The second-harmonic measurements are well described by the Sellmeier phase-matching equations for PPKTP [11], which allow us to

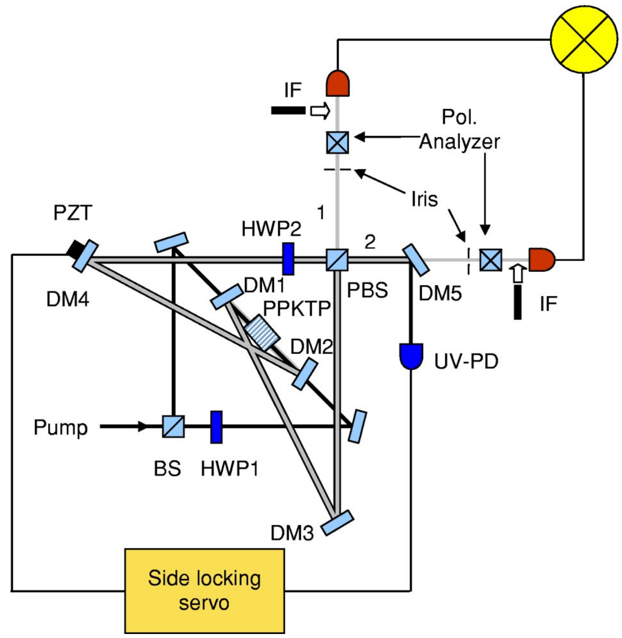

FIG. 2. Experimental setup. BS, 50-50 beam splitter; DM, dichroic mirror; PBS, polarizing beam splitter; HWP, half-wave plate; IF, 3-nm interference lter centered at 797 nm. HWP1 is used to balance the ux of down-converted photons in the two directions.

calculate the spatial and spectral properties of the down-converted photons, as well as the phase-matching angles' dependence on the crystal temperature. The latter predictions have been veri ed by imaging the emitted photons with a charge-coupled-device camera and narrow spectral lters.

The experimental setup is shown in Fig. 2. The frequency-doubled cw Ti:sapphire pump laser at 398.5 nm was split by a BS that had a splitting ratio of $\sim$50-50. To balance the powers of the two pump beams we inserted a half-wave plate (HWP1) to vary the horizontally polarized pump power in the (counterclockwise propagating) brighter path. The crystal was not phase matched for a vertically polarized pump. Each pump beam focused to a waist of $\sim$150 μm at the center of the PPKTP crystal. The generated beams were collimated with 300-mm radius-of-curvature dichroic mirrors (DM1,2) and combined at a PBS after the polarization of one of the beams was rotated by 90° with a HWP. The dichroic mirrors were coated for high re ectivity (HR) at 797 nm and for high transmission (HT) at 398.5 nm, with a residual re ectivity of 0.2% at the pump wavelength. The pump beams, which propagated collinearly with the down-converted beams, were weakly re ected by the four mirrors (DM1-4) and recombined on the PBS, which had a $\sim$20-80 splitting ratio at the pump wavelength. The resultant pump beam from port 2 of the PBS was directed by a dichroic mirror (DM5, HR at 398.5 nm, and HT at 797 nm) for detection with an ultraviolet photodiode. The BS and PBS in Fig. 2 formed a Mach-Zehnder interferometer for the pump and the detected fringes were used to stabilize the interferometer with a side-locking technique. This provided a convenient and robust way to control the phase ϕ of the output state in Eq. (2). By inserting a dispersive medium (such as a thin glass plate) in one of the arms of the Mach-Zehnder interferometer we introduced

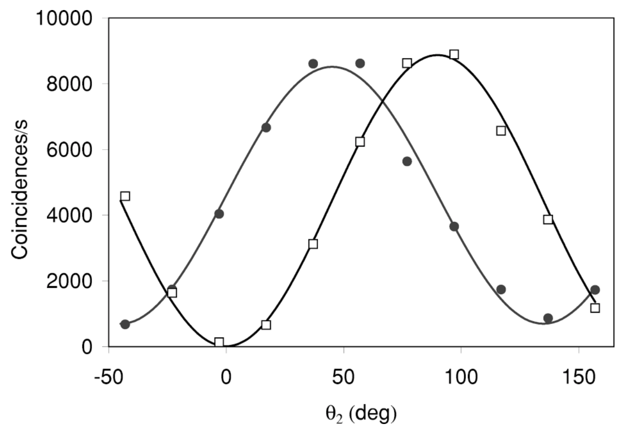

FIG. 3. Coincidence counts for the frequency-degenerate singlet state versus analyzer angle θ_2 in arm 2 for analyzer angle in arm 1 set at 45° (solid circles) and 0° (open squares). Aperture size: 4 mm; no interference lter was used; pump power: 0.7 mW. Each point is averaged over 10 s and the lines are a sinusoidal t to the data.

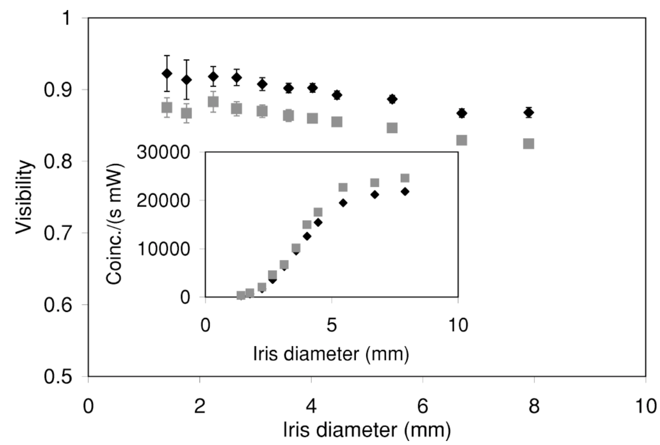

FIG. 4. Frequency-degenerate singlet state 45°-visibility versus iris diameter. In the inset: coincidence counts/s per mW of pump power versus iris diameter. No interference lter (squares) and 3-nm interference lter centered at 797 nm (diamonds).

a xed but variable offset between the phase of the pump fringes and the phase of the output state (the overall offset phase includes other dispersive elements in the interferometer). By varying this phase offset, we were able to lock the phase of the output state at an arbitrary value while optimizing the side-locking feedback signal.

We placed two irises in the output beam paths to control the acceptance angle of the detection system. We estimate that an iris diameter of 1 mm corresponded to an internal emission solid angle of ~3.5×10^{5} sr at the crystal. Flat dichroic mirrors (not shown in Fig. 2) similar to DM1 were used to eliminate residual pump light. The output photons were detected with single-photon Si detectors (Perkin-Elmer SPCM-AQR-14) through polarization analyzers (composed of a half-wave plate and a polarizer). The outputs of the single-photon detectors were counted and also sent to an AND gate (TTL logic family 74F) for coincidence counting. The coincidence window for this con guration was measured to be 39.4 ns. This parameter allowed us to correct for the rate of accidental coincidences in all of the data reported. For example, when 12 000 coincidences/s were measured, an average of 67 000 singles/s were detected at each single-photon detector and ~250 coincidences/s were due to accidental Poisson processes (better coincidence logic would make this correction unnecessary).

A summary of our experimental results, with the accidentals removed, is shown in Figs. 3–5 for $\phi=\pi$ (singlet). The temperature of the crystal was set to ~32 °C to ensure frequency degenerate operation. Figure 3 shows the quantum interference in the coincidence counts when the analyzer angle in arm 2 was varied for a xed angle in arm 1 with no narrow-band interference lter. We observed a visibility of (100±3)% [(85±3)%] when analyzer 1 is set to 0° (45°). In what follows we will use the 45° visibility as an indication of the quality of the state generated.

In Fig. 4 we report the 45° visibility for the singlet state as a function of the iris diameter. Two sets of data are shown, one using a 3-nm interference lters centered at 797 nm placed in front of the detectors (diamonds) and one in which the interference lter was removed (squares). In both cases the visibility is almost constant as a function of the iris diameter. This allows us to increase the pair ux (Fig. 4 inset) while preserving the purity of the output state. With the 3-nm lter we observed a visibility of 90% and a ux ≃12 000 pairs s^{1} mW^{1} with a 4-mm iris. Under this condition, following Ref. [12], we tested Bell's inequality and obtained $S=2.599\pm0.004$, violating the classical limit by more than 100σ.

Figure 4 can be compared with data obtained in a single-pass con guration with similar collection geometry properties reported in Ref. [9]. The visibility of quantum interference in the single-pass experiment drops much faster as the iris diameter increases than in this interferometric con guration. The nearly constant visibility in Fig. 4 arises from effective spatial and spectral indistinguishability in this dual-pumped interferometric con guration.

Two main factors limited the visibility: wave-front distortion and diffraction caused by the components of the inter-

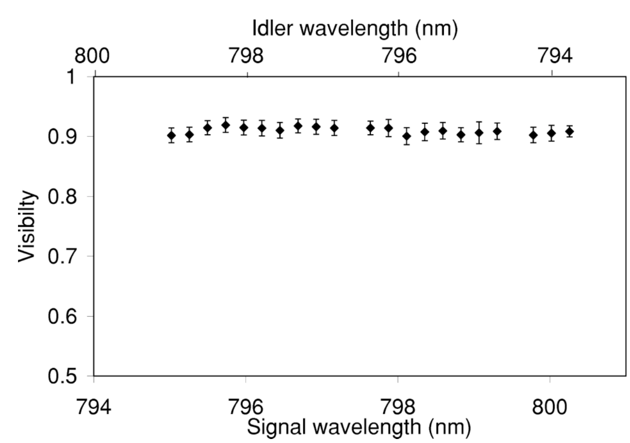

FIG. 5. 45° visibility (corrected for accidentals) versus signal wavelength (no interference lter, iris diameter 2.2 mm) with a measured ux of 3500 pairs s^{1} mW^{1}. The wavelengths on the abscissas are calculated from temperature tuning curves of the Sellmeier equations.

ferometer, and defects in the electric- eld poling of the crystal. Wave-front distortion and diffraction lead to spatial distinguishability between the two down-converted beams. Inhomogeneity in the crystal grating introduces a temporal mismatch between the two paths. Both these effects were mitigated somewhat by closing the iris and by adding spectral lters. To investigate the effects of wave-front distortion and diffraction we measured the interferometer visibility directly by injecting a laser beam at 797 nm through arm 2 of the PBS in Fig. 2 and observing the fringe signal in arm 1. The input and output beam diameters could be varied with irises. When we changed the diameter of the output beam for a xed input beam diameter, the visibility showed the same plateau for small iris diameters as in Fig. 4. When we decreased the input beam diameter for a xed output beam diameter the visibility increased linearly, approaching 100%. This suggests that the diffraction inside the interferometer was responsible for the at plateau in the visibility of Fig. 4. We note that a slight mismatch in the length of the two interferometric arms can also degrade the visibility.

No interference lter was used in obtaining the data shown in Fig. 5 and the iris diameter was xed at 2.2 mm. The temperature of the crystal was then scanned between 20 °C and 50 °C and the 45° visibility was measured. We used our knowledge of the Sellmeier equations, veri ed by down-conversion and second-harmonic generation measurements, to calculate the phase-matched signal and idler wavelengths for each temperature setting, and hence obtain the abscissas shown in this gure. Figure 5 shows that the 45° visibility is essentially independent of the signal and idler emission wavelengths for a range of $\sim$5 nm around degeneracy.

In conclusion, we have demonstrated a source of polarization-entangled photon pairs with high ux and state purity. The cw source is based on the interferometric combination of two coherently driven type-II sources of spontaneous parametric down-conversion from a single PPKTP crystal. This dual-pumped source is uniquely characterized by the fact that all the emitted photon pairs are polarization entangled, regardless of their wavelengths and directions of emission. Therefore it can be tuned, has a wide bandwidth, and an extended spatial pro le. We believe that our source produces spatial and spectral entanglement, in addition to polarization entanglement, thus providing additional degrees of freedom that can be used for quantum communication. Further work with this source is needed to experimentally demonstrate these additional forms of entanglement. If successful, we would then have a source that could be used to demonstrate fundamental quantum properties [13] and in cryptographic protocols with improved security [14].

This work was supported by a DoD Multidisciplinary University Research Initiative (MURI) program administered by the Army Research Of ce under Grant No. DAAD-19-00-1-0177, the Defense Advanced Research Projects Agency (DARPA) and Air Force Research Laboratory under Grant No. F30602-01-2-0546, the National Reconnaissance Of ce, and a DURIP Instrumentation Grant No. DAAD-19-01-1-0335.

[1] D. Bouwmeester *et al.*, Nature (London) **390**, 575 (1997).
[2] T. Jennewein, C. Simon, G. Weihs, H. Weinfurter, and A. Zeilinger, Phys. Rev. Lett. **84**, 4729 (2000); D. S. Naik, C. G. Peterson, A. G. White, A. J. Berglund, and P. G. Kwiat, *ibid.* **84**, 4733 (2000).
[3] P. G. Kwiat, P. H. Eberhard, A. M. Steinberg, and R. Y. Chiao, Phys. Rev. A **49**, 3209 (1994).
[4] P. G. Kwiat *et al.*, Phys. Rev. Lett. **75**, 4337 (1995).
[5] P. G. Kwiat, E. Waks, A. G. White, I. Appelbaum, and P. H. Eberhard, Phys. Rev. A **60**, R773 (1999).
[6] Y. H. Kim, M. V. Chekhova, S. P. Kulik, M. H. Rubin, and Y. Shih, Phys. Rev. A **63**, 062301 (2001).
[7] C. Kurtsiefer, M. Oberparleiter, and H. Weinfurter, Phys. Rev. A **64**, 023802 (2001); J. Völtz, C. Kurtsiefer, and H. Weinfurter, Appl. Phys. Lett. **79**, 869 (2001); M. Barbieri, F. De Martini, G. Di Nepi, and P. Mataloni, e-print quant-ph/0303018; M. Pelton *et al.* (unpublished).
[8] E. J. Mason, M. A. Albota, F. König, and F. N. C. Wong, Opt. Lett. **27**, 2115 (2002).
[9] C. E. Kuklewicz, M. Fiorentino, G. Messin, F. N. C. Wong, and J. H. Shapiro, Phys. Rev. A **69**, 013807 (2004).
[10] J. H. Shapiro and N. C. Wong, J. Opt. B: Quantum Semiclassical Opt. **2**, L1 (2000).
[11] H. Vaherzeele, J. D. Bierlein, and F. C. Zumsteg, Appl. Opt. **27**, 3314 (1988); W. Wiechmann, S. Kubota, T. Fukui, and H. Masuda, Opt. Lett. **18**, 1208 (1993).
[12] J. F. Clauser, M. A. Horne, A. Shimony, and R. A. Holt, Phys. Rev. Lett. **23**, 880 (1969); A. Aspect, P. Grangier, and G. Roger, *ibid.* **49**, 91 (1982).
[13] Z.-B. Chen, J.-W. Pan, Y.-D. Zhang, C. Brukner, and A. Zeilinger, Phys. Rev. Lett. **90**, 160408 (2003).
[14] M. Genovese and C. Novero, Eur. Phys. J. D **21**, 109 (2002).

Efficient and spectrally bright source of polarization-entangled photons

Friedrich König,* Elliott J. Mason, Franco N. C. Wong, and Marius A. Albota
Research Laboratory of Electronics, Massachusetts Institute of Technology, Cambridge, Massachusetts 02139, USA
(Received 23 September 2004; published 9 March 2005)

We demonstrate an ef cient ber -coupled source of nondegenerate polarization-entangled photons at 795 and 1609 nm using bidirectionally pumped parametric down-conversion in bulk periodically poled lithium niobate. The single-mode source has an inferred bandwidth of 50 GHz and a spectral brightness of 300 pairs/(s GHz mW) of pump power that is suitable for narrowband applications such as entanglement transfer from photonic to atomic qubits.

I. INTRODUCTION

The demonstration of the Einstein-Podolsky-Rosen (EPR) paradox is one of the most striking quantum effects observed to date. It reveals how entanglement of a nonseparable state produces nonlocal correlations that cannot be explained classically, as manifested in the violation of the Bell's inequalities [1]. Nonlocality is at the heart of a number of applications such as quantum cryptography and long-distance teleportation, which require ef cient distribution of entanglement over long distances. Photonic qubits are more easily transported over long distances than atomic qubits and, as a result, distribution of entangled photons is an essential part of a support infrastructure for quantum communications and distributed quantum computation networks.

In this work we report on a source of polarization-entangled photon pairs that is suitable for long-distance quantum information processing. Entangled photons at 795 and 1609 nm are created by nondegenerate parametric down-conversion with a spectral brightness that is suf cient for loading and entangling narrowband Rb-based quantum memories at 795 nm. The shorter-wavelength photon of this source can be used to directly excite a trapped Rb atom in a high- nesse cavity that serves as a local quantum memory. The other photon at 1609 nm is suited for ber -optic delivery because it lies in the low-loss transmission window of optical bers (1500–1650 nm).

In one proposed architecture for long-distance teleportation [2], a local and a remote Rb quantum memory are loaded using entangled photons. The stored atomic entanglement is then used to teleport an unknown atomic state from one location to the other [3]. Implicitly required for the architecture are the ef cient transport of entangled photons over long distances and wavelength matching between the entangled photons and the trapped atomic Rb. Because of unavoidable losses through long optical bers and the narrow bandwidth of atomic Rb of tens of MHz, it is essential to have a spectrally bright source of entangled photons at the above mentioned wavelengths. Note, however, that the entanglement of successfully delivered qubits is not degraded in this scheme [2]. For loading of the remote quantum memory, the 1609-nm photon has to be upconverted to the Rb wavelength at 795 nm with preservation of its polarization quantum state. 90%-ef cient upconversion [4] has recently been demonstrated at the single-photon level for a xed input polarization, and quantum-state preserving upconversion (for an arbitrary polarization qubit) is expected to have a similar conversion ef ciency .

Typical down-conversion sources using beta barium borate (BBO) crystals [5–7] are not suitable for narrowband applications such as quantum memory loading because of their large bandwidths of 1–10 nm. These sources also have relatively low ux, partly because of inef cient collection of the output photons in their emission cone and partly because of the small nonlinear coef cient of BBO. Down-conversion in waveguide nonlinear crystals [8,9] is much more ef cient but the outputs are still broadband and polarization entanglement using these waveguide crystals has not been reported.

We have previously demonstrated a high- ux source of nondegenerate photon pairs at 795 and 1609 nm in bulk periodically poled lithium niobate (PPLN) in a collinearly propagating geometry [10]. In the present work we have improved the source brightness to enter a regime suitable for narrowband applications such as atomic excitation and we have modi ed the apparatus for the generation of polarization-entangled photon pairs. PPLN has an effective nonlinear coef cient that is an order of magnitude larger than that of BBO and it can be tailored to phase match at any set of operating wavelengths within the transparency window of the crystal. In addition, PPLN has a wide temperature tuning range and is commercially available. Compared with more conventional noncollinear con gurations [5–7], collinear propagation in noncritically angle phase-matched down-conversion permits the use of a long crystal for more ef - cient generation. Moreover, the beamlike (instead of cone-like) output can be collected and ber -coupled more ef ciently for long-distance transport. This collinear geometry has recently been utilized in a type-II phase-matched periodically poled $KTiOPO_4$ (PPKTP) down-converter to ef- ciently generate polarization-entangled photons at 795 nm [11]. In a dual-pumping scheme with interferometric combination of the collinear type-II phase-matched PPKTP outputs a tenfold increase in ux has been demonstrated [12]. This dual-pumping method employs a single nonlinear crystal that is driven coherently by two counterpropagating pumps and is

*Now at School of Physics and Astronomy, University of St. Andrews, North Haugh, St. Andrews, Fife, KY16 9SS, Scotland.

suitable for nondegenerate operation with wavelength tuning.

For the current work, we have applied the dual-pumping technique to the generation of highly nondegenerate polarization-entangled photons using PPLN as the nonlinear crystal. By coupling the output signal and idler photons into their respective single-mode optical bers, we obtain single-spatial-mode photon pairs that are highly suited for spatial mode matching and ber -optic transport of the 1.6-μm light. Single-mode ber -optic delivery is particularly useful for applications such as the above-mentioned quantum-memory loading of a trapped atom in a high- nesse optical cavity. Fiber coupling of the outputs also allows one to select a mode-matched portion of the spontaneously emitted output eld from the crystal in order to limit the spectral bandwidth of the light. In our case, we have obtained a spectral bandwidth of $\sim$50 GHz which is less than the phase-matching bandwidth ($\sim$150 GHz) of our 2-cm-long PPLN crystal. We have achieved a spectral brightness that is suitable for narrowband wavelength-sensitive applications such as the proposed long-distance teleportation protocol [2].

In the next section we describe our dual-pumping generation scheme for the creation of polarization-entangled photon pairs in PPLN. In Sec. III, the characteristics of the PPLN source are presented when operated as a single-pass down-converter. Finally, in Sec. IV we describe the performance of the bidirectional pumping scheme and the violation of Bell's inequality as a measure of the purity of the polarization entanglement, before we conclude in Sec. V.

II. GENERATION OF POLARIZATION ENTANGLEMENT

Spontaneous parametric down-conversion (SPDC) in a nonlinear optical crystal is a standard technique for generating polarization-entangled photons. In SPDC, a pump photon is converted into two lower-frequency photons, called signal (S) and idler (I), that have de nite polarizations. For example, in a low-gain type-I phase-matched interaction, the signal and idler photons are copolarized with an output state (after ignoring the vacuum and higher-order modes) given by $|\Psi\rangle = |1\rangle_{S\bullet}|1\rangle_{I\bullet}$, where $\bullet$ refers to horizontal polarization. In this example, $|\Psi\rangle$ is a separable state and there is no polarization entanglement. It is clear that SPDC, by itself and without additional arrangements, does not produce polarization entanglement in which each photon of the down-converted pair appears to be randomly polarized and yet the pair is polarization correlated.

It was proposed [13,14] and recently demonstrated [12] in a type-II phase-matched system that polarization entanglement can be readily obtained if the outputs from two coherently driven identical down-converters are interferometrically combined. A remarkable property of such a bidirectionally pumped arrangement is that spatial, spectral, or temporal ltering is no longer necessary for obtaining high quality entanglement [12]. In our current experiment, we explore a type-I phase-matched system in a similar bidirectional pumping arrangement. Since PPLN is type-I phase-matched the signal and idler outputs have the same polarization, and hence they can only be separated if the outputs are very different in wavelength, using a dispersing prism or

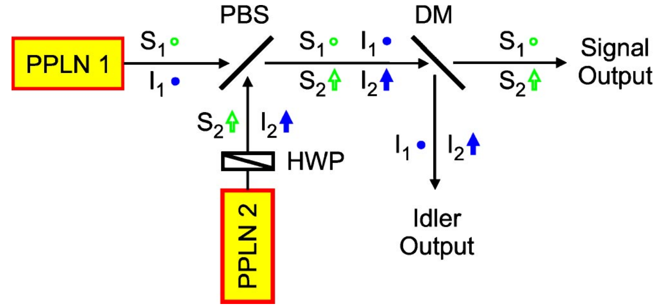

FIG. 1. Schematic view of two coherently driven and combined PPLN down-converters. Horizontal (vertical) polarization is denoted by $\bullet$ ($\uparrow$). HWP, half-wave plate; PBS, polarizing beam splitter; DM, dichroic mirror.

dichroic mirror, for example. A con guration combining two nondegenerate type-I phase-matched down-conversions in PPLN is schematically shown in Fig. 1. The horizontally polarized signal and idler elds in one direction (path 1) are combined with the vertically polarized signal and idler elds (after a $\pi/2$ polarization rotation) in the other direction (path 2) at the polarizing beam splitter. The signal and idler outputs are then separated at the dichroic mirror.

After the interferometric combination, the lowest-order nonvacuum output is the biphoton state

$$\begin{aligned} |\Psi\rangle &= \alpha|1\rangle_{S\bullet}|1\rangle_{I\bullet}|0\rangle_{S\uparrow}|0\rangle_{I\uparrow} + \beta|0\rangle_{S\bullet}|0\rangle_{I\bullet}|1\rangle_{S\uparrow}|1\rangle_{I\uparrow} \\ &= \alpha|H\rangle_S|H\rangle_I + \beta|V\rangle_S|V\rangle_I, \end{aligned} \tag{1}$$

where the complex coef cients α and β represent the eld strengths for the two down-converters and $\uparrow$ indicates vertical polarization. For a ber -coupled implementation of Fig. 1, $|\alpha|^2$($|\beta|^2 = 1 \;\; |\alpha|^2$) is proportional to the overall ef ciency for pair generation in path 1 (2) direction, and subsequent propagation and coupling into the signal and idler bers. The phase of α (β) is the sum of the phases of the horizontally (vertically) polarized signal and idler elds along their paths from the crystal to the dichroic mirror. Note that the common path for the signal and idler elds after the polarizing beam splitter adds a common phase to α and β, which yields an inconsequential overall phase for the state $|\Psi\rangle$. In Eq. (1), we have simpli ed the notation by not displaying the vacuum modes and by replacing $|1\rangle_\bullet$ and $|1\rangle_\uparrow$ with $|H\rangle$ and $|V\rangle$, respectively. Implicit in Eq. (1) is that the signal and idler photons have different wavelengths that allow them to be easily separated and individually manipulated. A key characteristic of this dual-pump con guration is that, with a proper choice of polarization basis, phases, and relative pumping strengths, one can in principle obtain any one of the four Bell states, independent of propagation or coupling losses. For instance, with $\alpha = \;\; \beta = 1/\sqrt{2}$ and a 90° rotation of the idler state, the singlet state $|\Psi \;\rangle = \alpha[|H\rangle_S|V\rangle_I \;\; |V\rangle_S|H\rangle_I]$ is obtained.

III. SINGLE-PASS DOWN-CONVERSION

Figure 2 shows a schematic of our experimental setup for implementing the polarization entanglement source with two

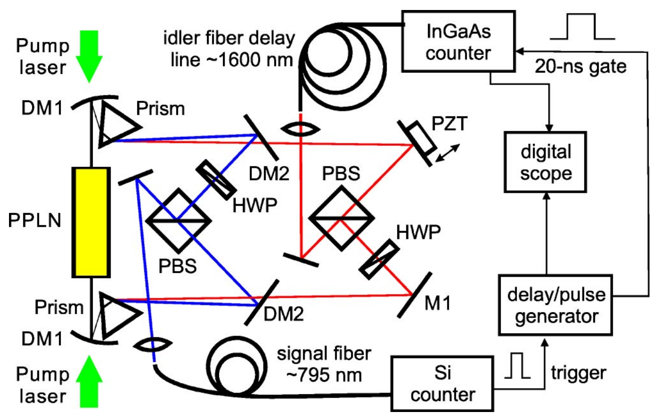

FIG. 2. Schematic of experimental setup used for single-pass and dual-pumped down-conversion. DM, dichroic mirror; HWP, half-wave plate; PBS, polarizing beam splitter; PZT, piezoelectric transducer.

identical down-converters. By using two counterpropagating pump beams to coherently drive a single PPLN crystal, the two down-converters can be made to be nearly identical (limited by the crystal grating uniformity). We rst describe and characterize our PPLN down-converter in single-pass operation with only one pump before detailing the coherent combining technique in the next section.

We employed a 2-cm long and 0.5-mm thick PPLN crystal with a grating period of 21.6 μm as the nonlinear medium. We previously fabricated the crystal for type-I third-order quasi-phase-matched SPDC to generate tunable signal and idler photons centered at $\sim$0.8 and $\sim$1.6 μm, respectively, from a continuous-wave (cw) pump at 532 nm [10]. The crystal was antire ection coated at the pump, signal, and idler wavelengths with re ectivities of $<1\%$, $<1\%$, $\sim 8\%$ per surface, respectively. Using difference-frequency generation (DFG) we observed a phase-matching bandwidth of $\sim$150 GHz at a xed pump wavelength and a xed crystal temperature. By varying the crystal temperature, we were able to tune the outputs over tens of nm, with a tuning coef cient of $\sim$150 GHz/°C. For outputs at 795 and 1609 nm, we operated the PPLN crystal at 176 ± 0.1 °C. From the DFG results we estimate the effective third-order nonlinear coef cient to be 3.8 pm/V, which is less than expected due to grating imperfections and mode mismatch in the DFG measurements.

The PPLN down-conversion source, including the ber-coupled pump input and the output ber couplers, was set up on a 38×74 cm^2 breadboard for improved mechanical stability and portability. The 532-nm pump was derived from a cw frequency-doubled Nd:YVO_4 laser (Coherent Verdi-8) with a maximum output power of 8 W. We coupled a small fraction of the laser power into a single-mode polarization maintaining ber which delivered the pump light to the PPLN source. This pump ber exhibited slight multimode behavior and the output was mode cleaned with a pinhole and then focused into the center of the crystal with a beam waist of 90 μm. Typical pump powers incident upon the crystal were 1 mW; however, the crystal could easily be pumped by a few hundred mW of cw power without damage.

The dichroic curved mirrors DM1 (highly re ecting at 0.8 and 1.6 μm and highly transmitting at 532 nm) in Fig. 2 served to focus the pump light into the crystal at the entrance and to remove the pump beam from the down-converted output at the exit. The DM1 mirror at the exit was also used to refocus the diverging down-converted output light. The down-converted light was spectrally separated into signal and idler beams with a dispersing prism which also steered the residual pump light away from the signal and idler paths. Signal and idler beams could then be individually manipulated before being coupled into their respective single-mode optical bers for transport or photon counting detection.

First we investigated the spontaneous emission characteristics of the bulk PPLN crystal. We passed the signal output through a 1-nm interference lter (IF) centered at 795 nm and imaged the output onto a high-resolution charged-coupled device (CCD) camera (Princeton Instruments VersArray: 1300B) with a detection sensitivity of a few photons. Figure 3 shows the evolution of the 795-nm output as a function of the crystal temperature from a conelike pattern, as in noncollinear SPDC, to a beam-like output, as in a collinear geometry. Figure 3(a) shows a typical ring pattern of the observed signal output emerging from the crystal. The ring diameter is directly related to the internal emission angle at which the output at the 795-nm wavelength was phase matched. By varying the crystal temperature the phase-matching angle for 795-nm emission was modi ed as shown in Figs. 3(a)–3(c). In Fig. 3(c) the output was collinear with a phase matching temperature $T=183.6$ °C.

We measured the ring diameters and hence the phase-matching angles of the 795-nm PPLN emission as a function of the crystal temperature. At each temperature T we obtained the corresponding collinearly phase-matched signal wavelength $\lambda_{CPM}(T)$ by DFG phase-matching measurements. Figure 4 shows the measured emission angles $\theta(T)$ relative to $\lambda_{CPM}(T)$, and compares them with the computed phase-matching angles obtained from the Sellmeier equations [15] for noncollinearly phase-matched PPLN. The excellent agreement between the experimentally observed signal emission angles and the theoretical values that we obtain without free parameters allows us to infer the mode characteristics of

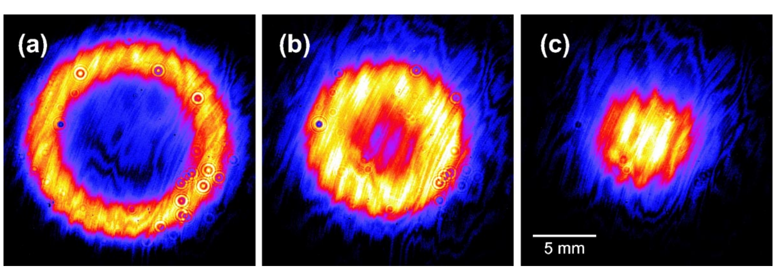

FIG. 3. Far- eld CCD camera images of spontaneously down-converted light through a 1-nm interference lter centered at 795 nm. PPLN temperatures were (a) 177.6 °C, (b) 180.6 °C, and (c) 183.6 °C. The 795-nm light was phase-matched at different angles as a function of temperature. Fringing is due to camera etalon effects.

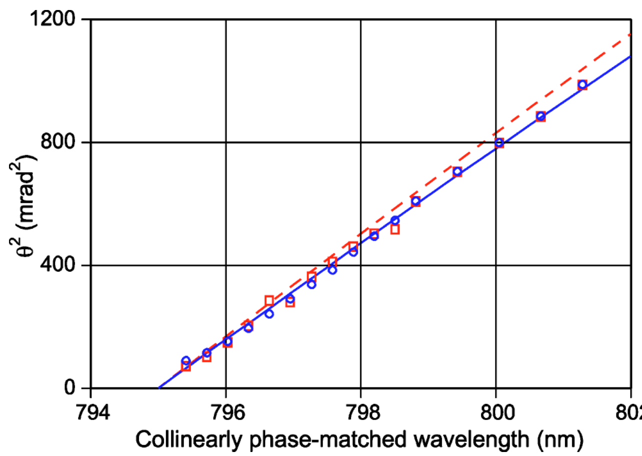

FIG. 4. Plot of external far- eld PPLN emission angles, as measured by the ring diameters of CCD images along the crystal's z axis (open circles) and y axis (open squares) as a function of the collinearly phase-matched wavelength $\lambda_{CPM}(T)$, where T is the PPLN crystal temperature. The solid and dashed lines are the theoretical emission angle curves corresponding to the crystal's y and z axes, respectively, obtained from the PPLN's Sellmeier equations with no adjustable parameters.

the idler output beam. In particular, because of the signal-idler wavelength difference, the 1.6-μm idler emission angle is twice the 0.8-μm signal angle, and the idler bandwidth in nm is four times as large as the corresponding signal bandwidth of the signal-idler pair emission.

The CCD camera was used to measure the emitted signal power within the 1-nm IF bandwidth. We integrated the pixel output voltages spatially over the ring structure and subtracted the background (obtained without input light) from it. The 795-nm signal power was measured as a function of crystal temperature within a 1-nm bandwidth. In Fig. 5 we plot the power versus the wavelength $\lambda_{CPM}(T)$, at which collinear phase matching was achieved at temperature T. Below $\lambda_{CPM} \approx 794$ nm, the 795-nm output was not phase-matched and the emission vanished. Beyond $\lambda_{CPM}=795$ nm, the output power remains more or less constant, indicating that the

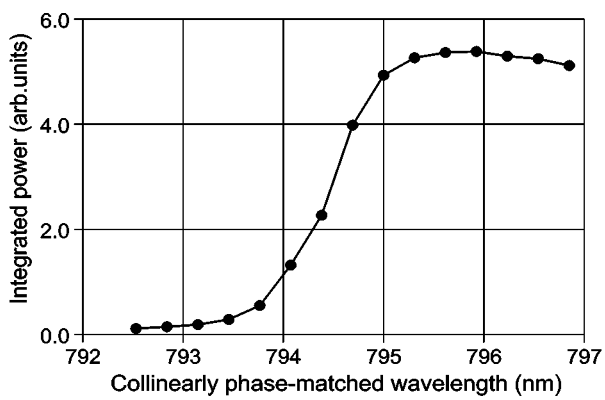

FIG. 5. Integrated power of output emission at 795 nm in a 1-nm bandwidth. PPLN crystal temperature T was set for collinear phase matching at the wavelength $\lambda_{CPM}(T)$. The total output power shows little dependence on the emission angles for $\lambda_{CPM} \geqslant 795$ nm.

integrated power was only weakly dependent on the phase-matching temperatures (and emission angles).

Next we optimized the coupling ef ciency of the photon pairs into single-mode bers by utilizing the mode structure information. In particular, we found that PPLN temperature tuning was a useful tool to vary slightly the down-converted beam parameters without affecting the down-conversion ef ciency . We measured the ber coupling ef ciencies at three different 795-nm IF bandwidths of 0.11, 1, and 3 nm for the signal photons. The PPLN temperature was nominally set for collinear phase matching at $\lambda_{CPM}=795$ nm and aspheric lenses of various focal lengths were used at each IF bandwidth setting. The signal photon ux before the signal ber was measured with a high-sensitivity Si photodiode under strong pumping. For measuring the ux after the single-mode ber we reduced the pump power and used a Si single-photon counting module (SPCM). After accounting for various losses and adjusting for the different pumping levels and different detection ef ciencies for the photodiode and the single-photon counter, the best ber coupling ef ciency of 18% for the signal beam was obtained using the 0.11-nm IF. In contrast, with the 3 nm IF the coupling was at least an order of magnitude less ef cient due to the much larger angular bandwidth of the output signal photons.

For a 3-nm bandwidth, we infer from the measurements a pair generation rate of $2\times10^7/(\mathrm{s\ mW})$ of pump power at the output of the crystal. The single-mode ber -coupled signal rate (corrected for detector ef ciency) was $5.1\times10^4/(\mathrm{s\ mW})$ of pump power within the same 3-nm spectral bandwidth. This rate was reduced from that at the crystal because of propagation and ber coupling losses.

We then studied the conditional detection probabilities by making signal-idler coincidence measurements, as shown in the schematic setup of Fig. 2. The 800-nm signal ber was connected to a ber -coupled Si SPCM (PerkinElmer AQR-13-FC) which produced a timing trigger upon detection of an incoming signal photon. A time-delay pulse generator then produced a bias gating pulse of 7–20 ns duration which was sent to a Peltier-cooled passively-quenched InGaAs avalanche photodiode (APD) operating in Geiger mode for the detection of the conjugate 1609-nm idler photon. The design and properties of our homemade InGaAs APD single-photon counter have been described elsewhere [10]. The main characteristics of this InGaAs single-photon counter are a dark count probability of 0.1% per 20-ns gate and a quantum ef ciency of 19.8% at a detector temperature of 50 °C. The generated electrical pulses from the detectors were then recorded by a computer and their timing information was used to identify rings of the Si and InGaAs counters corresponding to pair coincidences. Typically we used a coincidence window of 4 ns.

The conditional probability of detecting an idler photon, given the detection of a signal photon, was 9.4% using the narrowband 0.11-nm IF. In calculating this conditional probability we subtracted the background in the coincidence rate due to accidental and dark counts (probability of ~0.04%). This background rate was measured by offsetting the start of the gating pulse for the InGaAs counter by an amount greater than the 4-ns coincidence window. Given the 19.8%-ef cient InGaAs counter, this implies ~50% losses in idler propagation, mode matching, and ber coupling into the 1.6-μm optical ber , conditioned on signal photon detection. Single-mode pair generation is best characterized by the rate of photon pairs that are successfully coupled into their respective single-mode bers, i.e., the detected rate corrected for detector quantum ef ciencies. In the case of the 0.11-nm IF, we observed a signal-idler coincidence rate of 450/(s mW), from which we infer a single-mode ber -coupled pair ux of ~4100/(s mW) before detection. Without an IF the conditional probability decreased to 5.2% because additional spatial modes were coupling into the signal ber whose idler counterparts could not be all coupled simultaneously into the idler ber in an ef cient way. However, without using spectral lters we note that there were many more signal photons coupled into the signal ber (partly because of the absence of the propagation loss through the IF) and we measured a single-mode ber -coupled pair ux of 16 000/(s mW) before detection in this case.

IV. POLARIZATION ENTANGLEMENT BY BIDIRECTIONAL PUMPING

Coherent combination of two down-converters for the generation of polarization entanglement shown schematically in Fig. 1 was implemented with the setup of Fig. 2 which we have described for the single-pass case in the previous section. To ensure that the two down-converters were as identical as possible, a single PPLN crystal was pumped in counter-propagating directions along the crystal's x axis. The ber -coupled 532-nm pump light was split into two beams with a 50-50 beam splitter. Each of the pump beams was directed into the PPLN crystal as shown in Fig. 2 and the two outputs followed nearly identical paths as described in the previous section. In order to generate polarization entanglement, the signal and idler elds of one of the down-converters were rotated by 90° with half-wave plates (HWPs) before combining with the output from the other down-converter.

The spectral contents of the two down-converters were identical by our use of a single crystal. However, spatial and temporal mode matching were still necessary because there were four path lengths (two for the signals and two for the idlers) that must be properly adjusted for ef cient generation of polarization entanglement. When the two signal elds were combined at the polarizing beam splitter (PBS), the two spatial modes should be identical to avoid spatial-mode distinguishability, and similarly for the idler elds. This was accomplished by making sure that the two pump foci inside the crystal were the same in size and location, and the two signal and two idler path lengths were the same. The tolerance of the path length difference (a few mm) was dictated by the confocal parameters at the location of the PBS. Note that this mode overlap facilitated equal coupling to the respective signal and idler bers, where the elds were projected into a single spatial mode. A more stringent requirement is temporal indistinguishability. That is, the path length difference between the two combining signal elds should be the same as that between the two idler elds within the coherence length of the photons, which was determined by the

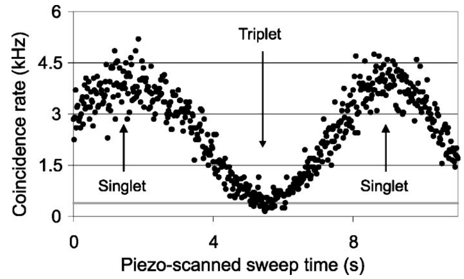

FIG. 6. Two-photon quantum interference from the bidirectionally pumped down-converter, showing the detected coincidence rate as a function of the PZT mirror sweep with crossed analyzers. The PZT changes the relative phase ϕ of the output state of Eq. (2), yielding a maximum rate for $\phi=0$ (singlet) and a minimum rate for $\phi=\pi$ (triplet). See text for experimental details.

bandwidths of the phase matching, the IF, and the ber coupling.

The photon bandwidth can be easily determined in a Hong-Ou-Mandel (HOM) interferometric measurement for degenerate signal and idler wavelengths. For nondegenerate wavelengths two-photon quantum interference visibility can be similarly utilized to measure the photon bandwidth. Quantum interference is also the basis for demonstrating Bell's inequality in the Clauser-Horne-Shimony-Holt (CHSH) form [1] that yields a measure of the quality of polarization entanglement.

The biphoton output state of the bidirectionally pumped down-converter, for equal pump power in both directions, is

$$|\Psi\rangle = (|H\rangle_S|V\rangle_I \quad e^{i\phi}|V\rangle_S|H\rangle_I)/\sqrt{2}, \tag{2}$$

where ϕ is the relative phase that is a function of the phase difference between the two pumps (hence coherent pumping is required), and the signal and idler phases acquired along the four path lengths. In the experiment, we controlled ϕ by a mirror mounted on a piezoelectric transducer (PZT) in one of the idler paths, as shown in Fig. 2. We note that the output state is a singlet polarization-entangled state for $\phi=0$.

For quantum interference observation and analysis, we installed polarization analyzers (a HWP followed by a horizontally-transmitting PBS) at the entrances to the signal and idler single-mode optical bers. The two analyzers were initially set parallel and oriented to transmit an equal amount of light from the two pumping directions (equivalent to transmission at 45° relative to the horizontal polarization). All angles of our analyzers were measured with respect to this initial orientation.

We rst demonstrated the generation of different two-photon states by varying the PZT mirror position, as manifested in the two-photon quantum interference. With the idler analyzer set orthogonal to the signal analyzer, the PZT was swept and the two-photon output state went through the singlet state at $\phi=0$ and the triplet state at $\phi=\pi$. We observed a sinusoidal modulation in the coincidence detection rate as a function of the PZT sweep, as shown in Fig. 6. At $\phi=0$, the singlet-state output is obtained which is invariant under coordinate rotation and signal and idler are always orthogonally polarized. Hence, a maximum in the coincidence rate

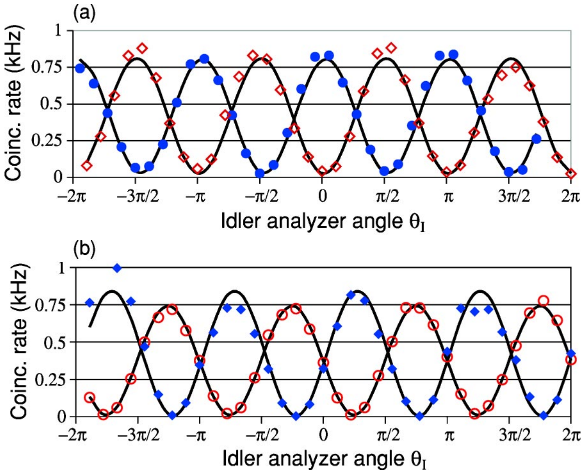

FIG. 7. Plot of coincidence rate as a function of idler polarization analyzer angle θ_I, where at $\theta_I=0$ the analyzer was set to couple equal amounts of idler from the two down-converters. (a) Signal polarization analyzer was set at $\theta_S=0$ (passing equal amounts of signal light from the two down-converters) for the singlet output state $\phi=0$ (open diamond) and the triplet output state $\phi=\pi$ (solid circle). (b) $\theta_S=\pm\pi/4$ to pass the output from the single down-converter pumped from below (open circle) or above (solid diamond). Below and above refers to pumping directions as indicated in Fig. 2.

was obtained for $\phi=0$. At $\phi=\pi$, the output state was transformed into a triplet state with parallel polarizations for signal and idler, thus yielding a minimum in the coincidence rate, as displayed in Fig. 6. For non-entangled photon pairs, the sweep would not produce any modulation in the coincidence rate, which would lie midway between the maximum and minimum values. We obtain a quantum-interference visibility of ~93% if dark counts and accidentals are subtracted (grey line in Fig. 6). The quantum interference coincidence measurements in Fig. 6 were made with ~80 mW of total pump power and the data were taken with the 0.11-nm IF. The interferometric setup was very stable such that no locking was required. The observed free-running phase drift after 5 minutes was much less than $\pi/4$. We used a high-speed multichannel analyzer (PicoQuant's TimeHarp 200) for time-resolved coincidence counting with an effective coincidence window of 4 ns. As the PZT was slowly swept the computerized data collection recorded the number of coincidences in 20-ms measurement time intervals. Note that the noise in Fig. 6 is Poissonian if we consider that the data were sampled in 20-ms time intervals. This initial set of measurements permitted us to further optimize the quantum-interference visibility and the coincidence rate.

Additional quantum interference measurements with the 0.11-nm IF were carried out and are shown in Fig. 7. In Fig. 7(a) the coincidence counts are plotted for the singlet (open diamond) and triplet (solid circle) states as a function of the idler analyzer angle θ_I when the signal analyzer angle θ_S was set to equally transmit light from both of the down-converters ($\theta_S=0$). Here we obtain quantum-interference visibility of 94% for the singlet and triplet in Fig. 7(a). In Fig. 7(b) a similar plot of the coincidence counts is made with the signal analyzer transmitting signal photons from the lower (open circle) and upper (solid diamond) pumping beams (Fig. 2), with $\theta_S=\pi/4$ and $\pi/4$, respectively. By setting the signal analyzer θ_S to pass the signal photons of just one of the down-converters, we were simply measuring the pair generation rate as a function of θ_I. For the data in Fig. 7(b), we obtained a higher visibility of 99.8% for the horizontal ($\theta_S=\ \pi/4$) and 98% for the vertical ($\theta_S=\pi/4$) orientation of the signal analyzer. We believe that the visibilities in Fig. 7(a) were not limited by spatial mode mismatch, temporal mismatch, or a rate imbalance of the two down-converters because the interfering signal elds shared the single mode of the ber and temporal overlap and rate balance were adjusted accurately. Therefore we conclude that a spectral distinguishability between the two down-converters is the most likely reason, caused by either a difference in the spectra of the ber -coupled signals and idlers or the crystal nonuniformity along its length.

We have used the quantum interference signature to measure the photon bandwidth of the ber -coupled photon pair in the absence of an IF. By translating the mirror $M1$ over a distance of a few mm in ne steps, we monitored the interference visibility as a function of distance. If the two orthogonal idler elds do not overlap in time, relative to the time difference of the two orthogonal signal elds, then the two-photon quantum interference disappears. We observed that the full distance at half of the peak visibility was 3.4 mm, or ~11 ps in time. If we assume that the ber coupling acts as a Gaussian lter , then the corresponding ber -coupled photon pulse width is 8.8 ps, or 50 GHz in spectral bandwidth. This narrow bandwidth was obtained for a particular mode matching con guration which ef ciently coupled only the light of this small bandwidth. This is a manifestation of the high degree of spatial and spectral correlation in the down-converted output. We have also performed a series of quantum interference measurements to demonstrate the violation of Bell's inequality in the CHSH form [1]. We follow the standard procedure of measuring coincidence rates at different polarization analyzer angles using the singlet state as the input. The drift of the dual-pumped down-converter interferometer was found to be negligible as it did not degrade the interference over the 6-minute measurement time, which included manually setting the analyzer angles. We measured an S parameter of 2.606 ± 0.010 for a pump power of 2.2 mW per beam. The results indicate a violation of 60 standard deviations over the classical limit of 2. Perfect polarization entanglement would have yielded maximum violation of the Bell's inequality with $S=2\sqrt{2}$.

V. SUMMARY

We have demonstrated an ef cient source of polarization-entangled photons at highly nondegenerate wavelengths using bidirectional pumping of a single PPLN crystal followed by coherent combination of the down-converted outputs. Our source is ber -coupled, widely tunable by tens of nm in wavelength via temperature tuning of the PPLN crystal, and takes advantage of a convenient, collinearly propagating geometry. Using third-order, type-I quasi-phase matching in a

2-cm long PPLN crystal, we have obtained a ber -coupled polarization-entangled pair ux of $\sim 16\,000/(\mathrm{s\,mW})$ of 532-nm pump power in a bandwidth of 50 GHz. For a bandwidth of 50 MHz, our source has a ux of $\sim 16/(\mathrm{s\,mW})$. This number can be scaled up by three orders of magnitude using a rst order grating (factor of 9 improvement) in PPLN with a better quality grating duty cycle (factor of 20%), and a higher pump power of 100 mW or more. These simple improvements can be implemented without changing the experimental con guration and would yield a photonic source of polarization entanglement suitable for entanglement transfer to atoms via direct atomic excitations which have bandwidths of tens of MHz. The source could be used for testing long-distance teleportation schemes, in which the entanglement is stored in trapped-atom quantum memories [2]. The bidirectional pumping con guration in our bulk PPLN system can be applied to a PPLN waveguide down-converter, thereby combining the signi cant ef ciency improvement of a waveguide con guration with the ease of generating polarization entanglement. Furthermore, the collinear geometry is suitable for implementing a cavity-enhanced parametric ampli er con guration [14], which should yield polarization-entangled photons that have bandwidths closely matching those of atomic excitations. Our source therefore is useful for a number of quantum information processing tasks such as long-distance teleportation and quantum cryptography.

ACKNOWLEDGMENTS

This work was supported by a DoD Multidisciplinary University Research Initiative (MURI) program administered by the Army Research Of ce under Grant No. DAAD-19-00-1-0177. We acknowledge substantial laboratory help from Christopher Kuklewicz.

[1] J. F. Clauser, M. A. Horne, A. Shimony, and R. A. Holt, Phys. Rev. Lett. **23**, 880 (1969).

[2] J. H. Shapiro, New J. Phys. **4**, 47.1 (2002).

[3] S. Lloyd, M. S. Shahriar, J. H. Shapiro, and P. R. Hemmer, Phys. Rev. Lett. **87**, 167903 (2001).

[4] M. A. Albota and F. N. C. Wong, Opt. Lett. **29**, 1449 (2004).

[5] P. G. Kwiat, K. Mattle, H. Weinfurter, A. Zeilinger, A. V. Sergienko, and Y. Shih, Phys. Rev. Lett. **75**, 4337 (1995).

[6] P. G. Kwiat, E. Waks, A. G. White, I. Appelbaum, and P. H. Eberhard, Phys. Rev. A **60**, R773 (1999).

[7] C. Kurtsiefer, M. Oberparleiter, and H. Weinfurter, Phys. Rev. A **64**, 023802 (2001).

[8] S. Tanzilli, H. De Riedmatten, H. Tittel, H. Zbinden, P. Baldi, M. De Micheli, D. B. Ostrowsky, and N. Gisin, Electron. Lett. **37**, 26 (2001).

[9] K. Banaszek, A. B. U'Ren, and I. A. Walmsley, Opt. Lett. **26**, 1367 (2001).

[10] E. J. Mason, M. A. Albota, F. König, and F. N. C. Wong, Opt. Lett. **27**, 2115 (2002).

[11] C. E. Kuklewicz, M. Fiorentino, G. Messin, F. N. C. Wong, and J. H. Shapiro, Phys. Rev. A **69**, 013807 (2004).

[12] M. Fiorentino, G. Messin, C. E. Kuklewicz, F. N. C. Wong, and J. H. Shapiro, Phys. Rev. A **69**, 041801(R) (2004).

[13] P. G. Kwiat, P. H. Eberhard, A. M. Steinberg, and R. Y. Chiao, Phys. Rev. A **49**, 3209 (1994).

[14] J. H. Shapiro and N. C. Wong, J. Opt. B: Quantum Semiclassical Opt. **2**, L1 (2000).

[15] R. C. Eckardt, C. D. Nabors, W. J. Kozlovsky, and R. L. Byer, J. Opt. Soc. Am. B **8**, 646 (1991).